Sede Amministrativa: Università degli Studi di Padova

Dipartimento di Medicina Molecolare

SCUOLA DI DOTTORATO DI RICERCA IN BIOMEDICINA

CICLO XXVII

G-QUADRUPLEXES IN THE HSV-1 AND HHV-6 GENOMES AS ANTIVIRAL TARGETS

Direttore della Scuola: Prof. Riccardo Manganelli

Supervisore: Prof.ssa Sara Richter

Dottorando: Sara Artusi

Index

List of abbreviations

3-MA	3-methyl adenine
ACV	acyclovir
B19	BRACO-19
bp	base pair
BSA	bovine serum albumin
C	cytosine
CC_{50}	50% cytotoxic concentration
CD	circular dichroism
cDNA	complementary DNA
CPE	cytopathic effect
DR	direct repeat
Ctrl	control
DR_L	direct repeat left
DR_R	direct repeat right
dsDNA	double-stranded DNA
E (or β)	early gene
ELISA	enzyme-linked immunosorbent assay
EC_{50}	50% effective concentration
FCV	famciclovir
g	glycoprotein
G	guanine
G-4	G-quadruplex
GCV	ganciclovir
h	hours
HCMV	Human cytomegalo virus
HIV	human immunodeficiency virus
HHV-6	human herpes virus-6
H/P	helicase/primase
h.p.i.	hours post infection
HPSG	heparan sulfate proteoglycan
HS	heparan sulfate
HSV-1	herpes simplex virus-1
HSV-2	herpes simplex virus-2
hTERC	human telomerase RNA component
hTERT	human Telomerase Reverse Transcriptase
HVEM	herpesvirus entry mediator
IC_{50}	50% inhibitory concentration
$^{tel}IC_{50}$	telomerase 50% inhibitory concentration
ICP	infected-cell polypeptide
IE (or α)	immediate-early gene
IF	Initiation factor
IR_L	inverted repeat long
IR_S	inverted repeat short
K^+	potassium
KCl	potassium chloride
kp	kilobase
L (or γ)	late gene
LTR	long terminal repeat

MOI	multiplicity of infection
MTT	3-(4,5-dimethylthiazol-2-yl)-2,5-diphenyltetrazolium bromide
Na^+	sodium
NaCl	sodium chloride
NDI	naphtalene diimide
nt	nucleotide
Ori	origin of replication
P2	TMPyP2
P4	TMPyP4
PAA	phosphonoacetic acid
PBMCs	peripheral blood mononuclear cells
PCV	penciclovir
PFA	foscarnet
PCR	polymerase chain reaction
PHA-P	phytohemagglutinin-P
PI3K	phosphoinositide 3-kinase
PKR	protein kinase RNA-activated
Pol	polymerase
PP1α	phosphatase-1α
QGRS	quadruplex forming G-rich sequences
Q-PCR	quantitative PCR
RQ	relative quantities
RT-PCR	real-time PCR
SP1	specificity protein 1
ssDNA	single-stranded DNA
SSRs	simple sequence repeats
TEM	transmission electron microscopy
T_m	melting temperature
TR_L	terminal repeat long
TR_S	terminal repeat short
TRS	telomeric repeat sequence
U	unique
U_L	unique long
U_S	unique short
VACV	valacyclovir
VZV	varicella-zoster virus
wt	wild-type

RIASSUNTO

Acidi nucleici ricchi di guanine possono formare una particolare struttura secondaria nota come G-quadruplex, il quale è implicato nella regolazione di importanti processi biologici a livello del genoma umano, di procarioti e virus.

Dato che il genoma dell'herpes simplex virus-1 (HSV-1) è notevolmente ricco in guanine, il nostro studio è stato mirato all'individuazione di sequenze virali in grado di foldare in G-quadruplex e, in secondo luogo, alla possibilità di colpire selettivamente questa conformazione non-canonica con specifiche molecole chimiche, al fine di sviluppare una terapia antivirale innovativa.

Il nostro studio dimostra la presenza di sei gruppi composti da sequenze altamente ripetute capaci di formare strutture G-quadruplex particolarmente stabili. Queste sequenze sono state individuate a livello delle regioni terminali del genoma di HSV-1 e all'interno di due regioni codificanti (geni ICP0 e UL36). Un cluster di sequenze G-quadruplex, inoltre, è situato nella regione promotoriale deputata all'espressione della proteina multifunzionale $\gamma_1$34.5.

Il trattamento di cellule infettate con BRACO-19 e TMPyP4 ha mostrato una significativa inibizione di HSV-1 e una riduzione dell'espressione di alcuni trascritti virali.

BRACO-19 si è dimostrato efficace nell'inibire l'elongazione di regioni G-quadruplex del genoma di HSV-1, da parte dell'enzima Taq; è stato in grado di diminuire il DNA virale intracellulare, opportunamente estratto da cellule infettate e trattate; inoltre, mentre nessun effetto è stato osservato sull'entry di HSV-1, l'ultimo step del ciclo virale inibito da BRACO-19 corrisponde alla replicazione del DNA virale.

Un diverso meccanismo d'azione è stato, invece, osservato in seguito al trattamento con TMPyP4. Nonostante questa porfirina sia riuscita ad inibire l'attività della Taq, non è riuscita,

al contrario, ad influenzare i livelli di DNA virali intracellulari. TMPyP4 sembra essere efficace nell'inibire la maturazione/uscita di HSV-1, attraverso un'induzione dell'autofagia.

In una seconda parte dello studio, abbiamo esteso questa promettente strategia antivirale all'herpes virus umano 6 (HHV-6), il quale presenta una caratteristica molto peculiare. Ad entrambe le estremità del suo genoma (D_R) contiene, infatti, numerose ripetizioni della sequenza telomerica umana $(TTAGGG)_n$. Questa caratteristica è ritenuta responsabile dell'integrazione di HHV-6 in alcuni cromosomi umani (1-2% della popolazione).

Ad oggi, la struttura G-quadruplex della sequenza telomerica è stata studiata in dettaglio e completamente caratterizzata. Abbiamo, quindi, testato BRACO-19 e TMPyP4 su cellule infettate sia con HHV-6A che HHV-6B, ottenendo anche in questo caso dei risultati molto incoraggianti.

Infine, in una terza parte del lavoro, è stato possibile visualizzare per la prima volta G-quadruplex virali a livello del DNA in cellule infettate, grazie all'impiego di anticorpi ad alta affinità per questa struttura. La specificità di segnale è data dal fatto che l'incremento di fluorescenza è avvenuto nel corso della replicazione virale in cui il DNA è presente come singolo filamento.

Questo lavoro, oltre a mostrare l'esistenza di estese regioni G-quadruplex in siti chiave del genoma di HSV-1 e HHV-6, mette in luce le potenzialità del G-quadruplex come target innovativo in terapie antivirali nuove e mirate, basate sull'impiego di leganti specifici per questa particolare conformazione secondaria del DNA.

ABSTRACT

Guanine-rich nucleic acids can fold into G-quadruplexes, four-stranded secondary structures which are implicated in important regulatory functions at the genomic level in humans, prokaryotes and viruses. Because the herpes simplex virus-1 (HSV-1) genome is remarkably rich in guanines, we aimed at investigating both the presence of G-quadruplex forming sequences at the viral genome level and the possibility to target them with G-quadruplex ligands to obtain anti-HSV-1 effects with novel mechanisms of action.

Here we show that HSV-1 displays six clusters of repeated sequences that form very stable G-quadruplexes. These sequences are located in the inverted repeats and in two gene-coding regions (ICP0 and UL36) of the HSV-1 genome. One G-quadruplex repeat is located in the promoter region of the multifunctional protein $\gamma_1$34.5.

Treatment of HSV-1 infected cells with the G-quadruplex ligands BRACO-19 and TMPyP4 induced significant inhibition of virus production and reduction of viral transcripts. BRACO-19 was able to inhibit Taq polymerase processing at G-quadruplex forming sequences in the HSV-1 genome, and caused a decreased intracellular viral DNA in infected cells. The last step targeted by BRACO-19 was viral DNA replication, while no effect on virus entry in the cells was observed. A different TMPyP4-mediated mechanism of action was on the contrary observed. Despite its capability to affect Taq polymerase processing, TMPyP4 did not inhibit intracellular viral DNA and it appeared to prevent HSV-1 maturation/egress by stimulating the autophagy process.

As a second part of the study, we extended this innovative antiviral approach to human herpes virus-6 (HHV-6). One of the main HHV-6 features is the presence of tandem repeats of the telomeric sequence $(TTAGGG)_n$ at the genome termini (D_R). This peculiarity is thought to be responsible for the viral integration in specific human chromosomes, occurring in the 1-2% of the world population. To date, the telomeric G-quadruplex structure had been extensively

characterized. We showed that BRACO-19 and TMPyP4 displayed a great antiviral activity against both HHV-6A and HHV-6B.

In the third part of this study, by using specific DNA G-quadruplex-interacting antibodies, for the first time we visualized viral DNA G-quadruplexes in infected cells at crucial time points for the viral replication cycle, in which viral DNA is likely in a single-stranded state.

This work, besides presenting the first evidence of extended G-quadruplex sites in key regions of the HSV-1 and HHV-6 genomes, points out G-quadruplexes as innovative potential antiviral targets in novel therapeutic interventions, based on the use of G-quadruplex ligands.

1 INTRODUCTION

1.1 G-QUADRUPLEX

The predominant structure adopted by the DNA is the double-helix, in which two complementary strands are held together by Watson–Crick base pairs (Figure 1.1.1a). However, DNA sequences can not only fold into the canonical duplex helix (B-DNA) but they can also form more than ten different types of non-B DNA structures under particular conditions, such as left-handed hairpin, Z-DNA, A-motif, triplex, tetraplex as G-quadruplex and i-motif (Zhang, et al., 2014).

G-Quadruplexes are non-canonical higher-order nucleic acid secondary structures formed from G-rich DNA and RNA sequences. Although the unusual ability of guanine-rich DNA solutions to form gelatinous aggregates was first noted in 1910 (Bang, 1910), their exact nature was not discovered until 1962. In fact, the first proof of the guanine (G) self-association called G-quadruplex was reported by Davies and co-worker in 1962 (Gellert, et al., 1962).

The existence of G-quadruplex was confirmed in several organisms such as bacteria, yeasts, in human telomere and genome as well as viruses. Most importantly, in the recent years their biological functions, presence in mammalian living cells and their stabilization by G-quadruplex ligands have been extensively demonstrated (Biffi, et al., 2013), (Henderson, et al., 2013). The formation of these particular structures can interfere with the biology that is crucial to sustain cellular homeostasis and metabolism via mechanisms that include transcription, translation, splicing, telomere maintenance and DNA recombination (Di Antonio, et al., 2012). Thus, the prospect of using G-quadruplex structures as novel targets for drug design, in the treatment of various disorders such as cancer and viral infections, is very attractive.

1.1.1 G-quadruplex general features

Guanine-rich nucleic acids can fold into non-canonical DNA secondary structures called G-quadruplexes. Guanine bases display the capability to self-associate through Hoogsteen hydrogen bonds to form planar G-quartets (also named G-tetrads), which are the building block of G-quadruplex (Figure 1.1.2a,b). Two or more G-quartets can stack on top of each

other to form the tetraplex G-quadruplex structure (Figure 1.1.1b). The sequences intervening between successive G-tracts, serving as links between G-quartets, are known as loops.

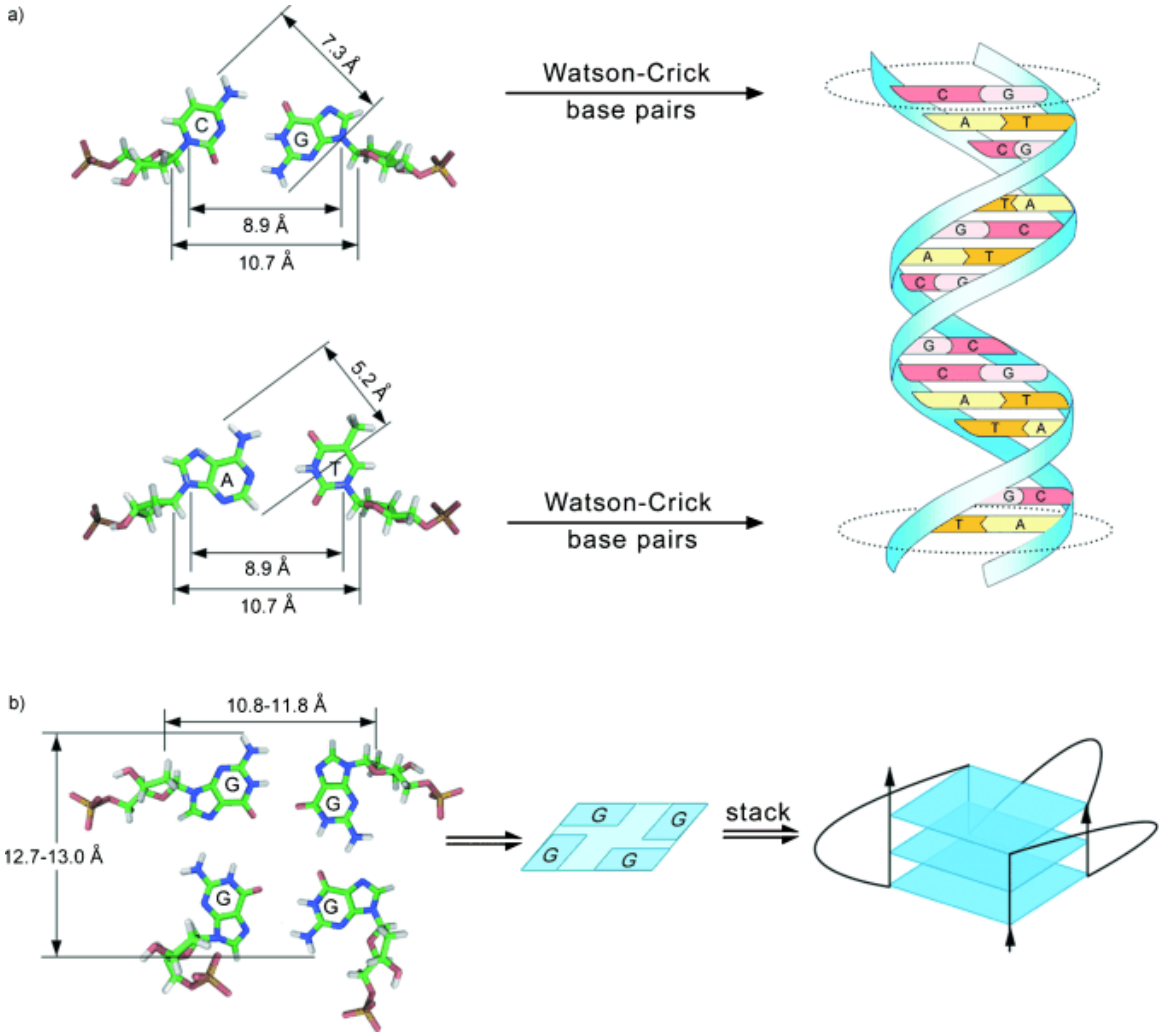

Figure 1.1.1 Representation of a) duplex DNA and b) G-quadruplex DNA structures (Ou, et al., 2008).

The formation of such guanine based supramolecular assemblies is particularly favored under physiological conditions, with respect to pH and the presence of alkali cations (Na^+ and K^+) (Di Antonio, et al., 2012). In fact, there is a strong negative electrostatic potential created by the guanine O_6 oxygen atoms, which form a central channel of the G-tetrad stack, with the cations located within this channel (Figure 1.1.2a,e).

Cations, such as Na^+ and K^+, can neutralize the electrostatic repulsions in the G-4 core. Moreover, because of their different size, the precise location of cations between the tetrads is dependent on the nature of the ion: Na^+ ions are positioned mainly in the plane of the G-tetrads, whereas K^+ ions are usually tetrad plane-equidistant, consequently forming a tetragonal bipyramidal configuration (Figure 1.1.2e) (Burge, et al., 2006).

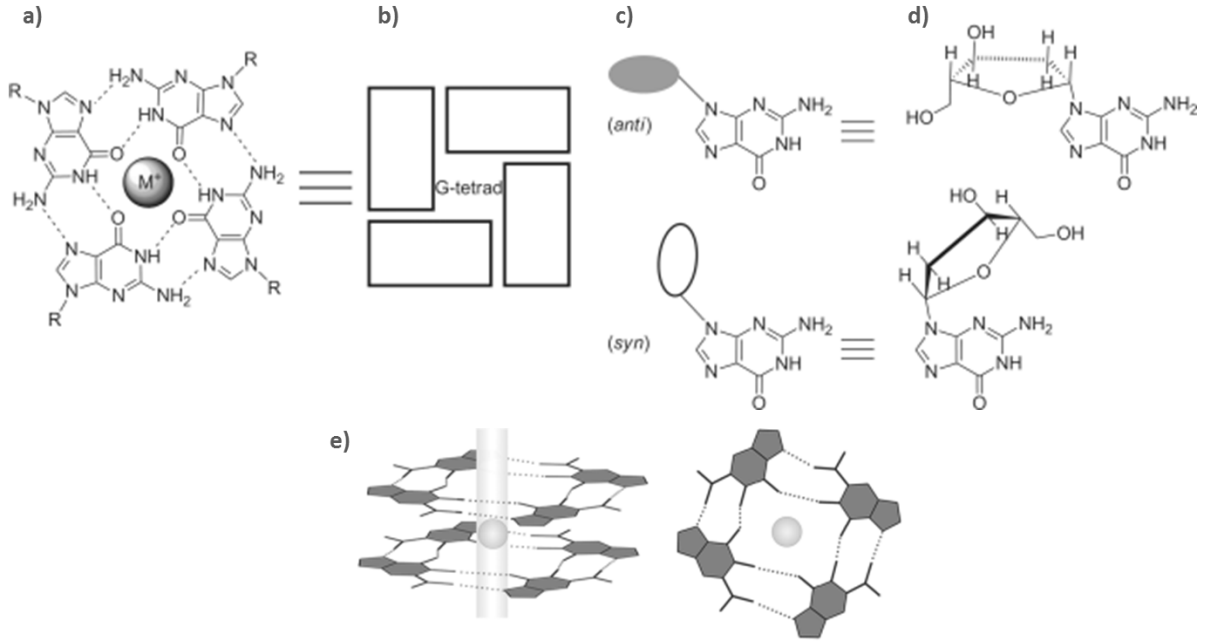

Figure 1.1.2 Representation of a G-quartet. a, b) A G-quartet structure formed by four coplanar guanines, each guanine is shown as a rectangle. c, d) Guanines in *anti* (pentoses as a grey ellipse) and *syn* (pentoses as a white ellipse) glycosidic conformations. (Zhang, et al., 2014). e) Monovalent cation location (K^+) in a G-quadruplex ion channel. (Ou, et al., 2008).

1.1.2 G-quadruplex polymorphism and topologies

G-quadruplex structures exhibit extensive structural diversity and polymorphism. In general, structural polymorphism arises mostly from the following factors: number of strands and orientation, G-tetrads number and composition, *anti*/*syn* glycosidic torsion of guanines, dimension of the four grooves and nature of the loops (Ou, et al., 2008) (Zhang, et al., 2014).

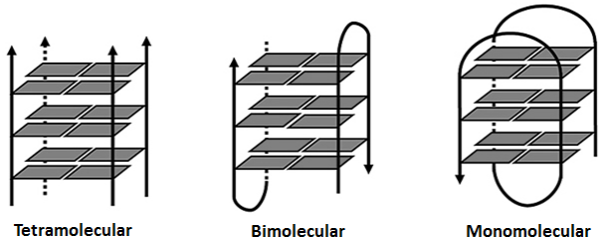

Figure 1.1.3 Different G-quadruplex topologies depending on the number of strands involved in the G-quadruplex formation: tetramolecular, bimolecular and monomolecular G-quadruplexes are represented.

First, depending of the number of strands three principal categories of quadruplex arrangement are possible (Zhang, et al., 2014) (Figure 1.1.3):

1. Monomolecular (or unimolecular or intramolecular): composed by one strand which forms four consecutive G-tracts
2. Bimolecular: formed by two strands, each normally having two G-tracts

3. Tetramolecular: given by four separate strands associating together, in which each strand shows a minimum of one G-tract.

Second, each G-quadruplex displays four parallel- or antiparallel- stranded G-tracts (or legs, Figure 1.1.4a–d). The orientation of adjacent legs may be parallel or antiparallel, this feature is related to the conformation of the guanine glycosidic torsion angles. Parallel G-quadruplexes have all guanines in an *anti* conformation, which implies that the four strands are parallel to each other (Figure 1.1.4a); antiparallel G-quadruplexes have both *syn* and *anti* guanines, consequently at least one of the four legs is antiparallel to the others (Figure 1.1.4b–d) (Zhang, et al., 2014).

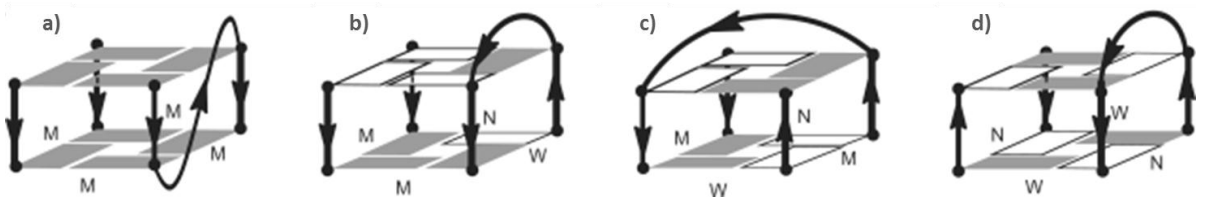

Figure 1.1.4 Scheme of four different G-quartets and three types of loops. a) Parallel G-quartet with an external loop. b) Hybrid/mixed G-quartet (3+1) and a lateral loop. c, d) Antiparallel G-quartets showing a diagonal loop (c) or a lateral loop (d). Arrows indicate 5′ to 3′ direction; N, M, and W represent narrow, medium, and wide grooves, respectively (Zhang, et al., 2014).

Each G-quadruplex contains a G-tetrad core that consists of at least two stacked G-tetrads. Based on the strand orientation, G-quartets show four possible conformations (Zhang, et al., 2014):

- Four strands in the same direction, and all guanines in an *anti* conformation (parallel G-quartet, Figure 1.1.4a)
- Three strands in the same direction and the fourth leg in an opposite direction, thus G-tetrads adopt *anti-anti-anti-syn* and *syn-syn-syn-anti* alignments (3+1 G-quartet, alternatively known as hybrid/mixed G-tetrad core) (Figure 1.1.4b)
- Two adjacent strands in the same direction and the remaining two legs in the opposite direction; all G-tetrads adopt a *syn-syn-anti-anti* conformation (Figure 1.1.4c)
- Two diagonally opposite strands in the same direction and the two other diagonally opposite legs in the opposite direction; all G-quartet adopt an *anti-syn-anti-syn* alignment (Figure 1.1.4d).

Moreover, loop regions can arrange in a number of distinct ways, so that a variety of quadruplex topologies can be formed. The loops can be classified into three major types (Zhang, et al., 2014):

- External loop (also named double-chain-reversal loop or propeller-type loop), which connects adjacent parallel strands (Figure 1.1.4a)
- Lateral loop (or edgewise loop), which connects adjacent antiparallel strands (Figure 1.4b,d)
- Diagonal loop, which connects diagonally opposite antiparallel strands (Figure 1.1.4c)

An additional structural feature differentiating between G-quadruplex and double helix DNA is represented by the four grooves (Figure 1.1.5a,b). In a G-quartet, there are at most three dimensions of grooves formed from two adjacent guanines (Zhang, et al., 2014):

- Medium grove: formed by two *anti* or two *syn* guanines (Figure 1.1.5a)
- Narrow groove: given by an *anti* and a *syn* guanine which is perpendicular to the anti guanine (Figure 1.1.5a,b)
- Wide groove: formed by an *anti* guanine perpendicular to a *syn* guanine (Figure 1.1.5a,b).

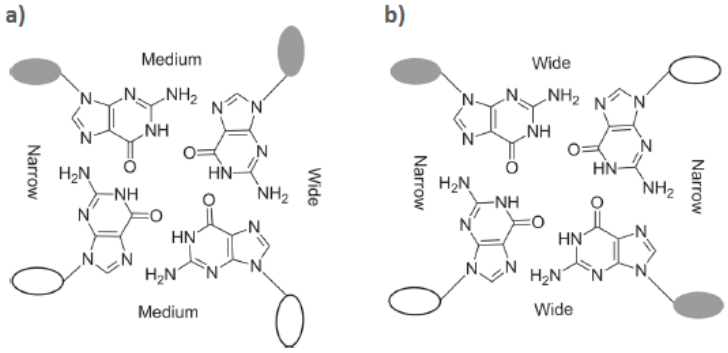

Figure 1.1.5 Scheme of different groove types within G-quartets. a) G-quartet formed from two pairs of adjacent parallel strands, having a narrow, a wide and two medium grooves. b) G-tetrad core composed by two pairs of diagonally opposite antiparallel strands, showing two narrow and two wide grooves. (Zhang, et al., 2014).

1.1.3 G-quadruplex as a drug target

In recent years, mounting evidence has indicated that G-quadruplexes formed in telomeric ends and oncogenic promoter regions play an important role in DNA replication, transcriptional regulation, and genome stability. These studies suggest that G-quadruplexes have a potential as drug targets. Hence, many scientists have refocused their research on seeking small molecular inducers and stabilizers of G-quadruplexes (Zhang, et al., 2014).

A structure-based design and synthesis approach has been generally adopted to develop new G-quadruplex-interacting lead compounds. In fact, the particular geometry of the G-quadruplex structure is thought to allow specific recognition by small ligands through various

binding modes in a manner analogous to that of double-helical DNA intercalators (Ou, et al., 2008). One of these G-4 peculiarities is the wide aromatic planar ring exhibited by G-quartets, in addition this wide aromatic surface generally possesses sites that can be protonated, thus improving the water solubility of the G-quadruplex ligands.

To date, numerous groups of compounds were identified and their binding to G-quadruplex extensively studied (Han, et al., 2001), however the exact interaction mode remained in some cases undefined *in vitro* (Ou, et al., 2008). Several interactions occurring between G-quadruplex and G-4-ligand have been identified (Figure 1.1.6):

- intercalation between G-tetrads
- stacking on the terminal G-tetrads (known as external stacking)
- groove binding mode
- combination of two or more of the previous binding modes.

Ligands with a wide planar aromatic surface interact with the G-quadruplexes mainly through π-π stacking on the terminal G-quartets and less through intercalating into the G-tetrads. The intercalation on the outer planes of G-quartets is poorly favored because of the highly stable and rigid G-quadruplex structure, which disruption requires an extremely high energy.

Electrostatic interactions between cationic ligands and the anionic central backbone of G-quadruplex are very important to improve their binding affinity (Ou, et al., 2008). Ligands containing amino groups and (or) side chains can interact with the grooves, loops, and the negatively charged phosphate backbone of the G-quadruplexes. In fact, the amino groups become positively charged by protonation or methylation, which may result in better recognition and stronger binding to the grooves as well as to the negatively charged phosphate backbone through electrostatic interactions (Ou, et al., 2008) (Zhang, et al., 2014).

G-quadruplex ligands are differently classified depending on their chemical features:

- Anthraquinons
- Acridine analogues
- Porphyrins
- Quindoline and quinacridine analogues
- Telomestatin
- Naphthalene diimmides

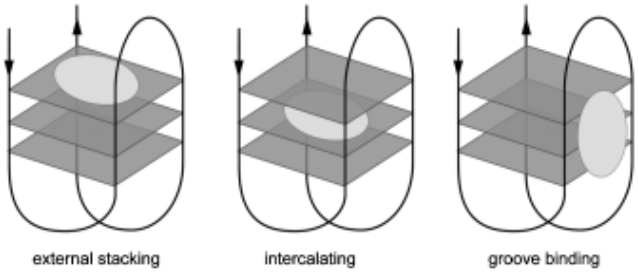

Figure 1.1.6 G-quadruplex ligand binding mode representation: on the left, an external stacking on the surface of the terminal quartet; in the middle, an intercalation between the tetrads and a groove binding mode on the right (Ou, et al., 2008).

1.1.3.1 Anthraquinones

The first developed anthraquinone was BSU-1051 (Figure 1.1.7), a 2,6-disubstituted aminoalkylamido anthraquinone with a telomerase inhibitory value ($^{tel}IC_{50}$) of 23 μM. This group of G-quadruplex ligands interacts with the G-tetrads through π- π stacking. A series of 2,7-fluorenone (2,7-FO) analogues (Figure 1.1.7)were designed to reduce the cytotoxicity and improve the inhibitory effect against telomerase. The most potent compounds showed an $^{tel}IC_{50}$ of 8-12 μM, with a 2-10 fold cytotoxicity decrease on several human-tumor-derived cell lines (Ou, et al., 2008).

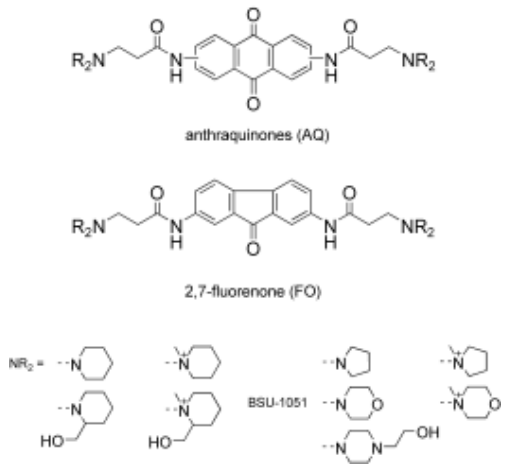

Figure 1.1.7 Chemical structures of anthraquinone analogues.

1.1.3.2 Acridines

The complementarity between negative electrostatic potential of G-quadruplexes and positively charged ring of small molecules was the impetus for the discovery of a new series of chromophore better known as acridines. 3,6-disubstituted and 3,6,9-trisubstituted acridines were developed.

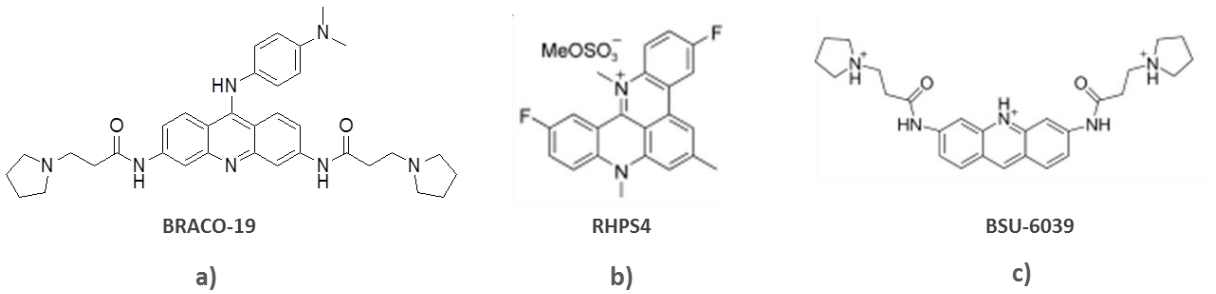

Figure 1.1.8 Chemical structures of some acridine analogues. a) the 3,6,9-trisubstituted acridine BRACO-19, b) the pentacyclic acridine RHPS4 and c) BSU-6039.

The 3,6-disubstituted analogues show approximately the same binding constant for duplex and quadruplex DNA. Furthermore, because of the weak basicity of the ring nitrogen atom for the poor electron-donating effect of the 3,6-bisamido groups, disubstituted acridines do not exhibit a higher inhibitory activity toward telomerase in comparison with the analogous 2,7-bisamidoanthraquinones (Ou, et al., 2008). On the contrary, the 3,6,9-trisubstituted acridines display a telomerase inhibitory activity in the range of 10–20 nM and they selectively bind to quadruplex DNA with 30–40-fold greater affinity over the duplex. BRACO-19 and RHPS4 are probably the most renown trisubstitued acridine, both entered in a preclinical development stage (Figure 1.1.8a,b) (Ou, et al., 2008).

Acridines mainly interact with the G-quadruplex grooves: the two substituent amido chains lies in the two widest grooves, the anilino group at the 9-position of the acridine fits into a third groove in this model, and the 9-substituent enhances the basicity of the acridine central ring nitrogen atom.

RHPS4 (Figure 1.1.8b), a pentacyclic acridine 3,11-difluoro-6,8,13-trimethyl(8H)-quino[4,3,2-kl]acridinium methylsulfate, is a potent telomerase inhibitor, it inhibits cell proliferation within 2-3 weeks at non-cytotoxic concentrations with an $^{tel}IC_{50}$ of 0.33 μM.

BRACO-19 (Figure 1.1.8a), a 9-[4-(N,N-dimethylamino)phenylamino]-3,6-bis(3-pyrrolodino-propionamido) acridine, efficiently stabilizes telomeric G-quadruplexes and acts as a strong telomerase inhibitor (Kim, et al., 1994), (Burger, et al., 2005).

The novel acridine derivative BSU-6030 (Figure 1.1.8c) interacts with the G-quadruplex in a 1:1 stoichiometry, showing a 70-100 fold greater selectivity than BRACO-19 (Figure 1.1.8a). The acridine ring stacks on one terminal G-tetrad of the G-quadruplex and interacts with the T_4 loop of the sequence $d(G_4T_4G_4)$ by forming intermolecular hydrogen bonds with the thymine residues of the loop (Zhang, et al., 2014).

1.1.3.3 Telomestatin

Telomestatin (SOT-095) (Figure 1.1.9a) is the most interesting neutral macrociclyc G-quadruplex ligand, it is one of the most efficient *in vitro* telomerase inhibitor with an $^{tel}IC_{50}$ value of 5 nM.

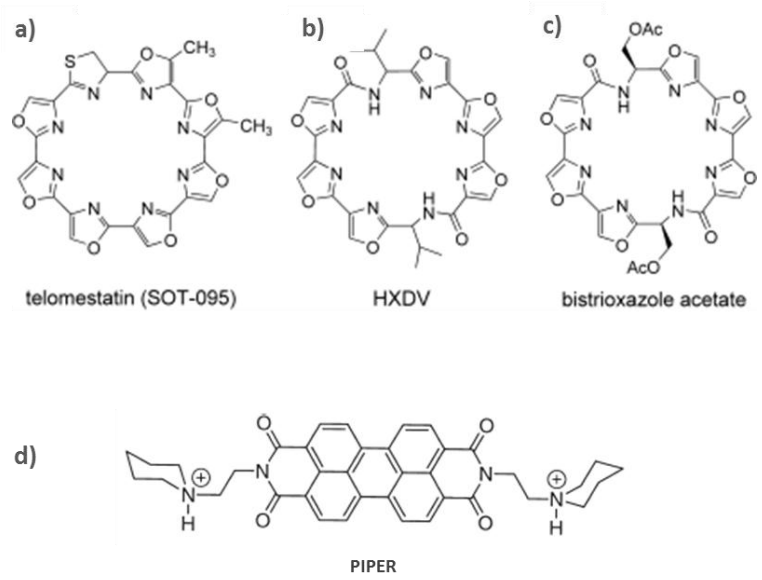

Figure 1.1.9 Chemical structures of some G-quadruplex ligands. a) Telomestatin, two telomestatin-analogues b) HXDV and c) bistrioxazole acetate. d) The perylene derivative PIPER.

Telomestatin is a natural small molecule consisting of seven oxazole rings and one thiazoline ring, normally isolated from the actinomycete *Streptomyces anulatus 3533-SV4*. It appears to interact preferentially with intramolecular G-quadruplexes rather than intermolecular quadruplexes, in addition it shows a 70-fold stronger binding affinity for G-quadruplex over duplex DNA (Ou, et al., 2008).

The main disadvantage of this G-quadruplex ligand is related to the very hard synthesis that has been recently reported (Doi, et al., 2006). Since then, some synthetic derivatives of telomestatin such as macrocyclic hexaoxazole (HXDV) (Figure 1.1.9b) and bistrioxazole acetate have been developed (Figure 1.1.9c).

1.1.3.4 Perylenes

PIPER is a polycyclic compound showing a perylene skeleton (Figure 1.1.9d). PIPER is an effective telomerase inhibitor, with an $^{tel}IC_{50}$ value which lies in the low-μM range. It binds to a variety of G-quadruplex structures with ligand/G-quadruplex stoichiometries of 1:2, 1:1, and 2:1, depending on the sequence of the G-4 DNA. PIPER appears to be able to perform

chaperone-like functions, capable of accelerating the assembly of G-quadruplex structures in a cell-free system (Ou, et al., 2008).

As mentioned above, the G-quadruplex is an extremely stable and rigid structure. The distortion of its integrity, necessary for intercalation of ligands within G-tetrads, should involve a very high energy cost (Hurley, 2000). For this reason, stacking of PIPER on the outer planes of G-quartets appears to be an energetically more plausible alternative.

1.1.3.5 Porphyrins

N-Methylated ligands, with a central aromatic ring in which four methylated nitrogen groups are located at the four corners of the aromatic surface, have been extensively used as G-quadruplex ligands. Their lower electron density improves the water solubility and π-stacking capability. TMPyP4, a (tetra-(N-methyl-4-pyridyl) porphyrin (Figure 1.1.10a), is representative of porphyrins family, it can inhibit telomerase activity and down-regulate the expression of oncogenes such as *c-myc*.

It has been extensively demonstrated that the planar arrangement of the aromatic rings in porphyrins bind to G-quadruplexes by stacking externally on the G-quartets, rather than by intercalating between G-tetrads. Porphyrins bind to and stabilize both parallel and antiparallel G-quadruplex structures, but with only twofold greater affinity for G-quadruplex over duplex DNA.

TMPyP4 was proved to inhibit telomerase by interacting with G-quadruplexes: the ligand/G-quadruplex binding occurs by stacking either on part of the external TTA loop structure in the telomere or at 5' region of the stacked quadruplex. The stacking interactions of TMPyP4 with the quadruplex involve the hydrogen bonded base pairs that are not involved in the formation of G-tetrads, thus precluding direct ligand interactions with the G-tetrads. This is consistent with the lower selectivity of TMPyP4 for quadruplex DNAs over duplex DNA (Ou, et al., 2008).

A complex between TMPyP4 and a parallel G-quadruplex formed in the *c-myc* promoter revealed that TMPyP4 stacks on one terminal G-tetrad of the G-quadruplex (Zhang, et al., 2014).

Differently the TMPyP4 conformational isomer, TMPyP2, a (tetra-(N-methyl-2-pyridyl) porphyrin with a N-methyl groups in the sterically hindered 2-position (Figure 1.1.10b), shows very weak activity (Ou, et al., 2008). Therefore, TMPyP2 is commonly considered a porphyrin with a much lower G-quadruplex binding affinity. Comparative studies using tumor

cell lines demonstrated that TMPyP4 has a greater slowing effect on cell growth than TMPyP2. TMPyP4 also induces anaphase chromosomal bridges in sea urchins, whereas TMPyP2 does not. This result indicates that G4-interactive compounds might target the telomeres directly inside cells (Han & Hurley, 2000).

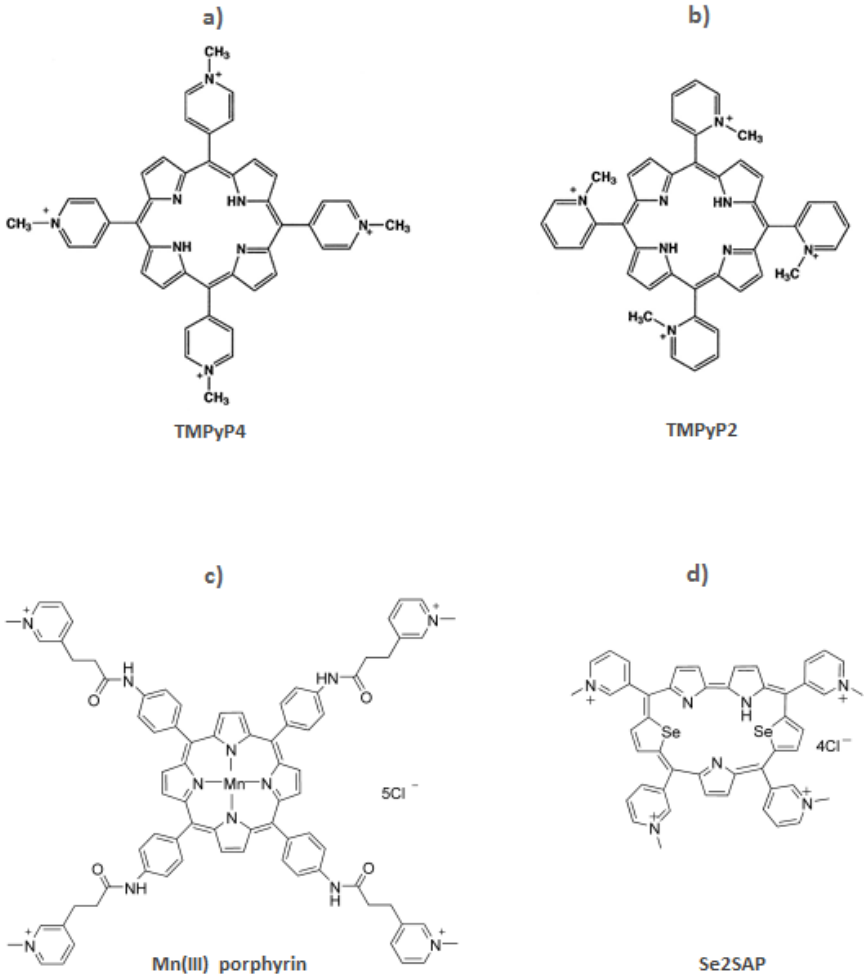

Figure 1.1.10 Porphyrin and derivatives. a) TMPyP4, b) TMPyP2, c) Mn(III) porphyrin and d) Se2SAP.

To overcome the restricted selectivity and better differentiate between G-4 over duplex DNA, a Mn(III) porphyrin composed by a central porphyrin ring and four flexible arms carrying methylated nitrogen groups was designed to target G-quadruplexes (Figure 1.1.10c). Mn(III) porphyrin exhibited both high affinity and excellent selectivity for G-quadruplexes. The complex between Mn(III) porphyrin and the human G-quadruplex telomere showed that the porphyrin ring was stacked on the terminal G-tetrads and the four flexible arms interacted with the grooves (Zhang, et al., 2014).

To achieve higher therapeutic selectivity for G-quadruplexes, it is necessary to design drugs that can discriminate different types of G-quadruplexes. To this end, a core-modified

expanded porphyrin analogue, Se2SAP (5,10,15,20-[tetra(N-methyl-3-pyridyl)]-26,28-diselenasapphyrin chloride), was synthesized (Ou, et al., 2008) (Figure 1.1.10d).

1.1.3.6 Other G-quadruplex ligands

Other small molecules can efficiently bind to G-quadruplex structures and further stabilize them. As described above, the size and shape of grooves discriminate between quadruplex and duplex DNA. These differences, resulting in a different binding site for the ligands, are used for a rational design of new selective compounds.

Non-planar alkaloids may represent a new class of G-quadruplex binders and, more importantly, that planar aromatic systems may not be essential groups for G-quadruplex ligands in some cases. This evidence is suggested by two novel G-quadruplex ligands, peimine (Figure 1.1.11a) and peiminine (Figure 1.1.11b), with non-planar aromatic structures. This new family of ligands displays high affinity for the grooves of parallel G-quadruplexes and also high selectivity for G-quadruplexes over duplex DNA. Both peimines and peiminines bind to the grooves through electrostatic interactions with a stoichiometry of 2:1.

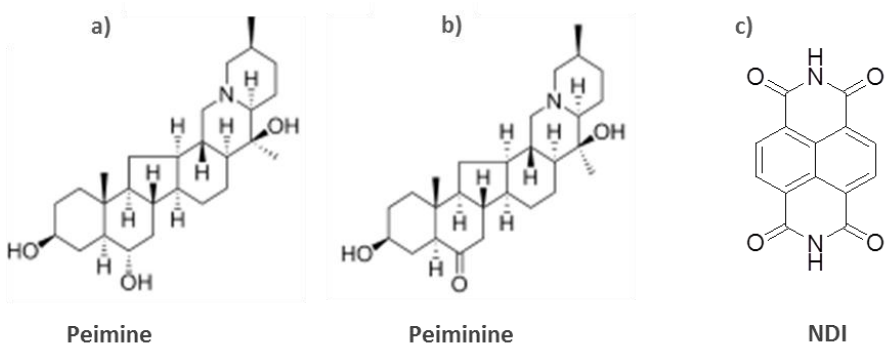

Figure 1.1.11 Chemical structures of a) peimine, b) peiminine and c) a naphthalene diimmide core.

A promising class of G-quadruplex ligands is represented by naphthalene diimmides (NDI) (Figure 1.1.11c). Among the 1,4,5,8-naphthalene tetracarboxylic diimides analogues, tri- and tetra-substituted NDIs show interesting G-quadruplex binding properties (Cuenca, et al., 2008). The chemical synthesis of NDIs permits to introduce up to four different side chains within the ND core, resulting in the design and development of new topology-selective G-quadruplex ligands. Moreover, NDIs with an extended core fused to 1,4-dihydropyrazine-2,3-dione, figured out as promising G-quadruplex ligands with an anticancer activity against different human telomerase-positive cell lines (Doria, et al., 2012).

1.1.4 The biological role of G-quadruplex

G-quadruplexes have been extensively studied *in vitro* and increasing evidences suggest a key biological role of the tetraplex structures *in vivo* (Biffi, et al., 2013), (Henderson, et al., 2013). It has been estimated that more than 300,000 distinct sites in the human genome have potential to fold in a G-quadruplex structure, suggesting an important role of these structures in regulating crucial biological processes (Huppert & Balasubramanian, 2005).

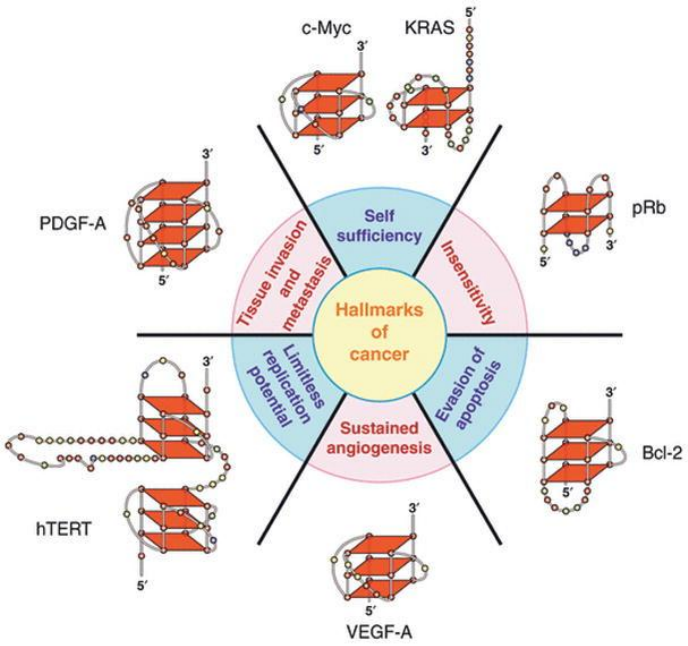

Figure 1.1.12 The six hallmarks of cancer, first proposed by Hanahan and Weinberg (Hanahan & Weinberg, 2000), here shown in association with the G-quadruplexes found in the promoter regions of these genes (Brooks, et al., 2010).

G-quadruplex DNA is a dynamic structure. Theoretically, the folding of a G-quadruplex DNA may initiate either from duplex or from single-stranded DNA, although it can mostly form in single-stranded G-rich sequences (Lopes, et al., 2011). Therefore, its formation depends on denaturation of the duplex, as occurs during replication, transcription or recombination (Maizels, 2006).

When DNA replication occurs, a replicative helicase divides the leading and lagging strands, this allows the DNA synthesis. During this process, there is a transient single-stranded DNA, which provides opportunities for a G-quadruplex formation (Figure 1.1.13a). Moreover, it has been reported that the G-quadruplex formation occurs mainly in the lagging strand template, that it is discontinuously replicated, triggering fork pausing and instability (Lopes, et al., 2011). A large number of natural proteins have been found to specifically interact with G-quadruplex structures (Wu & Brosh, 2010).

In vitro several DNA helicases, such as the mammalian BLM (Bloom syndrome protein) and WRN (Werner's syndrome protein) RecQ orthologues, PIF1, and FANCJ (Fanconi anaemia group J protein) unwind G-quadruplex structures (Maizels, 2006). PIF1 helicases was reported to specifically bind to G-quadruplex and efficiently unwind it (Figure 1.1.13b) (Sanders, 2010), (Mirkin, 2013).

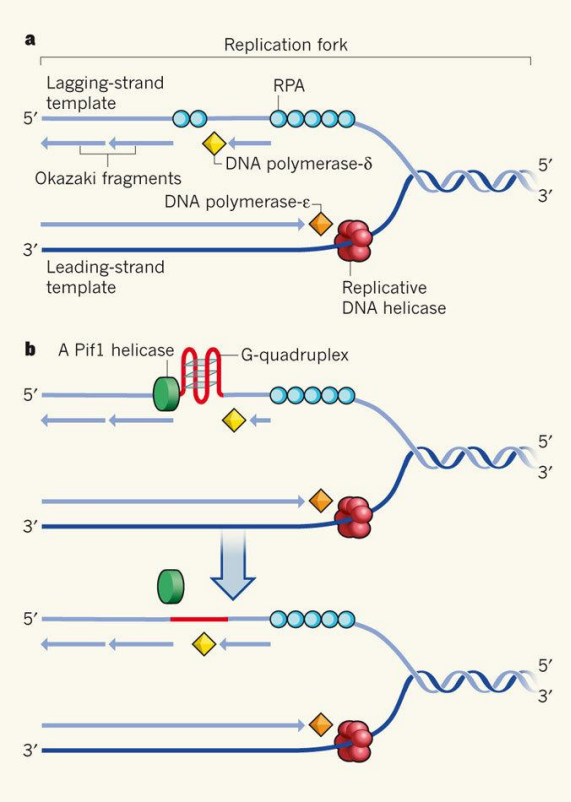

Figure 1.1.13 a) During DNA replication, replicative DNA helicases unwind the two strands into a leading- and a lagging-strand template to form a replication fork. b) PIF1 helicases was reported to efficiently unwind G-quadruplexes, allowing replication to progress past this obstacle (Mirkin, 2013).

The first biologically relevant G-quadruplex formation was observed in telomeric DNA (Yang & Okamoto, 2010). G-quadruplex potential folding sequences also occur in different regions of the human genome, such as oncogene promoters (Figure 1.1.12), ribosomal DNA, mini-satellites and the immunoglobulin heavy chain switch region (Ou, et al., 2008). Therefore, G-quadruplex is considered a very interesting innovative target in selective anticancer strategies.

1.1.4.1 Telomeres and cell proliferation potential

Telomeres, first described by Hermann Muller in 1938, are very unique structures. Muller coined the term "telomere" which comes from Greek, *telos* meaning end and *meros* meaning part (Bailey & Murnane, 2006).

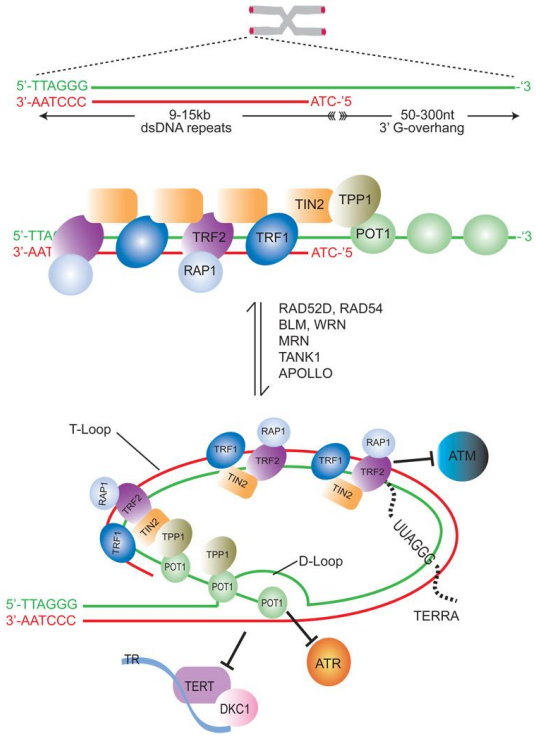

Figure 1.1.14 Human telomeres consist of $(TTAGGG)_n$ hexanucleotide repeats, with a G-rich leading strand and a C-rich lagging strand. The G-rich strand extends in the 3' direction, forming the G-tail. The shelterin complex is also shown (O'Sullivan & Karlseder, 2010).

Telomeres are non-coding DNAs located at the termini of linear eukaryotic chromosomes. They serve multiple functions in preserving chromosome stability, including protecting the ends of chromosomes from degradation and preventing chromosomal end fusion. In fact, the broken ends of chromosome can fuse end to end, leading to ring, dicentric or other unstable chromosome forms (Blackburn, 1991).

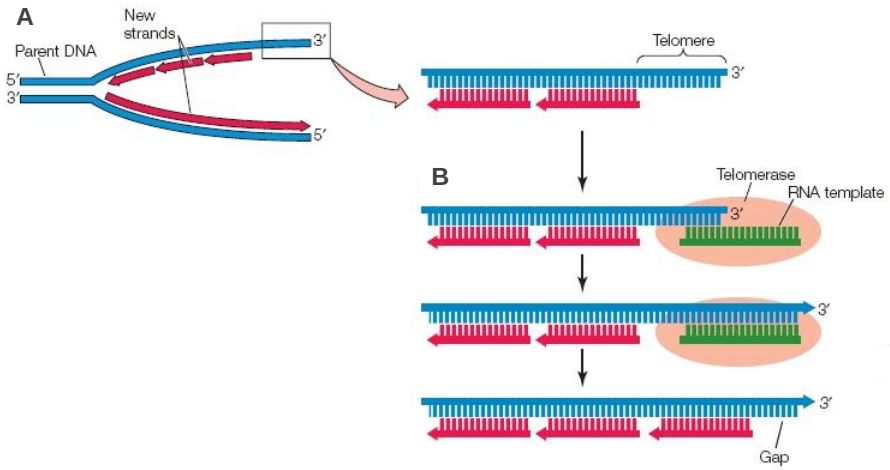

Figure 1.1.15 Mechanism of DNA replication of telomeric ends A) Semi-conservative replication of lagging strand B) Telomerase drives the synthesis of the G-rich tandem repeats at telomeric G-overhangs by using an RNA template (hTERC) (O'Connor, 2008).

Telomeres are characterized by different sequences depending on the organism. Human telomeres comprise tandem repeats of the short G-rich DNA motif (TTAGGG), oriented 5' to 3' towards the end of chromosomes, and an array of telomeric proteins better known as shelterin proteins. Telomeres consist of 9-15 kilobases (kb) long double stranded DNA and a 3' single-stranded overhang tail that ranges in length from ~50 to 300-400 nucleotides (nt) (Figure 1.1.14).

The shelterin complex consists of the double stranded telomeric repeat binding factors TRF1 and TRF2, the TRF2 interacting factor RAP1, the bridging molecules TIN2 and TPP1 and the telomeric protection factor POT1, together covering the double and single stranded repeats (Figure 1.1.14). Shelterin members interact with a large number of other factors that transiently localize to telomeres, frequently in a cell-cycle dependent manner. These factors aid in the generation of a protective structure at chromosome ends, here referred to T-loop (O'Sullivan & Karlseder, 2010). In fact, T-loop destabilization, resulting in the exposure of the 3' end, is recognized as a DNA damage signal by the cell, which starts a senescence process leading to the cell death (Li, et al., 2003). The T-loop is generated by invasion of the single stranded G-overhang into the double stranded TTAGGG repeats. The looped structure protects telomeres on several levels (Figure 1.1.14). Invasion effectively sequesters the G-tail, and allows distinction of natural chromosome ends from double stranded breaks (O'Sullivan & Karlseder, 2010).

During each cell cycle, 50–100 bp of telomeric DNA is lost because of the "end-replication problem" (Figure 1.1.15). This progressive shortening has been attributed to the inability of DNA polymerase to completely replicate the ends of chromosomal DNA during each S phase (Hanahan & Weinberg, 2000), (Phatak & Burger, 2007) (Levy, et al., 1991). When normal cells reach a critical telomere length called Hayflick limit, they exit the cell cycle, enter M2 phase (mortality stage) and undergo senescence. This mechanism is thought to be the clock that determines human life span (Phatak & Burger, 2007).

This is the reason why telomeres are thought to be essential in cellular aging and cancer, chromosome stability and genomic integrity (O'Sullivan & Karlseder, 2010). A stringent control of telomere length is important for cell cycle control, cellular immortalization, and tumorigenesis (Figure 1.1.16) (Ou, et al., 2008). Different cell types have different telomere dynamics. In normal somatic cells the average available telomere length is 10 kb, then their telomeres erode resulting in senescence. Stem cells of renewal tissues have an average telomere length of 12 kb, which shorten at reduced rates, whereas germ cells and fetal tissues have 15-20 kb. The average telomere length of cancer cells however, is only 5 kb (range 2-9

kb). During early tumorigenesis telomeres erode, but in the great majority of cases they are maintained at a stable length through the reactivation of telomerase (Phatak & Burger, 2007). Telomere shortening is thought to lead to the loss of structural integrity of the telomere nucleoprotein, thus resulting in the activation of p53 and Rb tumor suppressor pathways and cellular senescence, which is an important tumor suppressor mechanism. Telomere-induced senescence is as effective as apoptosis in decreasing cancer incidence, particularly in preventing oncogene-expressing cells from progressing to malignancy (Ou, et al., 2008).

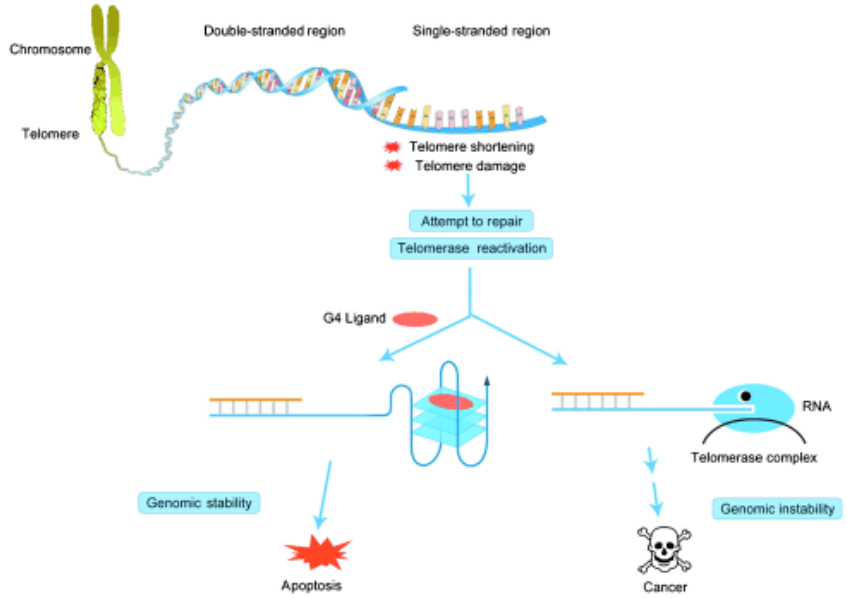

Figure 1.1.16 Structure and biological roles of telomeres. Repair mechanisms or telomerase reactivation is be triggered by telomere shortening or damage. While repair or reactivation in excess would induce or trigger tumorigenesis, G-quadruplex ligands could induce or stabilize the G-quadruplex structure in this region and thus block telomerase from binding to the terminal single-stranded end of telomeres (Ou, et al., 2008).

Telomerase, first identified by Carol Greider and Elisabeth Blackburn in 1985 (Greider & Blackburn, 1985), is a RNA-dependent DNA polymerase, almost universally conserved in eukaryotes. It allows cells to overcome one of the fundamental limitations to mammalian cell immortality, the progressive loss of telomeric DNA (Ou, et al., 2008).

Telomerase is a ribonucleoprotein reverse transcriptase, mainly composed of two distinct components: a human telomerase RNA component (hTERC or hTR), which acts as a template for addition of new telomeric repeats, and the catalytic subunit human telomerase reverse transcriptase (hTERT) (Figure 1.1.15). Cell populations that continue dividing throughout life, such as germ and stem cells, require the addition of new telomeres to their chromosomes to replace sequences lost during cell division. Differently cancer cells, which have acquired a high proliferative potential, surpass replicative senescence by activation of the telomerase (Phatak & Burger, 2007). This mechanism, termed alternative lengthening of telomeres

(ALT), can solve the end-replication problem, mentioned above. Telomerase is thought to be overexpressed in ~85-90% of cancer cells and primary tumors, but not in normal somatic cells (Balasubramanian & Neidle, 2009), (Ou, et al., 2008).

1.1.4.2 G-quadruplex at the telomeric ends

The single-stranded G-rich telomeric sequence can fold into G-quadruplex, which coexists with the T-loop structure in a dynamic equilibrium.

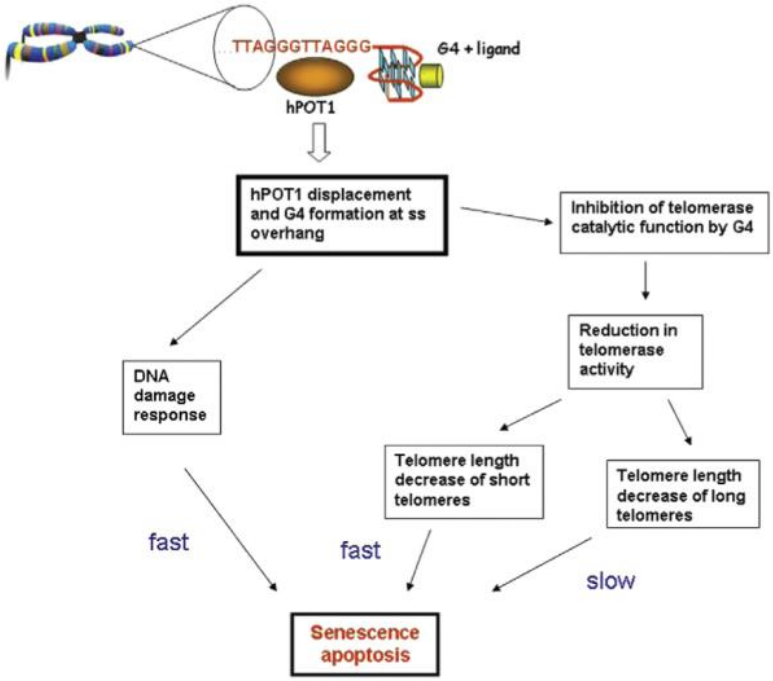

Figure 1.1.17 Anticancer effect induced by G-quadruplex ligands.

The folding and stabilization of a variety of G-quadruplexes in G-rich sequences at the end of telomeres may affect telomere length and hence the normal regulation of telomeres in the cell cycle, moreover the G-quadruplex formation can also inhibit the telomerase activity. In fact, as mentioned above, the physiological substrate for the enzyme is the single-stranded G-overhang of telomeres, which is recognized by the RNA template component of the telomerase complex (Figure 1.1.16, 1.1.17) (Ou, et al., 2008), (Balasubramanian & Neidle, 2009). This was first demonstrated using a disubstituted anthraquinone derivative (Ou, et al., 2008).

In addition, human POT1, a highly conserved telomeric protein that binds to the 3′ end of single-stranded telomeric DNA and plays an important role in telomere end-capping and protection, was shown to disrupt telomeric G-quadruplexes presumably by trapping the single-stranded form of telomeric DNA, thus allowing telomerase extension.

The effects of these structure stabilization by small ligands have been extensively studied over the past decade. The interactions of G-quadruplexes with ligands give rise to various effects on telomere functions (Ou, et al., 2008). Compounds that stabilize the DNA G-quadruplexes formed in the human telomeric sequence have been shown to inhibit the activity of telomerase, disrupt telomere capping and maintenance, induce senescence as well as cell growth and shortening of telomere length (Figure 1.1.17). Therefore, the human telomeric DNA G-quadruplex has become an attractive target for cancer therapeutic intervention and structural information of its topology under physiological conditions are fundamental for a structure-based rational drug design (Ou, et al., 2008), (Balasubramanian & Neidle, 2009).
The human telomeric G-quadruplex was extensively studied both in the presence of Na^+ and K^+, which is biologically more relevant because of its prevalence in physiological conditions.

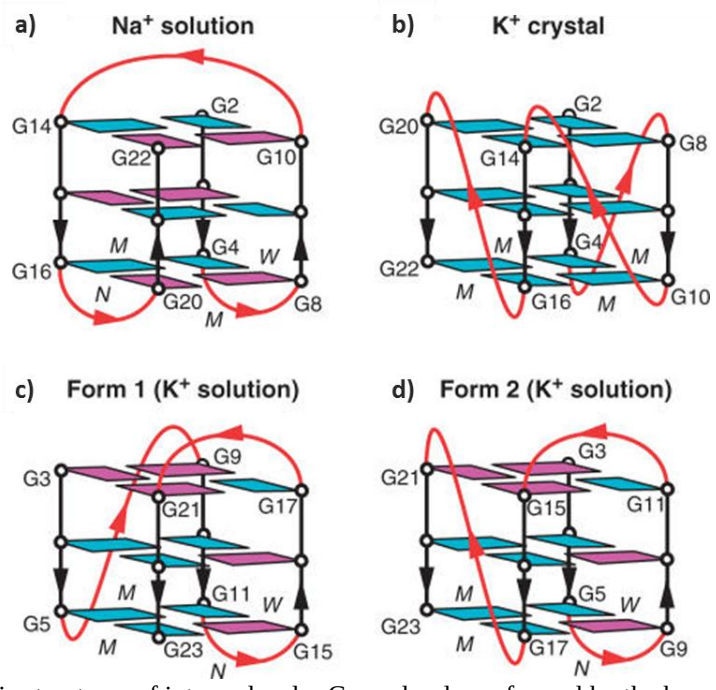

Figure 1.1.18 Schematic structures of intramolecular G-quadruplexes formed by the human telomeric sequences d[AGGG(TTAGGG)$_3$]: a) in Na^+ solution; b) in a K^+-containing crystal; c) in K^+ solution (natural-Form 1) and d) d[TAGGG(TTAGGG)$_3$TT] in K^+ solution (natural-Form 2). Loops are in red; *anti* and *syn* Gs are in cyan and magenta, respectively. W, M and N denote wide, medium, narrow groove, respectively (Phan, et al., 2007).

In 1993, the first four-repeat human telomere sequence, d[AGGG(TTAGGG)$_3$] in Na^+ solution, was characterized by a NMR-based solution structure. This sequence forms an intramolecular antiparallel G-quadruplex, which involves three stacked G-tetrads with *anti-anti-syn-syn* glycosidic orientations around each tetrad (Figure 1.1.18a). Three connecting TTA loops adopt successive edgewise, diagonal and edgewise alignments, such that each

strand has both parallel and antiparallel adjacent strands (Figure 1.1.18a) (Wang & Patel, 1993), (Phan, et al., 2007).

In 2002, a very different G-quadruplex structure of the same sequence was observed in a K^+-containing crystal by Stephen Neidle group. In this structure, all four strands are parallel, the connecting TTA loops are double-chain-reversal, and all guanines adopt anti glycosidic conformations. Subsequent studies from many laboratories indicated the presence of a mixture of multiple G-quadruplex forms for human telomere sequences in physiological K^+ solution conditions (Figure 1.1.18b) (Parkinson, et al., 2002), (Phan, et al., 2007).

In 2006, further studies showed that four-repeat human telomere sequences form at least two intramolecular G-quadruplexes of the (3+1)-type in K^+ solution (form 1 and 2 in Figure 1..1.18c,d), with one double-chain-reversal and two edgewise loops (Phan, et al., 2007).

1.1.4.3 G-quadruplex in gene promoters

Given the promising results of research on telomeric G-quadruplexes and the cellular consequences of targeting them with small molecules that stabilize these structures, interest in the more general therapeutic significance of G-quadruplexes has expanded during the past decade to include G-quadruplexes in gene promoters as targets (Balasubramanian, et al., 2011). An altered expression of these oncogenes is recognized as hallmarks of cancer, this evidence supports the therapeutic potential of targeting G-quadruplex for the treatment of human diseases, primarily cancer (Figure 1.1.19).

The most representative among these genes are *c-myc* (Siddiqui-Jain, et al., 2002), *c-kit* (Rankin, et al., 2005), KRAS, RET, *bcl-2* (Dexheimer, et al., 2006), pRb, *VEGF* (Sun, et al., 2002), *hTERT* (Palumbo, et al., 2009) and *PDGF-A* (Qin & Hurley, 2008) (Figure 1.1.12).

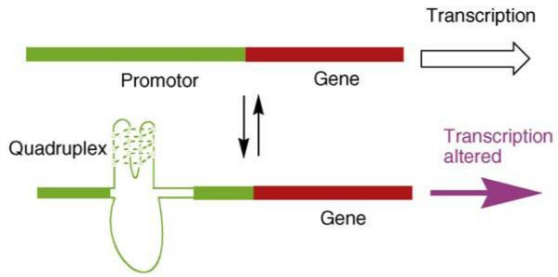

Figure 1.1.19 Schematic of the promoter-G-quadruplex hypothesis. G-quadruplex-forming sequence motifs in the upstream (promoter) region (in green) of genes (in red) may fold into G-quadruplex structures. The formation of G-quadruplex, rather than duplex, DNA structure in the promoter is associated with an altered state of transcription. This hypothesis would suggest that any molecule capable of interacting with the specific G-quadruplex could modulate the transcriptional activity of the associated gene (Balasubramanian & Neidle, 2009).

Promoters in each of these genes can form G-quadruplexes with vast diversity in their folding patterns and loop lengths, making them putatively amenable to specific drug targeting (Brooks, et al., 2010).

These G-quadruplexes include different numbers of tetrads, most commonly three, sometimes two or four. They also vary in their loop directionality, being parallel, antiparallel or mixed parallel/antiparallel. Most often the tetrads are continuously connected, but a snap-back configuration has been confirmed in at least one naturally occurring G-quadruplex formation, *c-kit* . The greatest variability among these secondary structures is found in loop lengths and constituent bases. Although the G-tetrad stacks are almost exclusively formed from guanines, there are no such limitations on bases in the loops. In these oncogenes, the loops are mainly 1–9 bases long. Shorter loops, especially in double-chain reversals, help stabilize the G-quadruplex. However, loop lengths have been seen to vary from only 1 base (the minimum required) to as many as 26 (forming their own secondary loop–stem structure in the *hTERT* promoter) (Brooks, et al., 2010).

Because of the diversity of G-quadruplex forming sequences in promoter elements, in 2010 Brooks and coworkers categorized promotorial G-quadruplexes in four distinct classes, summarized as follow (Brooks, et al., 2010):

- Class I: represented by a single G-quadruplex, in which many loop isomers are possible and loop sizes may vary. The *c-myc* G-quadruplex is the prototypical member of this class (Figure 1.1.20a)
- Class II: made of two distinctly different G-quadruplexes separated by about three turns of DNA. *C-kit* is the only example of this category (Figure 1.1.20b)
- Class III: including a pair of G-quadruplexes, but sufficiently close to form tandem G-quadruplexes, and together these tandem structures are more stable than the individual G-quadruplexes. Thus there are intermolecular interactions between the two adjacent G-quadruplexes. The two examples are *c-myb* and *hTERT* promoters (Figure 1.1.20c)
- Class IV: multiple overlapping G-quadruplexes exist in a dynamic equilibrium. The greatest example of this class is *bcl-2* (Figure 1.1.20d)

All these genes and their promotorial regions have a role in tumorigenesis. For example, the human *bcl-2* gene is a proto-oncogene with a GC-rich region upstream of the P1 promoter, which is critical for the regulation of *bcl-2* gene expression. *bcl-2* oncogenic property arises from decreasing the rate of cell death (Ou, et al., 2008).

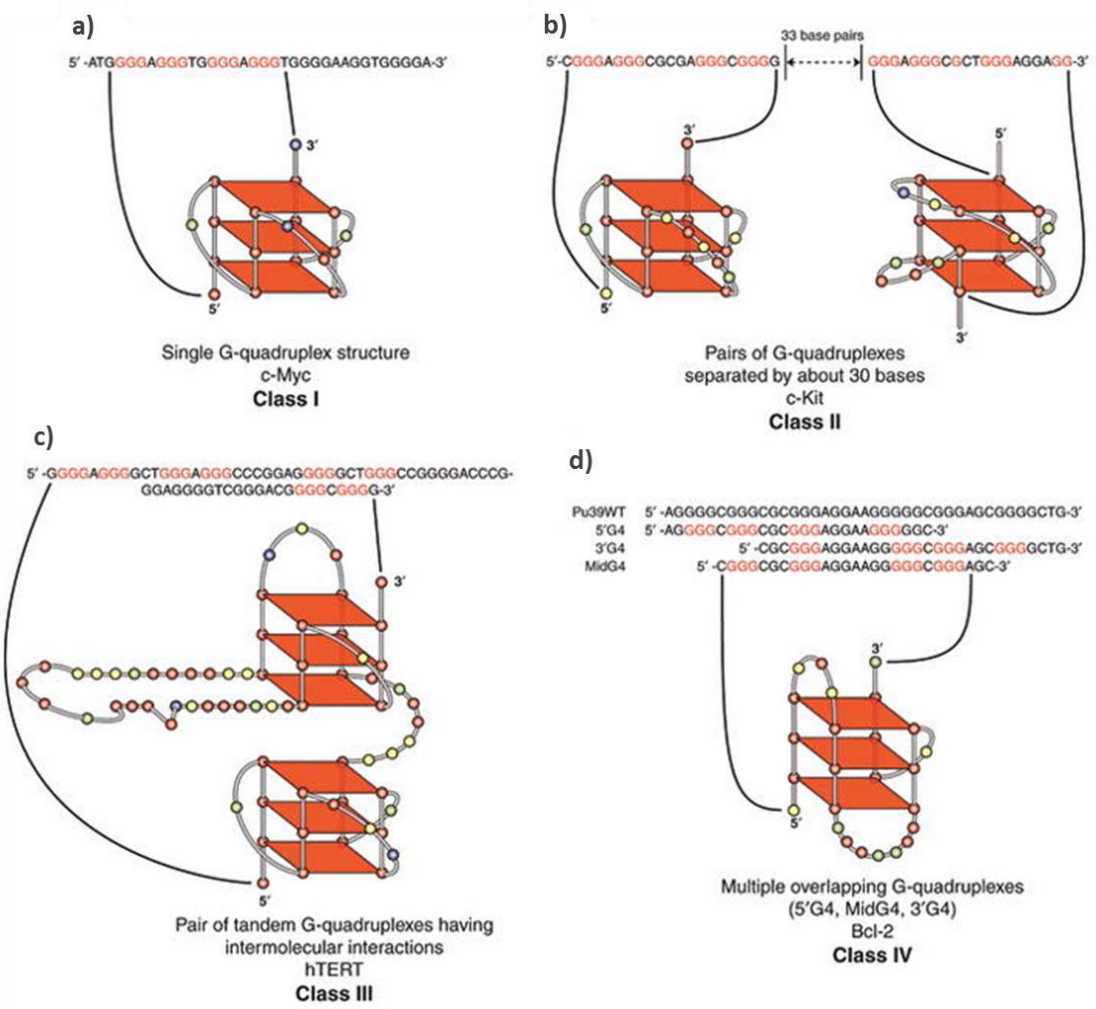

Figure 1.1.20 Four classes of G-quadruplexes found in eukaryotic promoter regions (Brooks, et al., 2010)**.**

The aberrant overexpression of *c-myc* is associated with a variety of malignant tumors including those of breast, colon, cervix, small-cell lung, osteosarcomas, glioblastomas, and myeloid leukemia. In particular, *c-myc* has been identified as one of the main activating factors for the human telomerase reverse transcriptase (*hTERT*) catalytic domain of the telomerase enzyme.

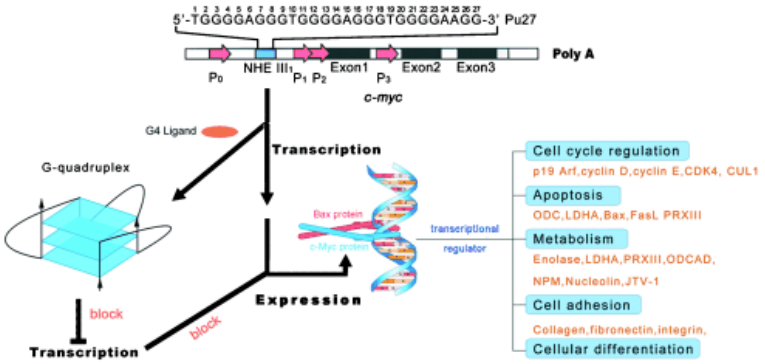

Figure 1.1.21 Structure and biological roles of *c-myc* (Ou, et al., 2008).

The nuclear hypersensitivity element III_1 (NHE III_1) upstream of the P1 promoter of *c-myc* is a G-rich strand containing a 27-base-pair sequence (Pu27). This sequence contains more than four consecutive G-strands, resulting in the formation of a dynamic mixture of four parallel G-quadruplex loop (Figure 1.1.21). The NHE III_1 region of *c-myc* controls 85–90% of transcriptional activation. The specific G-quadruplex structure formed in this region functions as a transcriptional repressor element. Stabilization of G-quadruplexes in this region by small molecular ligands can suppress *c-myc* transcriptional activation, down-regulate *c-myc* expression, inhibit cell proliferation, and induce delayed apoptosis of leukemia cells (Figure 1.1.21) (Ou, et al., 2008).

As a third example, two G-rich sequences (*c-kit* native and *c-kit 21*) within the promoter region of the human *c-kit* gene have been identified, and biophysical studies showed that these sequences can form G-quadruplexes. In the *c-kit* native sequence, 87-base-pairs upstream of the transcription start site of *c-kit* , a single intramolecular G-quadruplex structure forms in K^+ solution, as mentioned above. The proto-oncogene *c-kit* encodes a membrane bound glycoprotein of the family of growth factor receptors with tyrosine kinase activity, and it constitutes a cell signaling system that can stimulate cell proliferation, differentiation, migration, and survival. *c-kit* is closely related to the cell division regulation, thus its activity plays a very crucial role in human neoplasm (Ou, et al., 2008). *c-kit* expression is linked to several human solid tumors such as ovarian and breast carcinomas, lung cancer, gastrointestinal stromal tumors, mast and germ cell tumors, neuroblastoma and malignant melanomas.

1.1.4.4 G-quadruplex in viruses

Beside human genome, evidences of putative G-quadruplex forming sequences have been found in key regions of several organisms, such as other vertebrates (Verma, et al., 2008), bacteria as *E. coli* and yeasts such as *Saccharomyces cerevisiae* (Hershman, et al., 2008). Similarly to the human genome, in a number of organisms a computational analysis showed an analogous G-quadruplex motif distribution within the genome, and most importantly in promoter regions (Huppert & Balasubramanian, 2005).

Differently, to date little information about G-quadruplexes in viruses is available, therefore this area of research appears to be very promising. In 1992, for the first time Sundquist and Heaphy demonstrated a role of G-quadruplex during the dimerization of HIV-1 genome (Sundquist & Heaphy, 1993). Extensive recent studies, carried out by Prof. Richter's research group, strongly suggested the presence of putative G-quadruplex sequences within the HIV

genome (Perrone, et al., 2013a), (Perrone, et al., 2013b), and an antiviral activity induced by the G-quadruplex-interacting compound BRACO-19 against the virus was proved (Perrone, et al., 2014).

The Epstein Barr virus (EBV) encodes for the EBV nuclear antigen 1 (EBNA1), which is a virus-encoded protein that is critical for the replication and maintenance of the genome during latency in proliferating cells. In 2009, BRACO-19 was demonstrated to inhibit EBNA1-dependent stimulation of viral DNA replication and preferentially blocked proliferation of EBV-positive cells relative to EBV-negative cell lines. BRACO-19 treatment also disrupted the ability of EBNA1 to tether to metaphase chromosomes, suggesting that maintenance function is also mediated through G-quadruplex recognition. These findings suggest that the EBNA1 replication and maintenance function uses a common G-quadruplex binding capacity of the two EBNA1 linking region LR1 and LR2, which may be targetable by small-molecule inhibitors (Norseen, et al., 2009).

Moreover, highly conserved G-rich sequences showing a strong G-quadruplex folding propensity have been discovered within the human Papillomavirus (HPV) genome. Although the stability of these G-quadruplex structures, implications for a medical treatment of the HPV infection remain undefined so far (Tluckova, et al., 2013).

Overall, the presence and the biological roles of G-quadruplex in viruses remain elusive, making necessary further investigations in this promising research area. In the present study, the interest was focused on the herpesvirus family, with special attention to herpes simplex virus-1 and human herpes virus-6 (HHV-6).

1.2 HERPESVIRUSES

Herpesviruses are common causes of infections in humans, resulting in a spectrum of illness ranging from asymptomatic to life-threatening disease (Stewart, et al., 1995). The *Herpesviridae* family consists of large DNA viruses, which have been grouped together based on common biological features and virion. This family comprises three subfamilies designated *Alphaherpesvirinae*, *Betaherpesvirinae* and *Gammaherpesvirinae*. The first subfamily, *Alphahersvirinae,* includes herpes simplex virus type 1 and 2 (HSV-1 and HSV-2, respectively) and varicella-zoster virus (VZV or HHV-3). The *Betaherpesvirinae* subfamily includes human cytomegalovirus (HCMV or HHV-5) and human herpesvirus type 6 and 7 (HHV-6 and HHV-7, respectively). Whereas Epstein-Barr virus (EBV or HHV-4) and Kaposi's sarcoma-associated herpesvirus (KSHV or HHV-8) are part of the *Gammaherpesvirinae* subfamily (Figure 1.2.1a).

All herpesviruses exhibit a common virion structure, which is composed of four distinct elements: a core comprising the large double-stranded linear DNA, an icosahedral capsid, a tegument and an external envelope (Figure 1.2.1b).

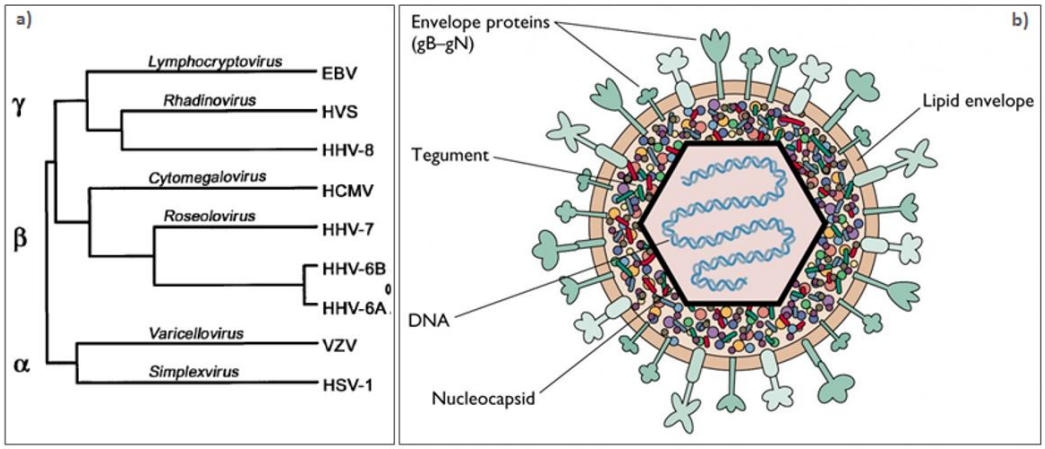

Figure 1.2.1 a) Herpesviruses, which belong to the *Herpesviridae* family, are shared into three different subfamilies: *Alphahersvirinae* (HSV-1, HSV-2, VZV), *Betaherpesvirinae* (HHV-5, HHV-6, HHV-7) and *Gammaherpesvirinae* subfamily (EBV and KSHV). b) Herpesviruses consist of core, containing the large double-stranded DNA, capsid, tegument and envelope with important glycoproteins.

The primary infection of herpesviruses starts by the interaction of viral envelope glycoproteins (g) with receptors at the plasma membrane of host cells. Entry consequentially occurs by fusion of the virion envelope with the cellular plasma membrane, a process which is still unclear at the molecular level, although several virally-encoded envelope glycoproteins have been shown to play essential roles in penetration. These glycoproteins include gB, gH,

and gL which are conserved throughout the *Herpesviridae* subfamilies. Subsequently, part of the tegument dissociates from the nucleocapsid and tegument proteins modulate the host cell to create an environment, which is beneficial for virus replication. Herpesviruses are transported along microtubuli to the nuclear pore and genomic viral DNA is released into the nucleus. Here viral genome transcription occurs in a cascade-like fashion resulting in immediate-early, early, and late viral mRNAs (Figure 1.2.6) (Mettenleiter, 2004). Therefore, viral DNA is replicated and assembled into nucleocapsids that egress by budding into the perinuclear cisterna, where they become enveloped. Thereafter, a de-envelopment during passing of the outer nuclear membrane occurs (Ahlqvist, et al., 2006). At this stage of maturation the tegument is formed around the now naked nucleocapsids (Mettenleiter, 2004). This is followed by a re-envelopment in the cytoplasm in close vicinity to the stacks of the Golgi apparatus, followed by egress of mature virions (Figure 1.2.6) (Ahlqvist, et al., 2006).
Interestingly, although the wide variety of tissue tropisms and the way of interaction with their natural hosts, all herpesviruses share a common mechanism by which they replicate their genomes during the lytic phase of the replication cycle. Moreover, in every herpesvirus the lytic DNA replication occurs by generating a long head-to-tail concatemers of viral genomes, that are cleaved to unit-length genomes during the process of encapsidation. This common replication mode reflects a conserved set of viral genes, encoding the basic components of the replication machinery.

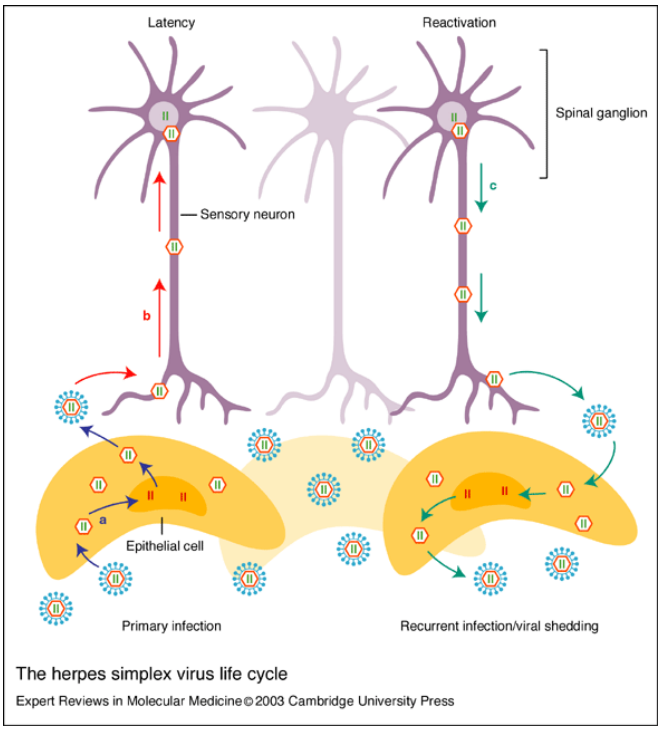

Figure 1.2.2 HSV-1 life cycle. Image from www.bio.davidson.edu.

Another common feature of herpesvirus biology is the capacity to remain latent in the infected host, but, unlike the case with lytic DNA replication, the mechanism by which the viral genomes are maintained during latency apparently differs considerably among the herpesviruses. After the primary infection all herpesviruses share the common ability to establish a lifelong infection by undergoing latency in their host. During latency, viral DNA is detectable in infected cells but no replication is observed, although the expression of some viral proteins. Upon stimuli not clearly defined, herpes viruses can reactivate and restart a lytic infectious cycle. Therefore, all of them have developed specific mechanisms to bypass the immune responses of the host to persist in it (Figure 1.2.2) (Vandevenne, et al., 2010).

1.2.1 Herpes simplex virus-1 (HSV-1)

1.2.1.1 General features and epidemiology

Herpes simplex viruses (HSV) are among the most ubiquitous of human pathogens, that evolved to use the human skin epithelium and mucous membrane epithelia as their port of entry into the human body (Stewart, et al., 1995). Human HSV infections were first documented in ancient Greece. Greek scholars, particularly Hippocrates, used the word "herpes" to describe spreading lesions. The classification now in use came into being in the late eighteenth century, although the vesicular nature of lesions associated with herpetic infections was previously well characterized, person-to-person transmission of HSV infections was recognized only in 1893 (Whitley, et al., 1998).

HSV-1 is the prototypical member of the *Herpesviridae* family and also the defining example of the *Alphaherpesvirinae*, the neurotropic subfamily of herpesviruses (Smiley, 2004). The frequency of HSV (HSV-1, HSV-2) infection is generally measured by testing various populations for the presence of antibodies. Worldwide, the global incidence of HSV-1 is ~90%, with a prevalence of 65% in the USA and 52–67% in northern Europe (Xu, et al., 2002). In the developing Countries HSV-1 is almost universal, and usually acquired from intimate contact with family in early childhood (Whitley, et al., 1998). After childhood, the HSV-1 prevalence rates increase minimally with age. Moreover, rates of HSV-1 infection are similar for men and women. The majority of infections are oral, although most are asymptomatic (Arvin, et al., 2007).

As previously mentioned, HSV-1 virion consists of four components: 1) an electron-dense core containing viral DNA, 2) an icosadeltahedral capsid, ~125 nm in diameter, 3) an amorphous, at times eccentric layer of proteins, designated tegument and 4) an envelope

(Figure 1.2.1). The capsid consists of 162 capsomeres and is surrounded by the tightly adhering tegument. The envelope surrounds the capsid-tegument structure and consists of at least 10 glycosylated and several nonglycosylated viral proteins, lipids, and polyamines (Whitley, et al., 1998). HSV-1 is a large double-stranded DNA virus characterized by a genome of approximately 152 kb, which encodes for more than 80 proteins and possesses complex transcriptional regulation mechanisms (Figure 1.2.3).

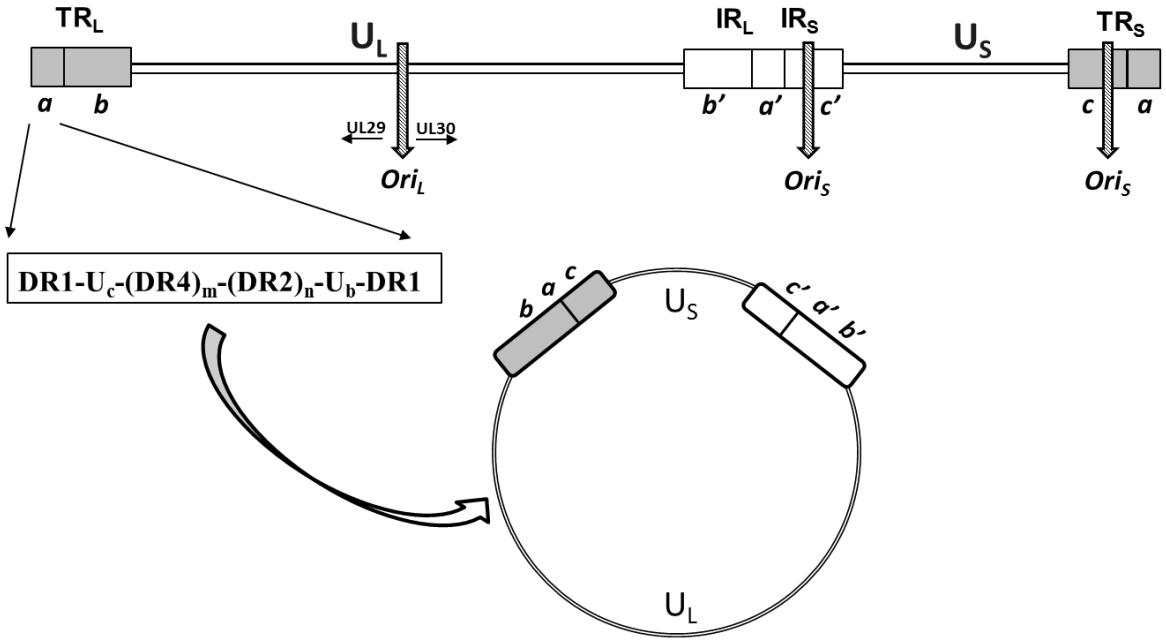

Figure 1.2.3 Scheme of the HSV-1 genome and episomal form of the virus after circularization.

The variability in size is due chiefly to the variation in the number of reiterations of specific terminal and internal sequences (Whitley, et al., 1998). A very particular HSV-1 genome feature is the high G+C content (68%) (Ouyang, et al., 2012). The genome of HSV-1 consists of two covalently linked components, designated as long (L) and a short (S) segment, each of which is composed of unique sequences (U_L and U_S, respectively), flanked by inverted repetitions (TR_L, IR_L, TR_S and IR_S) (Figure 1.2.3). The inverted repeat sequences flanking U_L are named *ab* and *b'a'*, whereas those flanking U_S are *a'c'* and *ca*. (Figure 1.2.3).

1.2.1.2 Primary infection of HSV-1 and entry

The initial step in HSV-1 entry begins with virus binding to heparan sulfate receptors on the cell surface membrane, followed by entry of the virus into host cells (Figure 1.2.4).

It was generally believed that HSV-1 entry into cells occurs by direct fusion of the virion envelope with the outer plasma membrane. Recently it has been reported, however, that at

least three different pathways are implicated in HSV-1 entry, depending on the cell types susceptible to infection: 1) via direct fusion with the plasma membrane, 2) via fusion within an acidic endosome, and 3) via fusion within a neutral endosome (Reske, et al., 2007).

The entry process is mediated by five viral surface glycoproteins, gB, gC, gD, gH, gL, and at least one cellular receptor for gD (Spear, 1993). These include a member of the TNF-receptor family named herpesvirus entry mediator (HVEM), a member of the immunoglobulin superfamily commonly known as nectin-1, and 3-O sulfated heparan sulfate (3-OS HS). gB and gC independently interact with heparan sulfate proteoglycans (HSPGs) to promote the initial attachment to the cell surface, in fact gC is not essential for viral entry and its absence decreases the overall viral binding to cell surfaces. gD is, then, required for entry of the virus into cells. Since gD does not have the characteristics of a fusion protein, it is assumed that the central fusion machinery involves gB and the heterodimer gH/gL. Therefore, the binding of gD to one of its potential entry receptors induces conformational changes in gD, that mobilizes a fusion active multi-glycoprotein complex involving gB, gD, gH and gL (Figure 1.2.4).

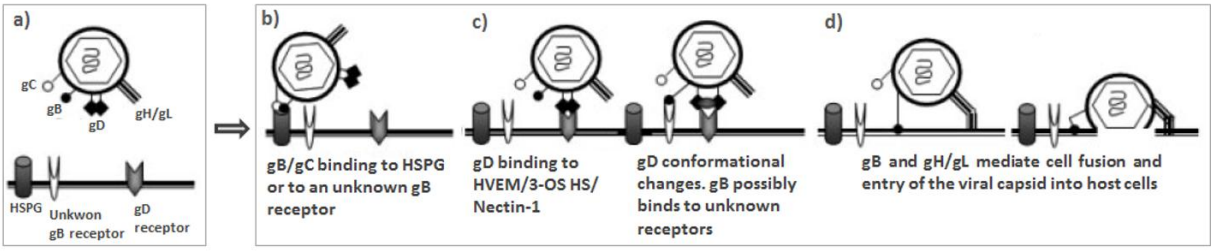

Figure 1.2.4 Scheme of HSV-1 entry into host cells. a) Host cell and HSV-1 representation. b) gB and gC bind to HSPG or an unknown gB receptor, in a HS-independent mechanism, allowing virus-cell attachment. c) gD binding to a cell surface receptor induces a gD conformational change. d) gB and gH/gL hypothetically form the fusion machinery (Reske, et al., 2007).

The fusion of the viral envelope with the cellular membrane is followed by the release of the viral nucleocapsid and tegument proteins into the host cytoplasm (Akhtar & Shukla, 2009), (Reske, et al., 2007). Thereafter, HSV-1 nucleocapsids dissociate with tegument proteins, the capsid is transported to the nuclear pores through a minus-end-directed microtubule motor protein dynein (Reske, et al., 2007), (Copeland, et al., 2009). During entry and transit to the nucleus, much of the tegument dissociates from the capsid, although at least two tegument proteins, VP1/2 and UL37, remain associated. Such partially tegumented capsids bind to the host nuclear pore complex (NPC), where the viral DNA is released, a process termed uncoating. The HSV-1 capsid remains on the cytoplasmic side of the NPC, while the DNA enters the nucleus by translocating through the pore (Copeland, et al., 2009).

The key events in viral replication that occur in the nucleus include transcription, DNA synthesis, capsid assembly, DNA packaging, and envelopment (Figure 1.2.6).

1.2.1.3 HSV-1 replication cycle

1.2.1.3.1 The DNA replication functional machinery

During the life cycle of HSV-1, the genome exists in at least three different states: linear, circular, and concatemeric, which may influence the outcome of infection. Within the virion, HSV-1 DNA normally exists in a linear double-stranded physical state, and it presumably assumes a circular form ("endless genomes") after entry into host cells. Although the kinetics of this genome circularization have not been fully established, the conversion from linear to circular form, also known as θ replication mode, has generally been assumed to be essential for replication (Poffenberger & Roizman, 1995). In 2003, however, Jackson and Deluca proved that θ replication does not occur during productive infection. The circular form of the viral genome, differently, is preferred for the establishment of latency, especially in the cells characterized by a low ICP0 expression (Jackson & DeLuca, 2003).

HSV-1 lytic infection involves the temporally regulated expression of three classes of viral genes: immediate early genes (α or IE), early genes (β or E) and late genes (γ or L). IE-genes are the first to be transcribed between 2 and 4 hours post infection (h.p.i.), followed by the early-genes which are transcribed between 5 and 7 hours after infection. Subsequently the expression of late-genes occurs between 12 and 17 hours post infection.

IE-promoters contain an enhancer element that responds to cellular factors but whose activity is greatly increased by a component of the virus particle known as virion protein (VP) VP16 (Everett, 1984). VP16 activates transcription by binding, along with the cellular factors Oct1 and host cell factor (HCF), to the TAATGARAT elements present in all IE promoters (Samaniego, et al., 1998). The expression of IE proteins, the infected-cell polypeptide ICP0 (α0 gene), ICP4 (α4 gene), ICP22 (α22 gene), ICP27 (α27 gene) and ICP47 (α47 gene), does not require prior viral protein synthesis. However, functional IE proteins are required for the optimal expression of both E and L gene products (Post, et al., 1981), (Everett, 1984), (Sampath & DeLuca, 2008). ICP4 is the principal regulatory protein of the virus, it plays a role as a transcriptional repressor or activator and it is necessary for the transition of viral gene transcription from the IE to the E phase. Binding to an array of cellular protein and not DNA, ICP0 acts as a potent transactivator of viral and cellular promoters, providing for efficient viral gene expression and growth *in vitro* and *in vivo*. Moreover, it is required both in

lytic viral growth and the efficient reactivation of the virus from the latent state (Whitley, et al., 1998), (Samaniego, et al., 1998). ICP0 has also been shown to interact with ND10 nuclear structures and components of the transcription, translation, cell cycle, and proteolytic machinery of the cell. Therefore, it has the potential to affect many aspects of host cell metabolism (Samaniego, et al., 1998). ICP27 regulates the processing of viral and cellular mRNAs, and it modulates ICP4 and ICP0 activities. ICP27 is required for an optimal viral DNA synthesis, in fact it increases the early-gene expression levels. Furthermore it contributes to an efficient late-gene expression, as well as ICP22. ICP22 has many other functions in viral proliferation. It mediates the formation of a novel phosphorylated form of RNA polymerase II (pol II), it regulates the longevity as well as the splicing pattern of the ICP0 mRNA. ICP47 may help the virus escape immune surveillance on the basis of its ability to block the presentation of antigenic peptides to $CD8^+$ cells (Whitley, et al., 1998) (Samaniego, et al., 1998).

The HSV-1 genome contains three origins of replication: Ori_S is present in two copies within the repeated *c* region of HSV-1, and Ori_L is present in U_L (Figure 1.2.3, 1.2.5c). Ori_L and Ori_S sequences are closely related, both contain an extensive inverted repeat sequence, the central 18 bp of which are exclusively AT base pairs (Figure 1.2.5c). Morever, both of them are located in the promoter-regulatory regions of divergently transcribed genes. Ori_L, the sequence of which comprises a 144-bp perfect palindrome, is located between the gene ICP8 (UL29) encoding a single-stranded DNA-binding protein, and the gene UL30 encoding the catalytic subunit of the polymerase (Pol) (Figure 1.2.3, 1.2.5c). Ori_S is located between genes encoding immediate early proteins such as ICP4 and either ICP22 and ICP47 (Weller & Coen, 2012), (Challberg, 1996). The significance of having three origins of replication in the HSV genome is not clear. Mutant viruses lacking Ori_L or one or both copies of Ori_S have been isolated and have no obvious growth defect either in cultured cells or in animal models. Thus, Ori_L and Ori_S serve as essential *cis*-acting functions during the replication of viral DNA *in vivo* (Igarashi, et al., 1993) (Poffenberger & Roizman, 1995), (Challberg, 1996). Ori_S is mainly composed of two components: the core origin containing UL9-binding sites showing several similarity with Ori_L, and flanking sequences that increase the efficiency of replication by 50-fold or more. The flanking sequences contain a number of consensus binding sites for transcriptional activator proteins such as SP1 and NFI, and the available evidence suggests that the binding of one or more of these transcriptional regulators to sites in close juxtaposition to the core sequence may be critical for enhancing DNA replication (Challberg, 1996). The core of Ori_S can be divided in at least five functional domains, essential for an

efficient replication of HSV-1 DNA: 1, 2) two high-affinity UL9-binding sites named site I and site II, which are separated by 3) an AT-rich region, 4) a sequence homologous to site I characterized by a lower affinity for UL9, known as site III, and 5) a binding site for an as-yet-uncharacterized cellular protein(s) called OF-1 (Challberg, 1996). It has been demonstrated that mutations in one or more of these functional domains lead to a significant less-efficient DNA replication. An interesting example of this evidence is the substitution of some AT pairs in the central AT-rich region of Ori_S with GC pairs (Lockshon & Galloway, 1988), (Werstuck, et al., 1990).

HSV-1 encodes seven essential replication proteins. Six of these play "core" replication roles at the replication fork and are conserved in all known herpesviruses: the single-strand DNA-binding protein ICP8 (or UL29), the two-subunit DNA polymerase (catalytic subunit Pol and processivity subunit UL42), and a three-subunit helicase/primase complex (H/P: UL5, UL8, and UL52). The remaining HSV-encoded protein is the origin-binding protein UL9 (Figure 1.2.5). Given the higher complexity of the replication origins in β and γ herpesviruses, UL9 homologs have never been identified.

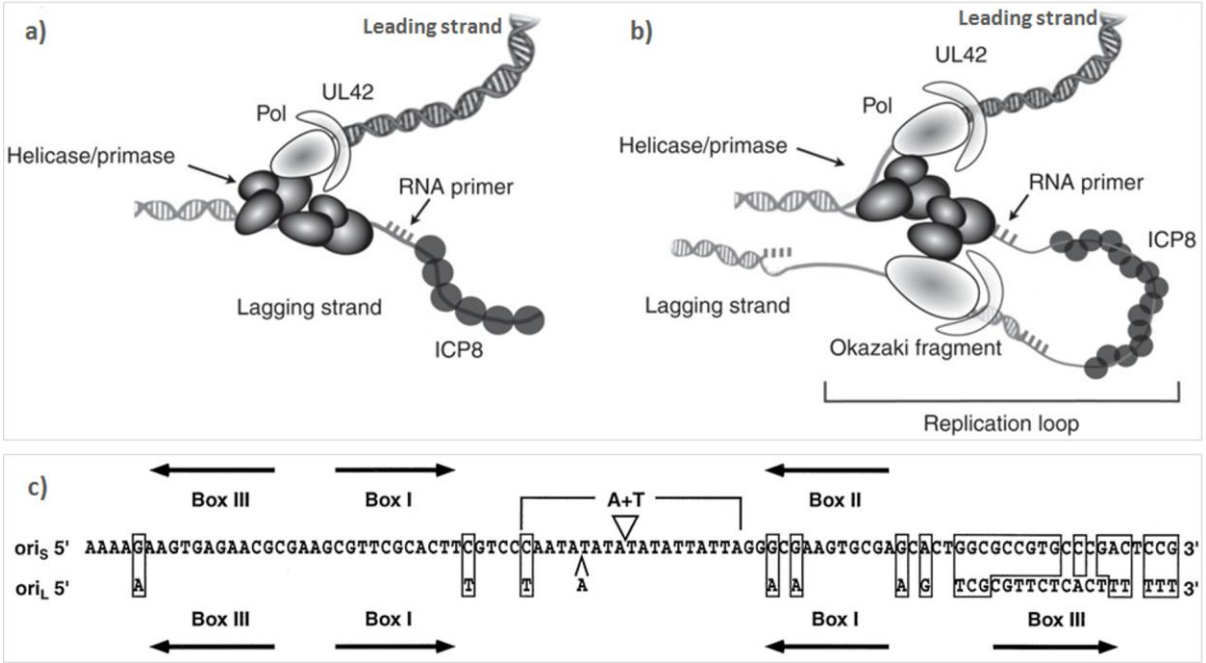

Figure 1.2.5 a) Organization of the HSV-1 replication fork: two heterotrimeric complexes of the helicase-primase (H/P) (dark gray spheres with white centers); the polymerase (white shapes with gray centers in which UL30, or Pol, is shown as an oval and UL42 as a crescent); a RNA primer depicted as hatched bars on the lagging strand of DNA; the ssDNA-binding protein ICP8 (uniformly dark gray circles). b) Coupled leading- and lagging-strand synthesis (Weller & Coen, 2012). c) Structure of the HSV-1 origins of replication, Ori_S and Ori_L (Lehman & Boehmer, 1999).

Therefore, although the similarities of the DNA replication cycle among all herpesviruses, the initiation of viral DNA synthesis may differ among the three herpesvirus subfamilies (Weller & Coen, 2012).

ICP8, an abundant HSV-induced protein of about 130 kD, is a particular helix-destabilizing proteins. It binds more tightly to single-stranded DNA than to double-stranded DNA, in a sequence-independent manner. The binding to the HSV-1 singl-stranded DNA (ssDNA), formed at the replication fork by the unwinding of the parental duplex DNA, favors the synthesis of the DNA templates by the DNA polymerase.

The polymerase is a heterodimeric complex composed of the catalytic subunit Pol (140 kD) and UL42 (52 kD), a phosphoprotein that binds tightly to double-stranded DNA. Pol contains an intrinsic 3'-5' exonuclease activity and a 5'-3' exonuclease/RNase H activity. The first one seems to increase the fidelity of DNA synthesis, while the second activity cooperates with the alkaline exonuclease UL12 in the removal of primers from the Okazaki fragments made on the lagging strand during semi-discontinuous synthesis (Figure 1.2.5) (Challberg, 1996).

1.2.1.3.2 HSV-1 DNA synthesis

Once the entry of viral genome into the nucleus occurs, HSV-1 infection determines a reorganization of the infected cell nucleus involving relocalization of cellular proteins and the ordered assembly of replication compartments, in which gene expression, DNA replication, and cleavage/packaging are thought to occur (Figure 1.2.5) (Weller & Coen, 2012).

HSV-1 DNA synthesis is believed to initiate at one of the three viral origins of replication, in which UL9 and ICP8 determine a distortion in the AT-rich origin spacer region. Hence, the helicase/primase complex unwinds the duplex DNA and synthesizes short RNA primers to start the DNA replication. The combinatory activity of the RNA primer and the H/P complex, which undergoes a conformational change, appears indispensable to recruit the two-subunit polymerase to the replication fork, thus promoting the synthesis of the viral leading and lagging strands. The recruitment of polymerase to the fork has been shown to involve direct interactions between the UL8 subunit of H/P and/or UL5 with Pol (Marsden, et al., 1996). Coupled leading- and lagging-strand DNA synthesis has now for the first time been reconstituted on synthetic minicircular DNA templates with the H/P, ICP8, and the viral polymerase (Pol/UL42) (Stengel & Kuchta, 2011).

Following the synthesis, HSV-1 DNA accumulates in the nucleus of infected cells as end-to-end long concatamers. The packaging machinery recognizes signals within the DNA to

generate unit length monomers, which are inserted into preformed capsids (Baines & Weller, 2005).

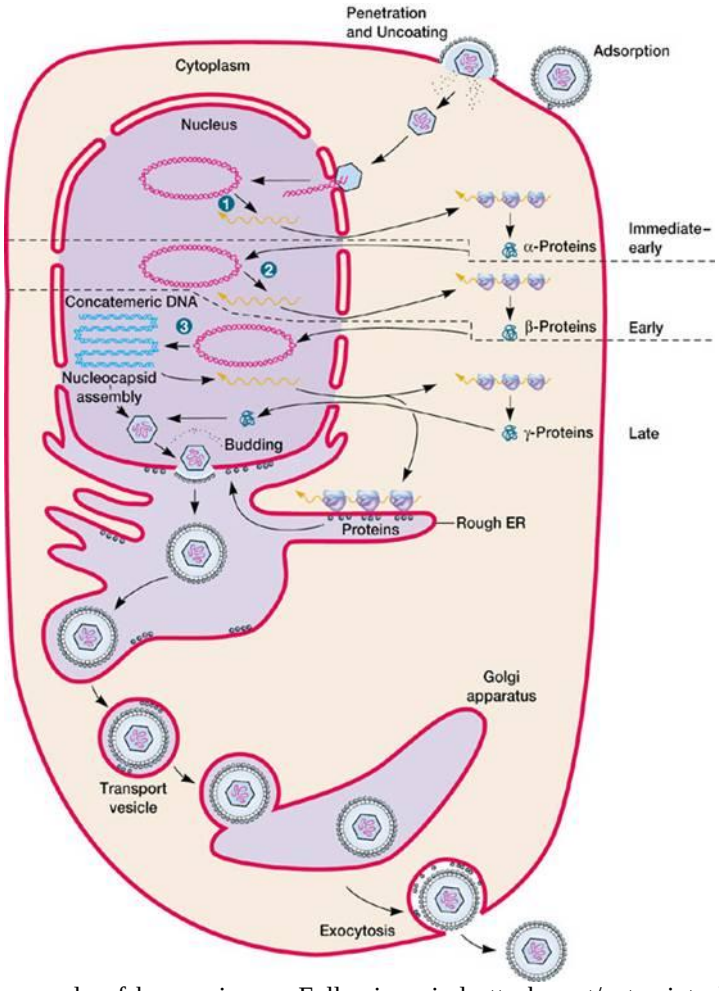

Figure 1.2.6 Replication cycle of herpesviruses. Following viral attachment/entry into host cells, 1) the viral genome circularize and the transcription of IE-genes occurs. 2) IE-proteins stimulate the transcription of E-genes. 3) E-proteins promote DNA replication and the formation of a concatemeric DNA, which is processed during cleavage/packaging, and DNA molecules are pre-encapsidated. Nuclear egress and maturation result in mature herpes virions.

1.2.1.3.3 Cleavage and packaging of HSV-1 DNA

The mechanism of cleavage and packaging of DNA is likely to be highly conserved among all herpesviruses. The terminally redundant *a* regions, containing several *cis*-acting sequences, are essential to successfully accomplish cleavage and packaging of the viral genomes. In HSV-1, these regions are 250-500 bp long, depending on the virus strain, for example in the strain F of HSV-1 the length is 391 bp long. The *a* sequence is in the same orientation at both termini of the genome, whereas it is present in inverted orientation at the L/S junction (indicated as *a'*): a single copy is detectable at the S terminus, differently one or more copies are present at the end of the L component. The *a* sequences are arranged as DR1-U_c-$(DR4)_m$-

$(DR2)_n$-U_b-DR1. Direct repeats DR1 (17-20 bp) flank each *a* sequence, with single copies of DR1 separating tandem *a* sequences. The core of the *a* segment comprises multiple repeats of one or two short sequences named DR2 and DR4 (not ubiquitously present), whereas very unique sequences are located between DR1 and either side of the DR2/DR4 repeats.

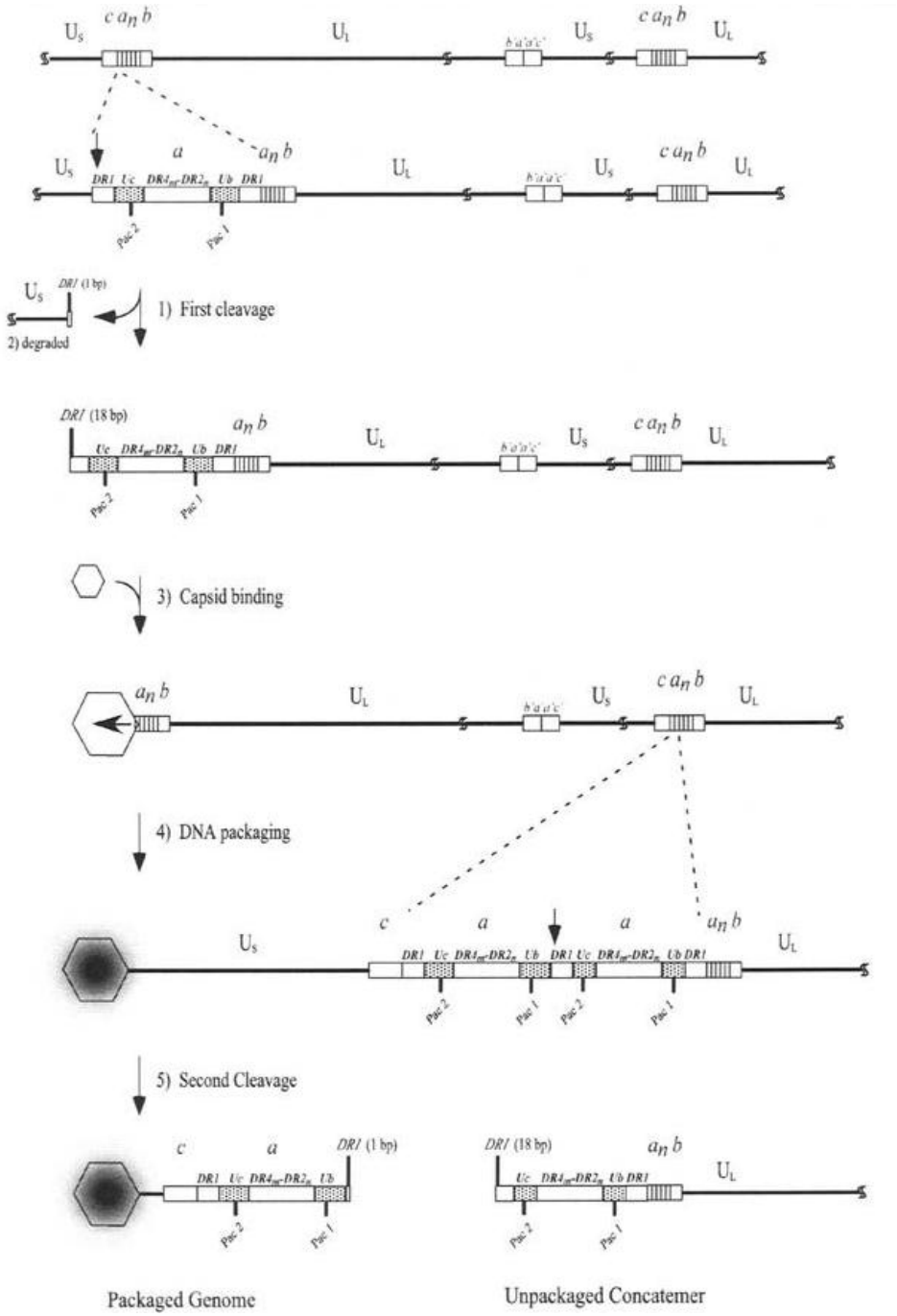

Figure 1.2.7 Scheme of the cleavage/packaging mechanism in HSV-1 (Baines & Weller, 2005).

These sequences, adjacent to the S and L components, known as U_b and U_c or *pac1* and *pac2* respectively, represent the signals to initiate DNA cleavage. The *pac1* and *pac2* domains

contain characteristic sequence motifs, also conserved among all herpesviruses. The T-rich element, within *pac1*, is one of the most conserved motif and, interestingly, it is flanked on each side by short GC-rich tracts. In *pac2*, the conserved T-rich element, frequently associated with the consensus motif CGCGGCG (from the proximal and distal GC-rich regions), is crucial to start the cleavage and packaging of DNA.

Genomic termini are generated by a cleavage event toward one end of DR1, and circularization of infecting genomes restores a complete *a* sequence. The *cis*-acting, sequences necessary for DNA packaging, are located within the approximately 200-bp fragment U*c*-DR1-U*b*, generated upon fusion of the genomic ends.

Cleaved viral genomes are not detected in cells infected with viruses that fail to assemble capsids, suggesting that capsids contain essential parts of the cleavage/packaging machinery (Baines & Weller, 2005). Four types of intracellular capsids have been identified by sucrose gradient sedimentation and electron microscopic analysis: procapsid (containing internal scaffold proteins), A capsids (empty), B capsids (containing scaffold protein) and C capsids (with DNA). The procapsid is the precursor of all capsid types, its shell is morphologically distinct from all other capsids and appears porous and roughly spherical. Differently, A, B and C capsids are more angularized icosahedrons of approximately 125 nm in diameter. The shells of all capsid types contain similar structural components such as VP5 (major capsid protein), VP19C, VP23, VP24 and VP26, differently VP21 and VP22 (UL26) are present in procapsid and B-type capsid only (Baines & Weller, 2005).

At least seven genes, UL6, UL15, UL17, UL25, UL28, UL32 and UL33, encode proteins that are required for the DNA cleavage/packaging process. Six of them, UL6, UL15, UL17, UL28, UL32, UL33, are required for the DNA cleavage, while UL25 performs a later function. Packaging, consisting in two distinct DNA cleavages, proceeds from *pac2* toward the *pac1* terminus. The putative terminase, composed of UL15 and UL28 proteins, binds viral DNA through a UL28-protein subunit, and dock with procapsids primarily through an interaction mediated by the UL6 protein (Baines & Weller, 2005). Interestingly, the UL28 component of the HSV-1 terminase enzyme is reported to binds to a specific conformation adopted by the region comprising the T element and G tracts, and this interaction is likely to be crucial for cleavage (Tong & Stow, 2010). The DNA concatemer is scanned by the capsid-associated terminase for the first *pac2* in proper orientation. Therefore, the first cleavage occurs at a fixed distance from *pac2,* which normally occurs within the upstream DRl, leaving a 18 bp truncated element and a single-base 3’ overhang (U_s end) (Figure 1.2.7). The first one, formed L-terminus with 18 bp of DRl followed by the rest of the *a* sequence, is inserted into the

capsid, on the contrary the cleaved U_s end is presumably degraded (Baines & Weller, 2005). Deletion, but not substitution, of the *pac2* GC element and unconserved region impaired DNA packaging, suggesting that the relative spacing of the cleavage site, T element and distal motifs, is crucial (Tong & Stow, 2010). The second cleavage is dependent on *pac1* domain, it occurs between the *pac1* T-element and the flanking G tracts. As a result, the terminus of the unpackaged concatemeric DNA is identical to the end to be packaging after the first DNA cleavage, and should therefore be able to initiate a subsequent round of packaging (Figure 1.2.7) (Baines & Weller, 2005).

1.2.1.3.4 Primary and secondary envelopment

Once completely assembled, nucleocapsids must be translocated through the nuclear membrane in the cytoplasm of the host cell, in which herpes virions mature. Both nuclear egress and the final maturation, also named primary and secondary envelopment respectively, involve different subcellular compartments and viral proteins. The first budding step in herpesvirus maturation occurs at the inner nuclear membrane, which provides the nucleocapsid with a first primary envelope (Mettenleiter, 2004).

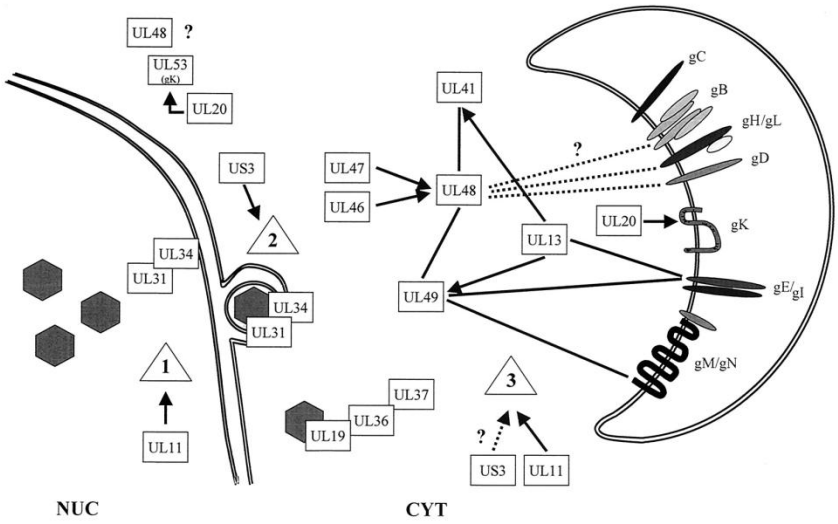

Figure 1.2.8 Scheme of the primary and secondary envelopment of HSV-1. Nuclear egress may involve the proteins UL34, UL31 and US3. The secondary envelopment is thought to require the cooperation of a number of HSV-1 late proteins, most importantly UL36 and UL37, and glycoproteins. Solid lines between gene products (rectangles) represent physical interaction, whereas arrows indicate functional effects (Mettenleiter, 2002).

Cooperating with two crucial protein, UL31 and UL34, conserved among all herpesviruses, nucleocapsids approach the inner nuclear membrane, bud into the perinuclear space and thus produce vesicular intermediates (Figure 1.2.8, 1.2.9). Upon fusion of these intermediates with

the outer nuclear membrane, capsids are released into the cytosol of infected cells and de-enveloped close to the Golgi area. Also the secondary envelopment process takes place in the cytoplasm of the cells and it produces intravesicular enveloped virus particles (Figure 1.2.9). Therefore, egress of virus progeny occurs by exocytosis of virus-containing vesicles (Figure 1.2.9) (Granzow, et al., 2001).

The molecular mechanism of this fusion process is unknown, moreover it is also unclear whether the UL34 protein, so far the only membrane protein unequivocally identified as a component of primary virions, is capable of mediating this fusion event either alone or in combination with other viral proteins such as UL31. Only one virally encoded protein, the product of the US3 genes, conserved exclusively in alphaherpesviruses, has been identified which plays a role in this fusion process. In the betaherpesviruses, other tegument components may also be added during primary envelopment, although it is not clear if they are retained or reacquired after de-envelopment (Mettenleiter, 2004), (Mettenleiter, 2002).

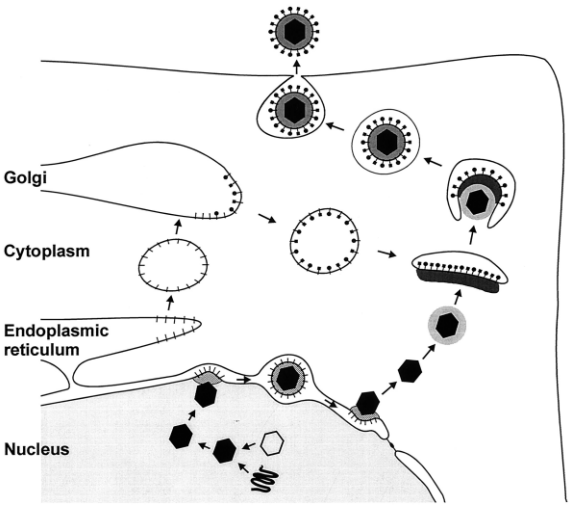

Figure 1.2.9 Scheme of the proposed pathway of herpesvirus egress (Mettenleiter, 2002).

After translocation into the cytosol, the alphaherpesvirus nucleocapsid has to collect more than 15 tegument proteins prior to acquisition of a lipid envelope, containing more than 10 viral glycoproteins. The betaherpes virion contains even more different proteins. Only a few of the components of the mature tegument and envelope are conserved, makes it difficult to propose a general pathway of virion formation for all herpesviruses. (Mettenleiter, 2004).

In fact, tegumentation requires an intricate network of protein-protein interactions (Mettenleiter, 2002). During the secondary envelopment, the UL36 gene product, the largest herpesvirus protein with more than 2000 amino acids, exhibits a crucial role in the tegumentation. In fact, the interaction between UL36 protein with the UL37 and UL19 gene

product is fundamental to the virus maturation (Figure 1.2.8). Two tegument components UL36 and UL37 are conserved among all herpesvirus subfamilies, therefore it is reasonable to assume that complex formation between UL36 and UL37 may also be a conserved property. In the absence of the UL36 protein, virion morphogenesis of HSV-1 is totally blocked and no infectious progeny arises. Lack of the UL37 protein yielded a similar effect in HSV-1 (Mettenleiter, 2004). Additional tegument-capsid interactions may occur, mediated by viral proteins (UL13, US3, UL41, UL46, UL47, UL49) and glycoproteins (gE/gI, gM/gN) but, unfortunately, these subsequent steps in tegumentation are still largely undefined (Figure 1.2.8, 1.2.9) (Mettenleiter, 2002).

1.2.1.4 HSV-1 pathogenesis and latency

The pathogenesis of human HSV-1 disease depends on intimate, personal contact between a susceptible seronegative individual and an individual who is excreting HSV-1. Virus must come in contact with mucosal surfaces or abraded skin for infection to be initiated (Whitley & Roizman, 2001). However, a great variability exists in the clinical symptomatology of primary HSV-1 infections, therefore asymptomatic infection is the rule rather than the exception (Whitley & Roizman, 2001). The most common manifestation of the HSV-1 disease comprises vesicular lesions affecting the mucous membranes principally of the mouth, nose, or eyes, and an increasing proportion of genital infections. HSV-1 is the cause of severe encephalitis and keratitis. Moreover, in 1979 HSV-1 has been also related to Alzheimer's disease (Itzhaki, et al., 1997), (Pyles, 2001).

A fascinating attribute of HSV-1 is its ability to enter a quiescent state and establish a lifelong latent infection (Kramer, et al., 2003). The latency of HSV-1 has been biologically recognized since the beginning of the century. Following entry and primary infection, HSV-1 is transported by retrograde movement to the nuclei of sensory ganglia (Figure 1.2.2). In the majority of the neurons, the viral genome remains in an episomal state for the entire life of the individual. The virus can later reactivate, generating a new virus progeny that is transported axonally back to the periphery and causes recurrent disease. Reactivation occurs following a variety of local or systemic stimuli, such as physical or emotional stress, fever, exposure to ultraviolet light, tissue damage and immunosuppression (Whitley & Roizman, 2001), and pathways such as the hormonal regulation of the thyroid hormone T3 (Bedadala, et al., 2010).

1.2.2 Human herpes virus-6 (HHV-6)

1.2.2.1 General features

In 1986, a new virus was isolated in the USA from patients affected by the acquired immunodeficiency syndrome (AIDS) as well as lymphoproliferative disorders. Initially designated human B-lymphotropic virus (HBLV), the virus was renamed human herpesvirus 6 (HHV-6), following herpesvirus nomenclature guidelines (Lusso & Gallo, 1995), (Ablashi, et al., 1987). To date, a number of strains were isolated from various geographic regions and clinical settings, included in two well-defined groups, HHV-6A and HHV-6B.

Historically, HHV-6A and HHV-6B have been treated as the same virus, mainly due to the lack of serological assays able to distinguish between the two variants (Ahlqvist, et al., 2006). However, these two variants showed different *in vitro* tropism for selected T cell lines, specific and conserved interstrain variations in their DNA sequences, specific immunological reactivity with monoclonal antibodies and distinct patterns of restriction endonuclease sites. As new evidence continued to accrue, several authors have suggested that the two variants be recognized as distinct viruses (Ablashi, et al., 2014). In fact, genomic sequencing confirmed distinctions between HHV-6A and HHV-6B and relationships to the herpesvirus family overall. Moreover, although the co-linear genome identity of 90%, HHV-6A and HHV-6B differ in some immediate-early gene functions, splicing patterns, specific amino acid signatures, biological and immunological properties, epidemiology and related diseases. Therefore, in 2012 the International Committee on Taxonomy of Viruses classified HHV-6A and HHV-6B as distinct viruses.

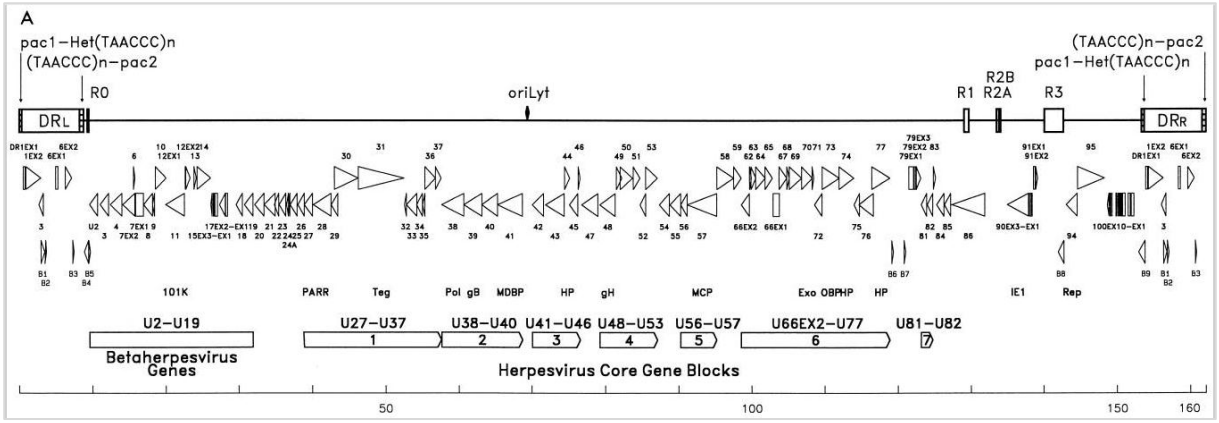

Figure 1.2.10 Genome of the human herpes virus type 6 (Braun, et al., 1997).

The HHV-6 genome is a linear double-stranded DNA molecule, 160 to 162 kb in size. It is composed of a ~145 kb long and A+T-rich unique (U) region, flanked by two identical G+C-

rich terminal direct repeats (DR) of ~9 kp, named DR_L (direct repeat left) and DR_R (direct repeat right) (Figure 1.2.10) (Morissette & Flamand, 2010), (De Bolle, et al., 2005), (Gompels & Macaulay, 1995). The terminal DR region are interrupted by three intermediate repeats, designated R1, R2, and R3, in the immediate-early A (IE-A) region (De Bolle, et al., 2005). Similarly to other herpesviruses, the G+C content across the genome is not uniform. The G+C content within the U region is estimated around 40-44%, whereas DR_L and DR_R are composed by a higher G+C composition ~59% (Gompels & Macaulay, 1995), (Martin, et al., 1991). The DRs contain the cleavage-packaging motifs, *pac-1* and *pac-2*, and reiterations of the hexanucleotide $(TTAGGG)_n$, which is a characteristic sequence of the telomeres of vertebrate chromosomes (De Bolle, et al., 2005), as abundantly described above. It has been suggested that one role of these repeats is to participate in the DNA packaging, in a manner analogous to the terminal repeats in HSV-1 (Figure 1.2.11) (Gompels & Macaulay, 1995), (Flint, et al., 2003). It is presumed that through homologous recombination between the telomeric repeat sequences (TR_S) present within the HHV-6 genome and the telomeres, the HHV-6 genome, or part of it, gets integrated within human chromosomes. In fact, all integration sites identified to date (1q44, 9q34.3, 10q26, 11p15.5, 17p13.3, 18p11.3, 18q23, 19q13.4, and 22q13.3) have been localized in the telomeric regions (Figure 1.2.11) (Morissette & Flamand, 2010). The protein U94 was shown to enable the establishment and/or maintenance of latent infection, it is expressed at low levels during lytic replication but is a major transcript during latent infection (Figure 1.2.11) (De Bolle, et al., 2005).

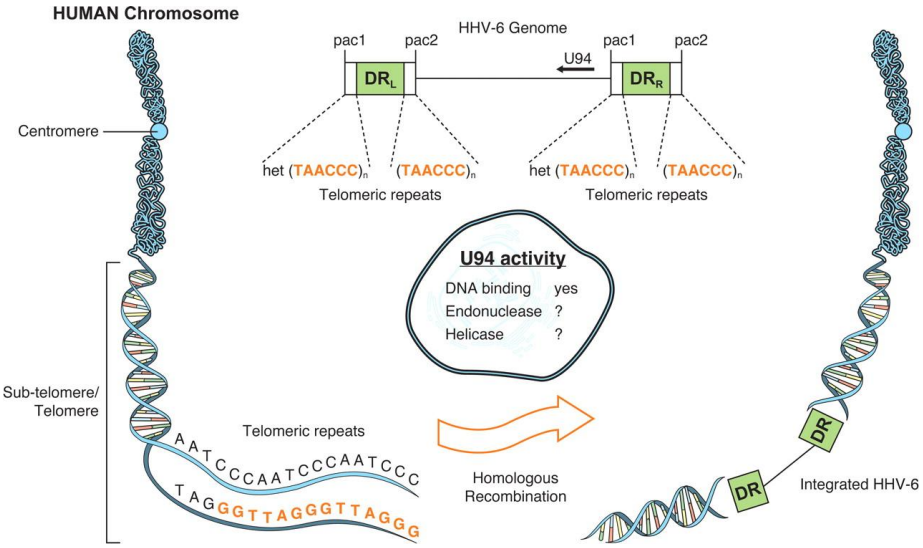

Figure 1.2.11 Genome structure of HHV-6, composed by a single unique long component (U_L) flanked by two identical direct repeats (DR_R and DR_L) (Morissette & Flamand, 2010).

1.2.2.2 The replication cycle of HHV-6

The entry of both HHV-6A and HHV-6B occurs via interaction through the human cellular receptor CD46, located on the membrane of all nucleated cells, and a number of glycoproteins, such as gH, gL, gM, gN, gQ and gB, are involved in the primary infection of HHV-6. However, the modality and affinity of the interaction between CD6 and glyproteins differ between the two viruses.

In the case of HHV-6A, the complex between the glycoproteins gH, gL and gQ (encoded by the genes U48, U82, and U100, respectively) serves as the viral ligand for CD46. The HHV-6 gB (encoded by U39 gene) is involved in viral attachment and fusion process as well, through an as-yet-undefined mechanism (Figure 1.2.12).

After the fusion of the viral envelope to the cell membrane, nucleocapsids is transported through the cytoplasm, most likely by association with the microtubule network, to nuclear pore complexes, where the viral DNA genome is released into the nucleus. The cytosolic transport mechanisms have not been investigated in detail for HHV-6, but they probably show strong similarity to those described for HSV-1 and HCMV (De Bolle, et al., 2005). Subsequently, similarly to HSV-1, the transcription of three kinetic classes of viral genes, IE-genes, E-genes and L-genes, are required for the viral DNA metabolism and replication.

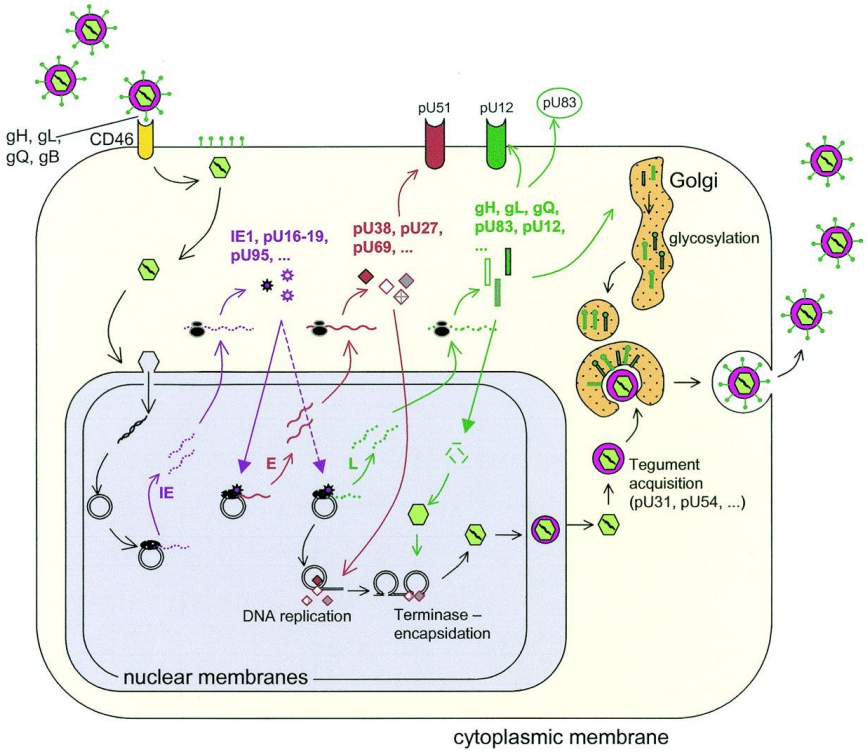

Figure 1.2.12 Scheme of HHV-6 DNA replication (De Bolle, et al., 2005).

HHV-6 DNA replication requires multiple virally encoded factors. First, the protein U73 binds to the origin of replication oriLyt, thus denaturing a portion of the circular viral DNA genome. This gap is maintained by the helicase/primase complex, consisting of the U43, U74, and U77 gene products, which also provides RNA primers for the lagging-strand DNA synthesis (Nicholas, 1994). The single-stranded DNA is stabilized by the major DNA binding protein U41, therefore HHV-6 DNA synthesis can be catalyzed by the DNA polymerase U38, driven by a processivity factor protein U27. The four proteins encoded by the U79 and U80 genes of HHV-6 are suspected of being involved in DNA replication as well, although their role is not yet understood. As the new strand grows, the circular replication structure is nicked to form a rolling circle intermediate. Long concatameric strands of progeny DNA are encapsidated by the interaction of cleavage and packaging proteins with specific packaging (*pac*) signals at the end of the viral genomes (Deng & Dewhurst, 1998). It is of interest that oriLyt and *pac* sequences are different for the A and B variants of HHV-6 (De Bolle, et al., 2005). The mature capsids bud out of the nucleus (thereby temporarily acquiring an intermediate membrane devoid of glycoproteins) into the cytoplasm, where they acquire a tegument and a secondary spiked viral envelope at the Golgi complex or at annulate lamellae, where viral glycoproteins accumulate (Cardinali, et al., 1998). These are sequentially glycosylated in transport vesicles prior to release of the mature virus particle into the extracellular space by exocytosis. The HHV-6 maturation pathway is different from that of the other herpesviruses in that no viral glycoproteins are detectable in the cell membrane of infected cells (De Bolle, et al., 2005).

1.2.2.3 HHV-6 primary infection, epidemiology and latency

HHV-6 is ubiquitous in general populations and it is normally acquired at a very early age (Braun, et al., 1997). Given that HHV-6 is most frequently detected in saliva and salivary glands, the transmission via saliva is considered the main route of infection, either from mother to child or between children. Remarkably, HHV-6B is usually isolated from saliva, whereas the detection of HHV-6 DNA in cord blood specimens of healthy newborns in the absence of serum immunoglobulin M (IgM) and in fetuses following spontaneous abortion supports the possibility of intrauterine transmission. The incidence of vertical HHV-6 transmission is about 1 to 2% of all births (De Bolle, et al., 2005).

In the USA, UK and Japan, 97-100 % of primary infections are caused by HHV-6B and occur between the ages of 6 and 12 months. HHV-6B primary infection normally causes acute

febrile illness and exanthem subitum (ES), also known as roseola infantum or sixth disease. Less is known about the epidemiology of HHV-6A. One report has indicated that HHV-6A infection is acquired later in life and that primary infection is typically without clinical symptoms (Ablashi, et al., 2014). HHV-6 has been associated also to several other diseases: epilepsy (Donati, et al., 2003), HIV/AIDS progression (Lusso & Gallo, 1995), chronic fatigue syndrome (CFS) (Watt, et al., 2012), cancer (Lacroix, et al., 2007), endocrine and autoimmune disorders (Caselli, et al., 2012), heart diseases, transplant complications, multiple sclerosis and, very recently, to Alzheimer disease (Carbone, et al., 2014).

Like other herpesviruses, HHV-6 can establish a latent or persistent infection which remains for the lifetime of the host and can reactivate during immunosuppression, under a number of stimuli. Whereas salivary glands and brain tissue are suspected of harboring persistent HHV-6 infection, candidate sites for latency are monocytes and early bone marrow progenitor cells. Low levels of HHV-6 DNA are also found in PBMCs from healthy individuals (De Bolle, et al., 2005).

1.2.3 Current antiviral treatments against HSV-1 and HHV-6

The nucleoside analogues represent the compound of choice to treat herpesvirus symptoms. However, herpesviruses remains in the body for life and can reactivate from time to time, since no cure, able to completely eradicate these viruses, has been developed so far. The most common compound for the prophylaxis and treatment of HSV-1 infection is acyclovir (ACV), a (9-[2-hydroxyethoxymethyl] guanine, that selectively inhibits viral DNA replication with a very low host-cell toxicity. Several nucleoside analogues, sharing the same mechanism of action, are currently used, such as ganciclovir (GCV), penciclovir (PCV), valacyclovir (VACV), famciclovir (FCV), foscarnet (PFA) (Figure 1.2.13).

HHV-6 infections in immunocompetent children are self-limiting and do not require treatment. In immunocompromised individuals, however, reactivation of latent virus may cause life-threatening complications. No controlled trials of antiviral therapy against HHV-6 have been conducted, and no compounds have been formally approved for the treatment of HHV-6 infections. Therefore, the drugs clinically used against HHV-6 are the nucleoside analogs GCV and valganciclovir, less frequently also ACV, VACV, cidofovir, and PFA (Figure 1.2.13) (De Bolle, et al., 2005).

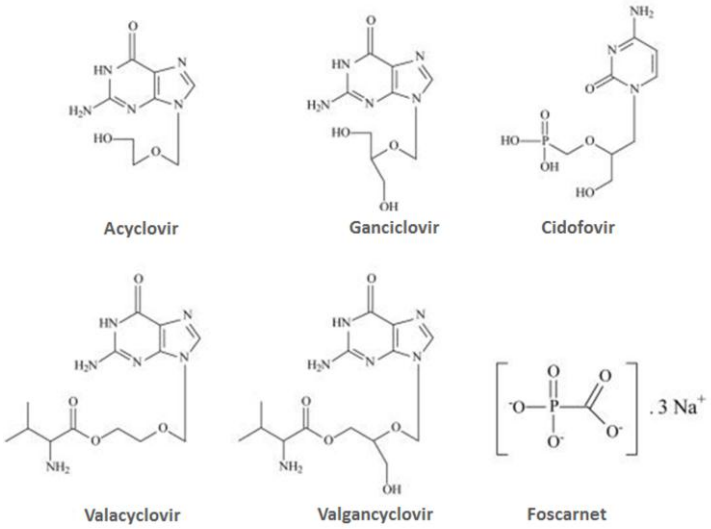

Figure 1.2.13 Chemical structures of the some nucleoside analogues.

The uptake of nucleoside analogs by infected cells is followed by phosphorylation of the drug to the monophosphate form, which occurs via HSV-encoded thymidine kinase (TK). Subsequently, the conversion to the triphosphate metabolite is catalysed by host cell enzymes. The triphosphate metabolites preferentially inhibit viral DNA polymerase, by competition with the natural substrate dGTP, over cellular DNA polymerase (Figure 1.2.14) (Snoeck, 2000). Unlike alpha- and gammaherpesviruses, betaherpesviruses do not express a TK enzyme but encode a phosphotransferase, which is capable of converting nucleoside analogs to their monophosphate (De Bolle, et al., 2005).

An emerging problem, which becomes particularly serious in immunocompromised patients, is related to increasing mutations within the gene TK. Therefore, new antiviral approaches able to suppress both lytic and possibly also latent infections are highly required.

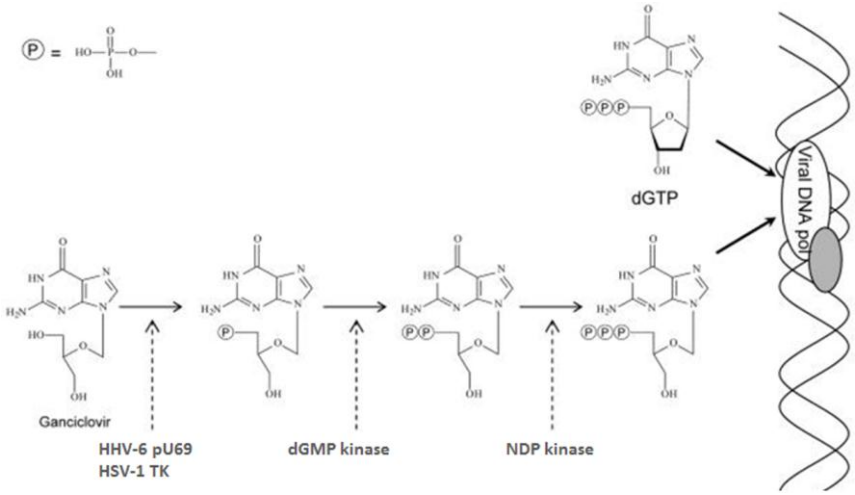

Figure 1.2.14 Diagram of the mechanism of action of nucleoside analogs as ganciclovir or acyclovir.

2 AIM OF THE STUDY

G-quadruplex structures are widespread within key regions of the human genome, such as telomeres and oncogene promoters. The additional stabilization of G-quadruplex structures by interacting with rationally-designed small molecules was proved to interfere with crucial biological mechanisms as replication and transcription. Therefore, this non-canonical secondary conformation of DNA has become an interesting therapeutic target in oncology.

Increasing evidences of putative G-quadruplex sequences in viruses, such as HIV, EBV and HPV, make G-quadruplex emerge also as a novel and very attractive antiviral target.

In the present study, efforts were focused on the family of herpesviruses with a particular attention to herpes simplex virus-1 (HSV-1) and human herpes virus-6 (HHV-6).

The main purposes of this study were:

1. Identification of putative and conserved G-quadruplex folding region in the genome of HSV-1 and HHV-6, and their ability to effectively fold in G-quadruplex in the absence or presence of G-quadruplex inducing/stabilizing small molecules *in vitro*.
2. Evaluation of the antiviral properties of commercially available G-quadruplex ligands on both HSV-1 and HHV-6 infected cells.
3. Study of the G-quadruplex ligand mechanism of action involved in the antiviral effect against these viruses.
4. Visualization of viral DNA-related G-quadruplex structures in infected cells.

3 MATERIALS AND METHODS

3.1 HSV-1 STUDY: MATERIALS AND METHODS

3.1.1 Selection of putative G-quadruplex sequences in HSV-1 genome

HSV-1 genome from the Pubmed database (http://www.ncbi.nlm.nih.gov/nuccore) was analyzed by QGRS Mapper (http://bioinformatics.ramapo.edu/QGRS/index.php). The following restrictions were applied to identify the putative G-quadruplex sequences: i) maximum oligonucleotide length of 30 nucleotides (nt), ii) minimum G-group size of 2-3 nt, iii) loop size from 0 to 20 nt. Oligonucleotide sequences are reported in Table 1 and Table 2.

Oligonucleotide	Sequence (5'→3')
gp054a	GGGGTTGGGGCTGGGGTTGGGG
gp054b	GGGGTTGGGGTTGGGGTTGGGG
gp054c	GGGGTTGGGGTTGGGGCTGGGG
gp054d	GGGGCTGGGGCTGGGGCTGGGG
gp054e	GGGGCTGGGGCTGGGGTTGGGG
gp054f	GGGGCTGGGGTTGGGGTTGGGG
un1	GGGGGAGAGGGGAGAGGGGGGGAGAGGGG
un2	GGGGGCGAGGGGCGGGAGGGGGCGAGGGG
un3	GGGAGGAGCGGGGGGAGGAGCGGG

Table 1 Oligonucleotide sequences selected through the analysis the HSV-1 genome.

HSV-1 packaging sequences (Adelman, et al., 2001) were provided by IDT (Integrated DNA Technologies, Belgium). The oligonucleotide *un1* was purchased from Invitrogen (Monza, Italy), whereas all other oligonucleotides were from Sigma-Aldrich (Milan, Italy).

Oligonucleotide	Sequence (5'→3')
HSV-1 pac1	CCCCC GGGGGG TGTGTTT CGGGG GGGG
mut L-poly G	CCCTA CCATGG TGTGTTT CGGGG GGGG
mut T-rich	CCCCC GGGGGG TGCGCCC CGGGG GGGG
mut R-poly G	CCCCC GGGGGG TGTGTTT CCCAT GGGG

Table 2 Wild-type and mutated HSV-1 (strain F) packaging sequences.

3.1.2 G-quadruplex ligands and other drugs

TMPyP4 and BRACO-19 were purchased from Calbiochem (Merck Millipore, Darmstadt, Germany) and ENDO-Therm (Saarbrücken, Germany), respectively. TMPyP2 was provided by Livchem Logistics GmbH (Frankfurt, Germany). Acyclovir (ACV), phosphonoacetic acid (PAA) and 3-methyl adenine (3-MA) were from Sigma Aldrich.

3.1.3 Circular dichroism and UV spectroscopy

Polarized light spectroscopy offers the possibility to characterize nucleic acid conformations and their complexes with proteins and other ligands. Circular dichroism (CD) is a useful indicator of G-4 folding topology and it can also provide structure information on its quadruplex-ligand complexes (Ou, et al., 2008). Circular dichroism spectra were recorded on a JASCO-810 spectropolarimeter and Chirascan^{TM} CD Spectrometer (Applied PhotoPhysics, United Kingdom), both equipped with a temperature controller (Peltier Jasco PTC-4235), using a 0.5 cm-path length quartz cuvette. DNA oligonucleotides (Table 1 and Table 2) were diluted to the final concentration of 4 μM in a buffer containing lithium cacodylate (10 mM, pH 7.4) and 0, 20, 50 or 100 mM KCl. All samples were denatured by heating at 95°C for 5 minutes, gradually cooled to room temperature and measured after 24 h with Nanodrop 1000 Spectrophotometer (Thermo Scientific, Illkirch Cedex, France). BRACO-19, TMPyP4 or TMPyP2 were added after DNA folding at a final concentration of 16 μM. CD experiments were performed using the following parameters: speed scanning 50-100 nm/min, response time 4 seconds, accumulation 2, wavelengths from 230-320 nm or 230-600 nm in the presence of compounds. CD spectra were baseline-corrected for signal contributions due to the buffer and obtained ellipticity (mdeg) was converted into molar ellipticity ($(\theta) = deg \times cm^2 \times dmol^{-1}$) based on sample concentration. Spectra were recorded at 20°C or over a temperature range of 20-95°C with temperature increase of 5°C.

UV spectra were carried out using a Lambda25 UV/Vis spectrometer (PerkinElmer) equipped with a Peltier temperature controller, and a quartz cell of 10-mm optical path length. Oligonucleotides were diluted to a final concentration of 4 μM in a lithium cacodylate (10 mM, pH 7.4) and KCl (0 mM or 100 mM) buffer. UV spectra were recorded at 295 nm over a temperature range of 20-95°C, with temperature increase of 5°C. A 5 min equilibration period at each measurement was allowed to ensure homogeneous sample temperature.

3.1.4 Electrophoretic mobility shift assay (EMSA)

All oligonucleotides were gel-purified before use and prepared in desalted/lyophilised form (Table 1). Oligonucleotides were 5'-end-labelled with [γ- ^{32}P]ATP by T4 polynucleotide kinase and purified by MicroSpin G-25 columns (GE Healthcare Life Sciences, Europe). They were next resuspended (1.8 μM final concentration) in lithium cacodylate 10 mM, pH 7.4, with or without 100 mM KCl, heat-denatured and folded. To check for the presence of oligomers, ^{32}P-labeled oligonucleotides (10 pmoles) were heat denatured and folded in the

presence of increasing amounts of cold oligonucleotides (10-290 pmoles), with or without KCl (100 mM), to a final concentration of 1.5-25 μM. All samples were loaded on 16% non-denaturing polyacrylamide gels, with or without 100 mM KCl, run for ~16 hours at 40 volts. Gels were visualized by phosphorimaging (Thyphoon FLA 7000, GE Healthcare Life Sciences, Europe).

3.1.5 Cell lines and Viruses

Vero cells (African green monkey from ATCC, CCL-81) were propagated in Dulbecco's modified Eagle's medium (DMEM GIBCO, Life Technologies, Monza, Italy or Corning Cellgro, Manassas, VA, USA) supplemented with 10% fetal bovine serum (FBS, GIBCO Life Technologies, Monza, Italy or Sigma Aldrich, Canada) supplemented with non-essential amino acids (Sigma-Aldrich), HEPES, sodium pyruvate (Multicell Wisent Inc., St-Bruno, Québec, Canada) and plasmocin 5 μg/ml (InvivoGen, San Diego, CA, USA) or PenStrep 1X (Life Technologies). Cell culture incubator was normally set at 37°C and 95% humidity, in an atmosphere of 5% CO_2.

The HSV-1 strain F was kindly provided by Dr. B. Roizman (University of Chicago, Illinois USA) and ATCC (VR-733).

3.1.6 Cytotoxicity

Cytotoxicity of the compounds was investigated by a 3-(4,5-dimethylthiazol-2-yl)-2,5-diphenyltetrazolium bromide (MTT) assay. Vero cells were plated at a density of 1×10^4 cells/well in 96-well tissue culture plates to a final volume of 100 μl and were grown overnight. Cells were treated with increasing concentrations of compounds, previously diluted in the appropriate solvent. Each sample was tested in triplicate. At 48 h post treatment cell survival was evaluated: 10 μl of freshly dissolved MTT solution (5 mg/ml in sterile PBS 1X, Sigma Aldrich) were added, cells were subsequently incubated for 4 h at 37°C, CO_2 5%. 100 μl/well of a SDS-HCl solution (sodium dodecyl sulphate 10%, HCl 0.01 M) were then added, cells were then incubated overnight at 37°C and absorbance was determined at 620 nm (Sunrise Tecan Spectrophotometer). Cell growth was also monitored by count: Vero cells were plated and treated with increasing compound concentrations every 24 h. Cell growth was assessed by counting cell number every 24 h (Cellometer Auto T4, Nexcelom Bioscience).

3.1.7 Viral titration assay

Vero cells were seeded at a density of 2.5×10^5 cells per well in 6-well tissue culture plates, pre-treated with BRACO-19, TMPyP4 or TMPyP2 (0.04 µM-25 µM) for 16 h, infected with HSV-1 strain F at a multiplicity of infection (MOI) of 1 Plaque Forming Units (PFUs). After 1 h infection at 37°C, cells were washed twice with PBS 1X and maintained in culture medium supplemented or not with G-quadruplex ligands (0.04 µM-25 µM). At 24 h post infection (h.p.i.), supernatants were collected, cleared by centrifugation at 300 rcf and stored at -80°C until assayed.

To test the autophagy hypothesis, 3-methyladenine was added at the final concentration of 1 mM, from -1 h.p.i. up to supernatant collection (24 h.p.i.).

Virus plaque assay was performed using confluent Vero cells in 24-well culture plates (1×10^5 cells/well). Cells were infected with 250 µl of serially-diluted (10-fold) supernatants. Every dilution was tested in triplicate. At 1 h.p.i., Vero cells were washed and incubated with 500 µl of DMEM supplemented with 2% FBS and 0.6% methyl cellulose (Sigma-Aldrich). Viral plaques were counted at 48 h.p.i. by fixing the cell monolayer with 1 ml/well of formaldehyde 5% (in PBS 1X) and crystal violet 0.8% (in ethanol 50%).

3.1.8 Time of addition and early-entry viral assay

Vero cells were seeded in 24-well at a density of 9×10^4 cells per well tissue culture plates. After 24 hours, to assess whether BRACO-19 had an impact on viral entry or fusogenic events, cells were treated at various time points (at -1, 0, 1, 2 h) relative to infection with HSV-1 strain F at a MOI of 1 PFU/cell. After 1 h at 37°C, cells were washed with PBS 1X and maintained in culture medium. Alternatively, to identify when G-quadruplex ligands mediate their effect within the HSV-1 replicative cycle, infected cells were treated every two hours (from 0 h.p.i. up to 12 h.p.i. and at 24 h.p.i.) with BRACO-19 (25 µM), or ACV (10 µM) as reference drug. At 30 h.p.i. supernatants were collected and titrated as described above.

3.1.9 Transmission electron microscopy (TEM)

Vero cells were infected with HSV-1 strain F and treated with BRACO-19 (5 and 25 µM) and TMPyP4 (1, 5, 25 µM), as described above. At 24 h.p.i., cells were washed twice with PBS 1X, detached with trypsin and collected by centrifugation at 300 rcf for 5 minutes at room temperature. Pellets were carefully resuspended with 2.5% glutaraldehyde (Sigma Aldrich) in

PBS 1X and incubated at room temperature for 4 hours, then stored at 4°C until processing and analysis with transmission electron microscopy (FEI Tecnai™).

3.1.10 Real-time PCR

Total HSV-1 intracellular DNA and RNA were collected from confluent Vero cells, similarly to the procedure used to collect viral supernatants, as described above. HSV-1 intracellular DNA was collected at 3 or 20 h.p.i. Infected and treated Vero cells were detached with trypsin (Wisent Inc.), centrifuged at 300 rcf and resuspended in 200 µl of PBS 1X. DNA extraction was performed using QIAamp DNA blood Mini Kit (QIAgen, Toronto, Canada), according to the manufacturer's instructions. RNA was isolated at 24 h using TRIzol reagent (Life Technologies), according to the manufacturer's instructions. All RNA samples were treated with RNase-free DNase I (Ambion Turbo DNA free, Life Technologies), resuspended in DEPC water (Sigma Aldrich) and stored at -80°C.

Reverse transcription was carried out using 1 µg of total RNA in a reaction mixture composed of buffer 1X, $MgCl_2$ 3 mM, dNTPs 0.5 mM, random hexamers 2 µM, RNase inhibitor 0.5 U/µl, MuLv 1.5 U/µl and DEPC water. Reverse transcription was performed under the following conditions: 10 minutes at 25°C, 60 minutes at 48°C and 5 minutes at 95°C using the Thermo Cycler Verity 96 (Applied Biosystem, Life Technologies, Monza, Italy). Forward/reverse primers and FAM-TAMRA fluorescent probes, used to perform TaqMan real-time PCR, were designed within conserved HSV-1 gene sequences, using Primer Express 3 (Applied Biosystem) (Table 3).

TaqMan real-time/sybr green primer sequences				
Gene	**Name**	**Primers (5'→3')**	**Probe (5'-FAM→TAMRA-3')**	**Amplicon length (bp)**
α-genes	US1	GGCCCGGAGTGTGATCTTAG GGTGGCATCGGAGATTTCAT	AGATTCATCTCAGCGCGAC AAGCGA	70
	US12	CAACGGGTTACCGGATTACG TTGGGTGTGGCACATCGA	ACTGTCGGTCACGGTCCCG CC	68
	UL54	ACATTGCATCCTTCGTGTTTGT AAGGGTCGCGTAGTCGATCTC	TTCTGGCCAGGCTCGCCAA CC	86
β-gene	UL30	TTCGACTTTGCCAGCCTGTA CAGGGAGAGCGTGCTGAAG	AGCATCATCCAGGCCCAC AACCTG	69
γ-genes	UL36	TCCGTCTCCCGAATGACATC GCACGTGCTGGACGAAAACT	ACAAGGATCAGCTTCGCC AGCGC	87
	UL37	CGGCTAACGGACGAAACG GTATGGATTGGTTACTGATGAA CGA	AAGCGCGAAACACGCCGT CG	81
Housekeeping gene	β-actin	TCACTGAGCGCGGCTACA CCTTAATGTCACGCACGATTTC	TCACCACCACGGCCGAGC G	69

Table 3 Primer sequences designed to perform TaqMan and SYBR® green real-time PCR.

All oligonucleotides (Table 3) were purchased from Sigma-Aldrich, and were tested for potential cross-reactivity with unrelated viral or other microbial sequences using BLAST alignment software (http://blast.ncbi.nlm.nih.gov/).

Each real-time PCR mixture contained: master mix 2X (Applied Biosystem), forward/reverse primer mixture 900 nM, probe 200 nM, sterile water and 5 µl of a 10-fold diluted complementary DNA (cDNA). Each sample was analyzed in triplicate. β-actin was used as housekeeping gene, whereas non-treated retro-transcribed HSV-1 RNA as a negative control. Real-time PCR experiments were performed in ABI 7900 HT – FAST Real Time PCR System under the following conditions: 2 minutes at 50°C (1 cycle), 10 minutes at 95°C (1 cycle), followed by 50 cycles of 15 seconds at 95°C and 1 minute at 60°C. Differently, isolated HSV-1 intracellular DNAs were analyzed by real-time PCR using SYBR® green as the detection reagent. The reaction was performed in a final volume of 20 µl containing SYBR® green fast 2X (QIAgen), forward and reverse primers at 500 nM (Table 3) (IDT, Coralville, USA) and isolated viral DNA at 100 nM. Data were collected using a Rotor Gene Q thermo cycler (QIAgen) with the following cycling conditions: 95°C for 5 minutes, followed by 40 cycles of 5 seconds at 95°C and 10 seconds at 60°C.

3.1.11 Taq-polymerase stop assay

Taq-polymerase stop assay was initially carried out using synthesized DNA oligonucleotides (Table 4). T4 polynucleotide kinase was from Invitrogen (Paisley, UK), [γ-^{32}P]ATP from Perkin Elmer (MA, USA). Primer (HSV Taq primer, Table 4) was 5'-end labelled with [γ-^{32}P]ATP using T4 polynucleotide kinase at 37°C for 30 min. The labelled primer (final concentration 72 nM) was annealed to the template (final concentration 36 nM) in lithium cacodylate buffer (10 mM, pH 7.4). Where specified, samples were incubated with KCl 10 mM in the presence or absence of BRACO-19 (0.5 µM, 1 µM) at room temperature. Primer extension was accomplished with 2 U of Ampli*Taq* Gold DNA polymerase (2 U/reaction, Applied Biosystem, Carlsbad, California, USA) at 60°C for 30 minutes. Reactions were stopped by ethanol (EtOH) precipitation, primer extension products were separated on a 15% denaturing gel, and finally visualized by phosphorimaging (Typhoon FLA 9000).

In addition, Taq polymerase stop assay was performed on the full length HSV-1 DNA previously extracted from semi-confluent Vero cells infected with HSV-1 strain F. At 90% cytopathic effect (CPE), the cell monolayer was lysed with repeated freeze/thaw cycles, the HSV-1-containing supernatant was collected and cleared by centrifugation at 11000 rcf. HSV-

1 DNA was isolated by incubation at 56°C for 10 minutes with 500 µl Lysis buffer (Biomerieux) and 20 µl proteinase K, following extraction on easyMAG (Biomerieux). An appropriate volume of a 10-fold diluted HSV-1 DNA was denatured at 95°C for 10 min and gradually cooled to room temperature. After 90 minutes, increasing concentrations of BRACO-19 or TMPyP2 were added and samples stored overnight at 4°C. DNA amplification was achieved both by standard PCR, stained with GelRed in 1% agarose gel and visualized with Typhoon FLA 9000, and real-time PCR and detected with SYBR® green. Standard PCR was performed using Verity 96 Thermo Cycler under the following conditions: 95°C for 5 minutes followed by 35 cycles of 1 minutes at 94°C, 30 seconds at 58°C, 1 minutes at 72°C and finally 3 minutes at 72°C. PCR mixtures were composed of buffer 1X, $MgCl_2$ 2 mM, dNTPs 0.2 mM, primers 0.2 µM, sterile water and 5 µl of HSV-1 DNA treated with increasing compound concentrations (500 nM-16 µM, 1:2 dilutions) or sterile water. PCR reagents were provided by Fermentas (Milan, Italy). Real-time PCR was performed using ABI 7900 HT – FAST Real Time PCR System with the following conditions: 95°C for 10 minutes followed by 40 cycles of 30 seconds at 95°C and 30 seconds at 58°C, 1 minutes at 72°C. The mixtures were composed of SYBR® green PCR Master Mix 2X (Applied Biosystem), primers 0.18 µM, sterile water and 5 µl of HSV-1 DNA treated with increasing compound concentrations (250 nM-4 µM, 1:2 dilutions). All primer sequences were synthesized by Sigma Aldrich (Table 4).

Taq polymerase stop assay (on designed oligonucleotide templates for sequencing)			
Oligonucleotide name	**Oligonucleotide function**	**Oligonucleotide sequence (5'→3')**	**Amplicon length (bp)**
HSV Taq primer	primer	GGCAAAAAGCAGCTGCTTATATGCAG	-
HSV Taq non-G4 control	template	TTGTCGTTAAAGTCTGACTGCGAGCTCTCAGATCCT GCATATAAGCAGCTGCTTTTTGCC	60
un2	template	TTTTTGGGGGCGAGGGGCGGGAGGGGGCGAGGGGT TTTTCTGCATATAAGCAGCTGCTTTTTGCC	65
un3	template	TTTTTGGGAGGAGCGGGGGGAGGAGCGGGTTTTTCT GCATATAAGCAGCTGCTTTTTGCC	60
gp054a	template	TTTTTGGGGTTGGGGCTGGGGTTGGGGTTTTTCTGCA TATAAGCAGCTGCTTTTTGCC	58
gp054d	template	TTTTTGGGGCTGGGGCTGGGGCTGGGGTTTTTCTGC ATATAAGCAGCTGCTTTTTGCC	58
Taq polymerase stop assay primer sequences (for full length HSV-1 DNA)			
un	primer	GTGTCACGGGGAAAGAGCA CCAAGTGTTTGCCCAGTAACAC	288
gp054	primer	AGGGAGGATGCCCACGAA GACCGTCAGCCGCCTGTC	357
non-G4 control	primer	AGGGAGGATGCCCACGAA TCCGCGTCTTCCACAAATC	68

Table 4 Primer and template sequences of oligonucleotides used to perform Taq-polymerase stop assays.

3.2 HHV-6 STUDY: MATERIALS AND METHODS

3.2.1 Analysis of the HHV-6 genome

The genome of both HHV-6A (GS and U1102 strains) and HHV-6B (Z29 and HST strains), from the Pubmed database (http://www.ncbi.nlm.nih.gov/nuccore), were analyzed by QGRS Mapper (http://bioinformatics.ramapo.edu/QGRS/index.php). As described above for HSV-1, the following restrictions were applied to study the leading and lagging strands of the viruses: i) maximum oligonucleotide length of 30 nucleotides (nt), ii) minimum G-group size of 2-3 nt, iii) loop size from 0 to 20 nt.

3.2.2 Cell lines and Viruses

Molt-3 (ATCC, CRL-1552), HSB-2 (ATCC, CCL-120.1) and pheripheral blood mononuclear cells (PBMCs) were propagated in RPMI-1640 medium (Corning Cellgro) containing 10% FBS (Sigma-Aldrich) and supplemented with HEPES and plasmocin 5 μg/ml (InvivoGen). PBMCs were isolated from blood samples using a lymphocyte separation medium (Wisent Inc.). Cell lines were normally grown at 37°C and 95% humidity, in an atmosphere of 5% CO_2.

HHV-6B (Z29 strain) was provided by the HHV-6 Foundation, HHV-6A (GS strain) was purchased from the NIH AIDS Repository.

3.2.3 G-quadruplex ligands and other drugs

TMPyP4 was purchased from Calbiochem, whereas BRACO-19 from Sigma-Aldrich. TMPyP2 was provided by Livchem Logistics GmbH.

3.2.4 Cytotoxicity studies

Cytotoxicity of TMPyP4, BRACO-19 and TMPyP2 was investigated by a 3-(4,5-dimethylthiazol-2-yl)-2,5-diphenyltetrazolium bromide (MTT) assay, following the cell growth every 24 hour post treatment. HSB-2, Molt-3 and PBMCs were plated in 96-well tissue culture plates (final volume of 100 μl/well), at a density of 3.5×10^4 cells/well, 2.5×10^4 cells/well and 5×10^4 cells/well, respectively. Therefore, cells were treated with increasing concentrations of these compounds (concentration range from 1 nM up to 1 mM), and incubated at 37°C. At 48 hours post incubation, cells were treated a second time. Every sample was tested in triplicate. Cell survival was evaluated at 96 h post treatment, by adding

12 μl/well of MTT solution (TACS TMM cell proliferation assay, R&D systems), subsequently cells were incubated for 4 hours at 37°C, CO_2. 110 μl/well of a SDS-HCl solution (sodium dodecyl sulphate 10%, HCl 0.01 M) were then added and cells were incubated overnight at 37°C. The absorbance was determined at 620 nm (Tecan Spectrophotometer).

Cell growth was also monitored by count: the cells were plated at a density of $5x10^4$ in 96-well tissue culture plates (final volume 200 μl), and treated with increasing concentrations of compounds at 0 and 48 hours (day 1 and 3, respectively). Cell growth was assessed by counting the cell number every 24 h (Cellometer Auto T4, Nexcelom Bioscience). Cell viability was also assessed monitoring the cell growth by counting the cells every 24 h.p.t with Cellmeter Auto T4 (Nexcelom Bioscience).

3.2.5 Antiviral activity studies against HHV-6 and nucleic acid isolation

The different cell tropism of HHV-6A and HHV-6B required distinct procedures to properly investigate the activity of TMPyP4, BRACO-19 and TMPyP2 against the viruses. Molt-3 cells were infected with HHV-6B (strain Z29) at a MOI of 0.5 in complete RPMI-1640, for 4 hours at 37°C. After the infection, cells were washed twice in PBS 1X, resuspended in the appropriate volume of complete medium and distributed at a confluence of 5×10^5 cells/ml in 6-well tissue culture. The cells were treated with increasing concentrations of TMPyP4 (2-fold dilutions from 1 μM to 0.125 μM or 10-fold dilutions from 1 μM to 0.01 μM), BRACO-19 (2-fold dilutions from 2 μM to 0.25 μM or 2-fold dilutions from 3 μM to 0.1875 μM) or TMPyP2 (2-fold dilutions from 1 μM to 0.125 μM) at 0 h.p.i. (day 1 p.i.), 48 h.p.i. (day 3 p.i.), 96 h.p.i. (day 5 p.i.) and eventually 144 h.p.i. (day 7 p.i.). Aliquots of supernatants and cells, previously centrifuged at 300 rcf for 3 minutes, were collected at 48 h.p.i. (day 3 p.i.), 96 h.p.i. (day 5 p.i.), 144 h.p.i. (day 7 p.i.), and eventually 192 h.p.i. (day 9 p.i.).

HSB-2 cells were infected with HHV-6A (strain GS) at a MOI of 0.5 or 1 in complete RPMI-1640, for 6 hours at 37°C. After the infection, cells were washed in PBS 1X, resuspended in complete medium at a confluence of 7.5×10^5 cells/ml and grown in flasks, to increase the infection rate. At 48 h.p.i., cells were distributed in 24-well tissue culture plates and treated with increasing concentrations of TMPyP4 (2-fold dilutions from 1 μM to 0.125 μM or 10-fold dilutions from 1 μM to 0.01 μM) or TMPyP2 (2-fold dilutions from 1 μM to 0.125 μM) at 48 h.p.i. (day 3 p.i.), 96 h.p.i. (day 5 p.i.), 144 h.p.i. (day 7 p.i.), and eventually 192 h.p.i. (day 9 p.i.). Aliquots of supernatants and cells, previously centrifuged at 300 rcf for 3

minutes, were collected at 96 h.p.i. (day 5 p.i.), 144 h.p.i. (day 7 p.i.), 192 h.p.i. (day 9 p.i.), and eventually 240 h.p.i. (day 11 p.i.).

PBMCs were isolated from blood samples of donors aged between 18 and 50 years old, in accord to the CHU de Quebec ethics committee. PBMCs were extracted by centrifuging venous blood samples over a Ficoll gradient, cells were then washed with PBS 1X, counted and stimulated for 48 h with PHA-P (10 µg/mL) (Sigma-Aldrich). After this time, PBMCs were infected with HHV6-B (strain Z29) or HHV-6A (strain GS) at a MOI of 0.5 or 1, as described for Molt-3 and HSB-2.

In all cases, collected pellets and supernatants were stored at -80°C until DNA isolation.

Infected and treated cell growth was monitored by counting the cells every 48 h, using an automatic cell counter (Cellmeter Auto T4, Nexcelom Bioscience).

3.2.6 HHV-6 DNA isolation

Intracellular HHV-6 DNAs were isolate using QIAamp DNA blood mini kit (QIAgen), in accord to the manufacturer's instructions.

Differently, viral DNA from supernatants was isolated as follow: each supernatant was treated with 20 µl DNAse buffer 10X (Tris 100 mM, pH=7.5, $MgCl_2$ 25 mM, $CaCl_2$ 5 mM), 5 µl of DNAse (Roche) and incubated at 37°C for 30 minutes, followed by a further incubation at 70°C for 10 minutes in the presence of 7.5 µl/sample of EDTA (200 mM). Viral DNA extraction was completed with QIAamp DNA blood Mini Kit, in accord to the manufacturer's instructions. Before DNA elution, $1x10^6$ copies/sample of a GAPDH-containing plasmid were added, as a control to normalize data.

3.2.7 Q-PCR experiments

The Q-PCR mixture was composed of multiplex mix 2X (Invitrogen, Life Technologies), forward/reverse/probe primers (Table 5) at a final concentration of 500 nM, sterile water and 4-5 µl viral DNA isolated from supernatants or a total of 100 ng of DNA extracted from cells. The housekeeping gene GAPDH used as control.

Primer sequences were purchased from IDT. Q- PCR experiments were recorded with Rotor Gene Q thermo cycler (QIAgen) under the following conditions: 5 minutes at 95°C (1 cycle), followed by 40 cycles of 15 seconds at 95°C and 15 seconds at 60°C.

Primers	Forward/Probe/Reverse primer sequences (5'→3')
U65-U66	GACAATCACATGCCTGGATAATG 56FAM / AGCAGCTGGCGAAAAGTGCTGTGC / 3BHQ_1 TGTAAGCGTGTGGTAATGGACTAA
GAPDH	AAATGAGCCCCAGCCTTC 5HEX / CGACGTACT / ZEN / CAGCGCCAGCATC / 3IABkFQ AATCCCATCACCATCTTCCAG

Table 5 Forward/probe/reverse primer sequences adopted to perform Q-PCR experiments with HHV-6.

3.2.8 Circular dichroism

Circular dichroism spectra were recorded with a Chirascan^{TM} CD Spectrometer (Applied PhotoPhysics), equipped with a temperature controller, using a 0.5 cm-path length quartz cuvette. HHV-6 packaging sequences (Table 6) (Thomson, et al., 1994) were diluted to the final concentration of 4 μM in a buffer containing lithium cacodylate (10 mM, pH 7.4) and 0 or 100 mM KCl. All samples were measured with Nanodrop 1000 Spectrophotometer (Thermo Scientific) and denatured by heating at 95°C for 5 minutes, gradually cooled to room temperature. CD experiments were performed using the parameters mentioned above. CD spectra were baseline-corrected for signal contributions due to the buffer and obtained ellipticity (mdeg) was converted into molar ellipticity based on sample concentration. Spectra were recorded over a temperature range of 20-90°C, with temperature increase of 5°C.

Oligonucleotide	Sequence (5'→3')
HHV-6A pac1	CCCC CGGGGGG GCT AAAAAA AGGGGG GTAA
HHV-B pac1	CCCC GGGGGGG TTA AAAAAA GGGGGG TAT

Table 6 HHV-6A (U1102 strain) and HHV-6B (Z29 strain) packaging sequences.

3.3 VIRAL G-QUADRUPLEX VISUALIZATION: MATERIALS AND METHODS

3.3.1 Antibodies

The plasmid pSANG-BG4, used to produce BG4, was kindly provided by Prof. S. Balasubramanian (Cambridge, UK) (Biffi, et al., 2013). 1H6 antibody was kindly provided by Prof. P. M. Lansdorp (University of Groningen, The Netherlands) (Henderson, et al., 2013).

3.3.2 BG4 production and purification

BL21DE3-RIL (Cml^R) competent cells were transformed with the plasmid pSANG-BG4, plated in the presence of Luria-Bertani (LB) agar medium, supplemented with kanamycin (50 μg/ml) and chloramphenicol (25 μg/ml), and incubated overnight at 37°C. 5 ml of a single-colony LB preculture were inoculated in 500 ml of LB with kanamycin (50 μg/ml) and chloramphenicol (25 μg/ml), and incubated at 37°C, 250 rpm. When the OD_{600} reached 0.4-0.5, the inoculum was induced with isopropyl β-D-1-thiogalactopyranoside (IPTG) 0.3 mM, then incubated overnight at 20°C, 250 rpm. The culture was centrifuged at 6000 rpm for 15 minutes, at 4°C. The pellet was resuspended in binding buffer (sodium phosphate 20 mM, pH 7.4, NaCl 0.5 M, imidazole 20 mM), sonicated for 2-3 minute in water/ice and spun down again at 12000 rpm for 10 minutes at 4°C. Subsequently, the supernatant was filtered and BG4 was purified on HisTrap column (Qiagen) using an elution buffer with an imidazole-increasing gradient (sodium phosphate 20 mM, pH 7.4, NaCl 0.5 M, imidazole 500 mM).
Dialysis in 4 liters of PBS 1X at room temperature for 4 h was performed to remove salts (3500 as molecular weight cut-off of the membrane), followed by BG4 quantification with both Bradford assay and bovine serum albumin (BSA) curve.

3.3.3 ELISA assay

The binding affinity and specificity of both BG4 and 1H6 for G-quadruplex DNA was assessed using enzyme-linked immunosorbent assay (ELISA). 96-well plates (NUNC™ medi-sorp surface, Thermo Scientific) were coated with 100 μl/well of an avidin solution (5 μg/ml) (Life Technologies) and incubated overnight at 37°C.
Biotinylated G-quadruplex folding oligonucleotides (Table 7) were diluted at 2 pmoles/60 μl in annealing buffer(Tris-HCl 10 mM, pH=7.5; KCl 100 mM) and denatured by heating at 95°C

for 10 minutes, gradually cooled to room temperature overnight, and bound (2 pmoles/60 µl) to the avidin-coated plates by incubation at 37°C for 1 h, followed by repeated washing in PBS-T (0.1% Tween 20 in PBS 1X). After a 1 h incubation with BSA 3% (in PBS-T) to prevent aspecific interactions, biotinylated oligonucleotides were incubated with BG4 (0-200 nM, 2-fold dilutions) or 1H6 (0-40 ng/µl, 2-fold dilutions) for 1 or 2 h respectively, and washed. In the case of BG4, an additional incubation of 1 h in the presence of an anti-mouse α-flag secondary antibody (dilution 1/2500 in PBS-T) (Anti-D Tag, abm) was performed. The binding between G-4 structures and BG4 or 1H6 was detected with an anti-mouse horseradish peroxidase (HRP) antibody (dilution 1/20000 in PBS-T) (Jackson ImmunoResearch, USA), by incubating the plates in the dark for 1 h. Subsequently, 100 µl/well of TMB (3,3',5,5'-tetramethylbenzidine, HRP substrate, BD OptEIA^{TM}, Thermo Scientific) were added, followed by addition of 50 µl/well of H_2SO_4 2N to stop the reaction. Plates were read with TECAN at λ=450 nm, using a reference wavelength of λ=570 nm.

HSV-1 sequences (5'→3')	
gp054a	TTTTTGGGGTTGGGGCTGGGGTTGGGGTTTTT
un2	TTTTTGGGGGCGAGGGGCGGGAGGGGGCGAGGGGTTTTT
un3	TTTTTGGGAGGAGCGGGGGGAGGAGCGGGTTTTT
HHV-6 sequence (5'→3')	
hTELO	TCGAGGGGTTAGGGTTAGGGTTAGGGTTAGGGTTAGGGTTAGGGTTAC
HIV sequences (5'→3')	
LTRII+III+IV	TTTTTGGGGACTTTCCAGGGAGGCGTGGCCTGGGCGGGACTGGGGAGTGGTTTTT
LTRIII+IV	TTTTTGGGAGGCGTGGCCTGGGCGGGACTGGGGAGTGGTTTTT
LTRIII+IV M5	TTTTTGGGAGGCGTGGCCTGGGCGTGACTGGGGAGTGGTTTTT
LTRIII+IV M4+5	TTTTTGGGAGGCGTGGCCTGTGCGTGACTGGGGAGTGGTTTTT
Reference sequences (5'→3')	
c-myc	GGCATAGTGCGTGGGCG
Negative control sequences (5'→3')	
ss-DNA	GGCATAGTGCGTGGGCG
ss-DNA long	ACTACTACTGGCATAGTGCGTGGGCGTGAGGGTAG
ss-DNA high G-content	ACTACTACTGGGTGTGTGGTGTGTGTGTGGGTGTG
TERC DNA	GTGGCCATTTTTTGTCTAACCCTAACTGAGAAGGGCGTAG
H6 TR_S	CTAACCCTAACCCTAACCCTAGGCCCTAACCCTAACCCTAGGTCTAACCCT

Table 7 Sequence of biotinylated oligonucleotides (biotin at 5' end) used to perform ELISA assay. *ss-DNA* sequence was reported by Biffi, et al **(Biffi, et al., 2013)**. hTELO is the telomeric sequence.

3.3.4 Circular dichroism

Negative control sequences (TERC DNA, H6 TR_S, *ss-DNA*, *ss-DNA long*, *ss-DNA high G-content*) (Table 7), used to perform ELISA assay, were analyzed by circular dichroism to assess their capability to fold into G-quadruplex. Circular dichroism spectra were recorded with a JASCO-815 spectropolarimeter, using a 0.5 cm-path length quartz cuvette. As

described above, DNA oligonucleotides were diluted to the final concentration of 4 μM in a buffer containing lithium cacodylate (10 mM, pH 7.4) and KCl 100 mM. All samples were measured with TECAN, denatured by heating at 95°C for 5 minutes and gradually cooled to room temperature. CD spectra were recorded at 20°C, under the following parameters: speed scanning 100 nm/min, response time 4 seconds, accumulation 2, wavelengths from 230-320 nm. CD spectra were baseline-corrected for signal contributions due to the buffer and obtained ellipticity (mdeg) was converted into molar ellipticity ($(\theta) = deg \times cm^2 \times dmol^{-1}$) based on sample concentration. All oligonucleotides were purchased from IDT.

3.3.5 Cell lines and Viruses

As mentioned above, Vero cells (ATCC, CCL-81) were propagated in Dulbecco's modified Eagle's medium (Life Technologies or Corning Cellgro) supplemented with 10% FBS (Life Technologies or Sigma Aldrich) supplemented with non-essential amino acids (Sigma-Aldrich), HEPES, sodium pyruvate (Multicell Wisent Inc.) and plasmocin 5 μg/ml (InvivoGen) or PenStrep 1X (Life Technologies). The HSV-1 strain F was purchased from ATCC (VR-733), whereas the GFP-expressing recombinant virus V41 was kindly provided by Professor P. O'Hare (La Boissière, et al., 2004).

Molt-3 (ATCC, CRL-1552) were propagated in RPMI-1640 medium (Corning Cellgro) containing 10% FBS (Sigma-Aldrich) and supplemented with HEPES and plasmocin 5 μg/ml (InvivoGen). HHV-6B (Z29 strain) was provided by the HHV-6 Foundation.

3.3.6 Immunofluorescence

For HSV-1 G-quadruplex visualization, Vero cells were seeded at 5-7x10^4 cells/well in 8-well plates (8-well cultureslide, BD Falcon™) and grown overnight at 37°C. The cells were infected with the GFP-expressing recombinant virus V41 at a MOI of 0.5 (occasionally also 0.2, 1 or 4) for 1 h at 37°C, then washed with PBS 1X and incubated at 37°C in complete DMEM. Cells were also treated with PAA (400 μg/ml), or ACV (200 μM), as control.

At different time post infection (2, 4, 6, 8, 9, 12, 14, 16, 18 and 20 h.p.i.), cells were fixed in 4% paraformaldehyde (Sigma Aldrich) in PBS and then permeabilized with 0.5% tween 20 in PBS 1X for 50-60 minutes at room temperature. At this step, cells were eventually treated with 40 μg/ml of RNase A in PBS 1X (Thermo Scientific) or 0.12 U/μl of DNAse I (Fermentas) in buffer 1X (Ambion Turbo DNA free, Life Technologies) for 1 h at 37°C. Subsequently, Vero cells were blocked with 5% normal FBS (Life Technologies) in PBS 1X

for 12 h at 4°C. Cells were then incubated with 1H6 (diluted to 1 µg/ml in PBS 1X), for 2 h at room temperature. Cells were washed with 0.2% PBS-T, and incubated in the dark for 1 h at room with alexa Fluor-546 anti-mouse IgG (Life Technologies). Following repeated washing in 0.2% PBS-T and PBS 1X, the nuclear staining for DNA was obtained by incubating the cells in the dark with DRAQ5® at a dilution of 1:1000 (Cell Signaling Technologies), for 5 minutes at room temperature. Cells were washed and mounted in Dako mounting medium (Dako, Denmark). Slides were analyzed using a confocal microscope Nikon A1R+.

Although the many similarities, some different working conditions were necessary to test BG4 on infected Vero cells: the blocking step was performed by incubating the cells for 1 h with 3% BSA. BG4 was diluted to 1/100 in 3% BSA (stock concentration 520 ng/µl) and cells were incubated for only 1 h at room temperature. BG4 also required a further incubation of 1 h with an anti-mouse α-flag secondary antibody, diluted to 1/500 or 1/1000 in PBS 1X (stock concentration 100 µg/µl**)**. Moreover, detection was reached by incubating the cells, in the dark, for 1 h with alexa Fluor-488 anti-mouse IgG or alexa Fluor-568 anti-mouse IgG (Life Technologies). Slides were mounted using the slow-fade, containing DAPI for the DNA nuclear staining (Life Technology). Slides were analyzed with an Olympus BX-51 upright microscope, using a 40x or 60x UPlan Apo objective and processed with ImagePro 4.5.1 software (Media Cybernetics, Silver Spring, MD).

To detect G-quadruplex structures within the genome of HHV-6, Molt-3 cells were infected and treated as described above. Cells were centrifuged, counted and resuspended in order to distribute 10^5 cell/10 µl in each well of multitest slides (MP Biomedicals, LLC., Germany). Cells were fixed in cold acetone 100% at -20°C for 10 minutes, and re-hydrate in PBS 1X for 5 minutes. An additional permeabilization in 0.5% tween 20 in PBS 1X was eventually performed to improve the interaction with 1H6. The remaining consecutive steps were carried out as described above for BG4.

4 RESULTS AND DISCUSSION

4.1 HSV-1: RESULTS AND DISCUSSION

4.1.1 Analysis of herpes simplex virus-1 genome

Following the observation that GC content of the HSV-1 genome is extremely high (68%, with peaks of 84.7% in simple sequence repeats) (Ouyang, et al., 2012), we initially investigated the theoretical possibility of G-quadruplex folding by an online algorithms-based software for recognition and mapping of putative Quadruplex forming G-Rich Sequences (QGRS) (http://bioinformatics.ramapo.edu/QGRS/index.php) (Kikin, et al., 2006), on both the leading and lagging strands.

Among several hits, we selected nine regions that presented highly repeated putative QGRS (Table 1, Table 8 and 9). Six of them (named *gp054a-f*) were mainly found in the leading strand of the *gp054* gene (positions 71.527-71.728 bp, Gene Bank Accession Number GU734771.1) (Figure 4.1.1) which encodes UL36, the largest viral protein and essential viral tegument component (McNabb & Courtney, 1992). Two repeats of *gp054b* were additionally identified in the leading and lagging strand of the gene encoding the ubiquitin E3 ligase ICP0 (RL2) (Table 9).

Name	Sequence (5'→3')	G-score*
gp054a	GGGGTTGGGGCTGGGGTTGGGG	63
gp054b	GGGGTTGGGGTTGGGGTTGGGG	63
gp054c	GGGGTTGGGGTTGGGGCTGGGG	63
gp054d	GGGGCTGGGGCTGGGGCTGGGG	63
gp054e	GGGGCTGGGGCTGGGGTTGGGG	63
gp054f	GGGGCTGGGGTTGGGGTTGGGG	63
un1	GGGGGAGAGGGGAGAGGGGGGAGAGGGG	62
un2	GGGGGCGAGGGGCGGGAGGGGGCGAGGGG	62
un3	GGGAGGAGCGGGGGGAGGAGCGGG	36

Table 8 The analysis of HSV-1 genome allowed to select nine putative G-quadruplex forming sequences named *gp054* (*a-f*) and *un* (*1-3*). DNA sequences and G-scores are shown. *G-score: propensity of a sequence to fold into unimolecular G-quadruplex assigned by the QGRS software.

The *gp054* series sequences displayed the $G_4XTG_4XTG_4XTG_4XT$ common motif, where X was either a T or a C base. All *gp054* sequences were highly conserved among four reference HSV-1 strains. On the whole, *gp054* sequences were repeated 13-14 times and covered about 220 bps. Three more putative QGRS were found clustered at the terminal and internal repeats (both long and short) of the HSV-1 genome (Figure 4.1.1 and Table 8, 9). The exact role of

these regions is as yet unknown and thus the QGRS in these positions were named "*un*". In the leading strand, *un1* and *un2* sequences were located in segments *b* of TR_L and *c* of TR_S, respectively; *un3* laid in segment *a* of both TR_L and TR_S. Identical "*un*" sequences were also found in the lagging strand: *un1* was found in segment *b'* of IR_L, *un2* and *un3* in segments *c'* of IR_S and *a'* of IR_S/IR_L, respectively (Figure 4.1.1 and Table 9). Each "*un*" sequence was highly repeated (5-18 times) and conserved among different HSV-1 strains (Table 9). On the whole, the *un* sequences covered about 900 bps in the leading strand and 700 bps in the lagging strand.

Name	Strains	Positions		Repeats and genes	
		Leading strand (5'→3')	Lagging strand (5'→3')	Leading strand	Lagging strand
gp054a	F	71527-71620	-	4 UL36	-
	17	71612-71705	-	4 UL36	-
	H129	71561-71654	-	4 UL36	-
	KOS	71580-71757	-	4 UL36	-
gp054b	F	4121-4142/71587-71608	30075-30096	1 UL36, 1 TRL (RL2)	1 IRL (RL2)
	17	4138-4159/71672-71693	29987-30008	1 UL36, 1 TRL (RL2)	1 IRL (RL2)
	H129	4114-4135/71621-71642	29892-29913	1 UL36, 1 TRL (RL2)	1 IRL (RL2)
	KOS	71616-71637	-	1 UL36	-
gp054c	F	71593-71632	-	1 UL36	-
	17	71678-71717	-	1 UL36	-
	H129	71627-71666	-	1 UL36	-
	KOS	71574-71661	-	2 UL36	-
gp054d	F	71623-71722	-	4 UL36	-
	17	71708-71807	-	4 UL36	-
	H129	71657-71756	-	4 UL36	-
	KOS	71652-71739	-	3 UL36	-
gp054e	F	71707-71728	-	1 UL36	-
	17	71792-71813	-	1 UL36	-
	H129	71741-71762	-	1 UL36	-
	KOS	71562-71745	-	2 UL36	-
gp054f	F	71581-71626	-	2 UL36	-
	17	71666-71711	-	2 UL36	-
	H129	71615-71660	-	2 UL36	-
	KOS	71568-71655	-	3 UL36	-
un1	F	8966-9147	34922-35103	5 TRL (b)	5 IRL (b')
	17	9049-9213	34898-35062	5 TRL (b)	5 IRL (b')
	H129	9010-9174	34804-34968	5 TRL (b)	5 IRL (b')
	KOS	8997-9161	34768-34932	5 TRL (b)	5 IRL (b')
un2	F	150989-151306	25157-25474	9 TRS (c)	9 IRS (c')
	17	151064-151381	25090-25407	9 TRS (c)	9 IRS (c')
	H129	150962-151279	25087-25404	9 TRS (c)	9 IRS (c')
	KOS	150854-151171	25009-25326	9 TRS (c)	9 IRS (c')
un3	F	93-296/151880-152083	26047-26250	8 TRL,8 TRS (a)	8 IR (a')
	17	106-309/151929-152132	25955-26158	8 TRL,8 TRS (a)	8 IR (a')
	H129	106-333/151771-151974	25896-26111	9 TRL,8 TRS (a)	9 IR (a')
	KOS	118-309/151734-151925	25889-26080	8 TRL,8 TRS (a)	8 IR (a')

Table 9 Location and sequence repeats of the selected putative G-quadruplex forming oligonucleotides, in the genome of HSV-1, are shown.

To note that all identified sequences, apart from *un3*, were characterized by four GGGG-tracts, therefore possessing the ability to fold into 4-tetrad stacked G-quadruplex. This kind of tetraplex is in principle very stable, as denoted by the high G-scores obtained by these oligonucleotides (Table 9). The *un3* sequence displayed four GGG-tracts therefore gaining a lower G-score. However, three Gs were additionally present in each of the two 6-base-long loops. Because increasing evidence demonstrates the possibility that non-sequential G bases take part to G-quadruplex formation (Mukundan & Phan, 2013), more options for the building of a very stable quadruplex structure are also available for the *un3* sequence.

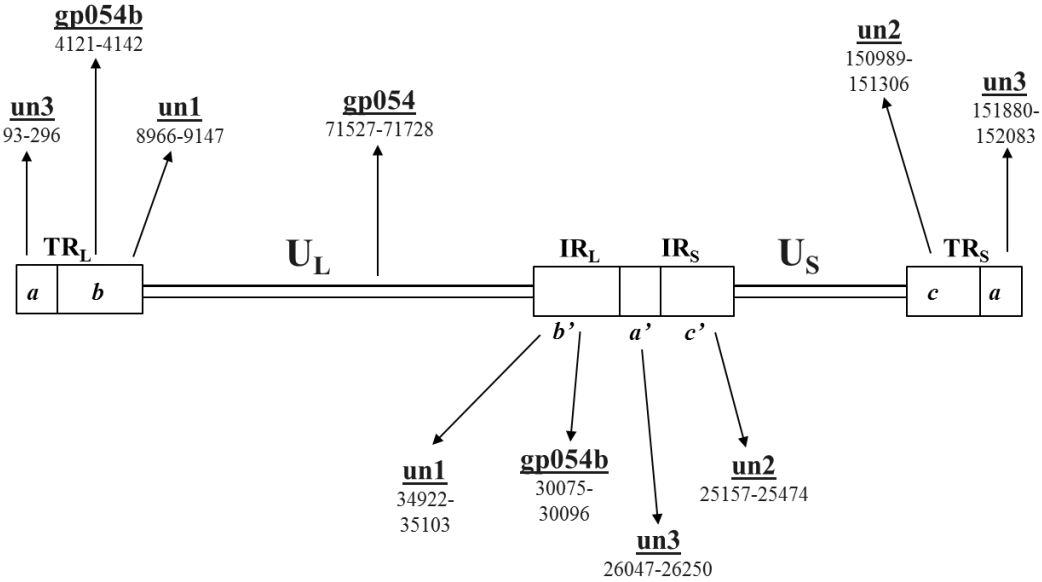

Figure 4.1.1 Schematic representation of the HSV-1 genome. G-quadruplex forming regions and their position within the genome are indicated. The terminal (TRL and TRS) and internal (IRL and IRS) repeats are shown as rectangles. The leading and lagging strands are depicted by a thick and thin line, respectively.

4.1.2 Biophysical characterization of selected HSV-1 putative G-4 sequences

To determine the possibility of G-quadruplex formation and the likely topology of the HSV-1 putative QGRS, circular dichroism spectroscopy was carried out.

Parallel G-4 structure usually shows a strong positive band at 265 nm and a minimum around 240 nm; CD spectra with a maximum around 295 nm and a negative peak around 260 nm typically display an antiparallel conformation; two peaks at both 265 nm and 295 nm are characteristic of a mixed-type G-4 structures which indicate the coexistence of distinct parallel and antiparallel folded species in solution (Bugaut & Balasubramanian, 2008).

In the presence of physiological concentrations of K^+, all tested oligonucleotides displayed CD G-quadruplex signatures. In particular, *gp054* oligonucleotides exhibited a maximum at

290 nm and a shoulder at 260 nm, indicative of a hybrid G-quadruplex (Figure 4.1.2a); *un2* presented two positive peaks at 290 nm and 240 nm and a negative peak at 260 nm, characteristic of an antiparallel topology, while *un1* and *un3* showed a main positive peak at 260 nm and a negative peak at 240 nm, signature of a parallel conformation (Figure 4.1.2b).

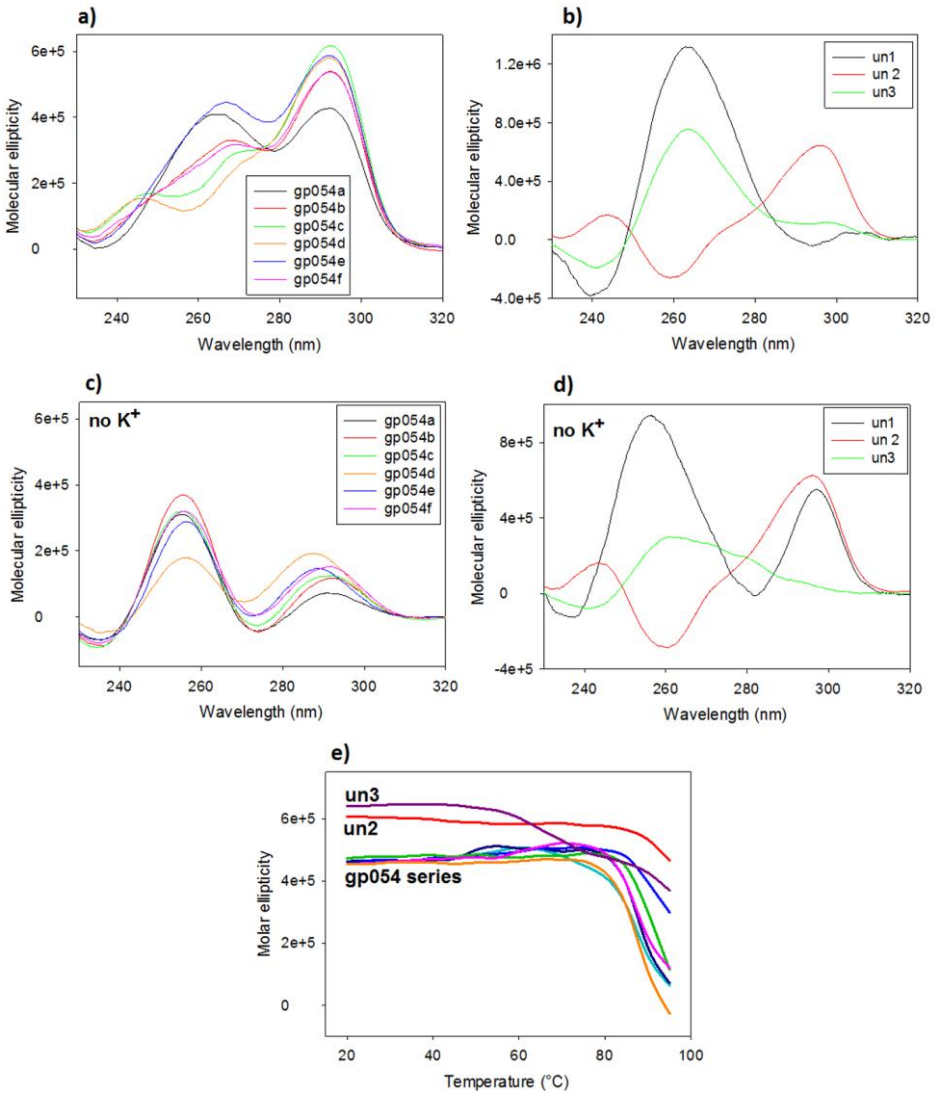

Figure 4.1.2 CD analysis of HSV-1 G-quadruplex forming sequences in the absence or presence of K^+ 100 mM. CD spectra of the *gp054* series oligonucleotides a) in the presence or c) without K^+. b) CD spectra of the *un* series oligonucleotides with K^+ 100 mM and d) in the absence of K^+. e) Thermal unfolding analysis of HSV-1 G-quadruplex sequences. Molar ellipticity at the peak wavelength has been plotted against temperature.

Usually, G-quadruplex folding occurs in the presence of K^+, while in the absence of this monovalent cation oligonucleotides are mostly unfolded. The HSV-1 oligonucleotides, however, displayed positive peaks at 290 and 260 nm, characteristic of G-quadruplex conformation, even in the absence of K^+ (Figure 4.1.2c,d), indicating strong propensity to fold into the tetraplex structure. Stability of HSV-1 G-quadruplexes in the presence of K^+ was

assessed by thermal denaturation experiments monitored by CD (Figure 4.1.3) and UV spectroscopy (Figure 4.1.2e). As shown in Figure 4.1.2e, 4.1.3 and Table 10, in the presence of K^+, all *gp054* series oligonucleotides were stable up to 80°C and unfolded only at higher temperature, with T_m values around 90°C. *Un2* was even more stable, with T_m above 95°C, while *un3* showed two transitions with T_m at 65°C and above 95°C, indicating the presence of at least two conformations (Table 10).

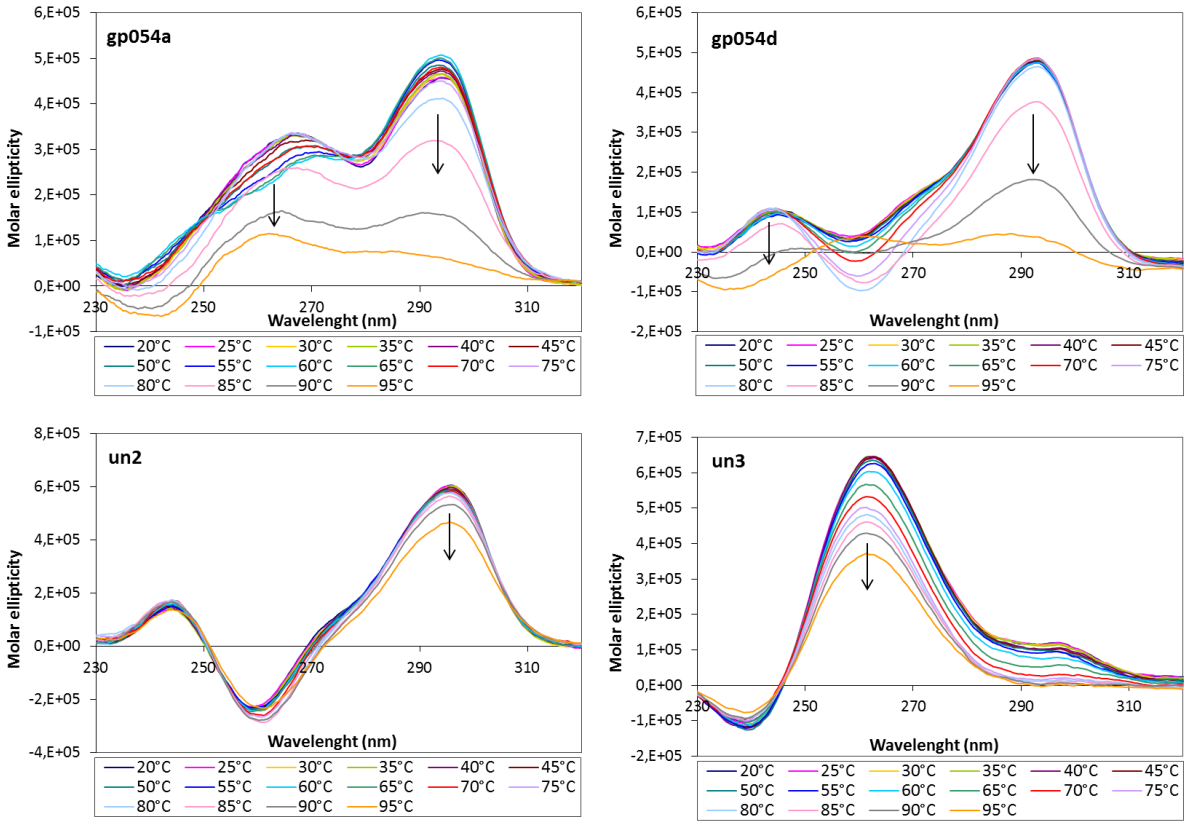

Figure 4.1.3 CD thermal denaturation analysis. Spectra of the indicated oligonucleotides, in the presence of K^+ 100 mM, during thermal unfolding are shown. Arrows indicate spectra progression during temperature increasing.

Sequence	Tm (UV, 100 mM K+)	Tm (CD, 100 mM K+)	Tm (CD no K+)	ΔTm[100 mM/no K+] (CD)
gp054a	87.4 ± 0.4	88.1±1.3	24.7±0.7/48.0±1.1	63.4/40.1
gp054b	88.0 ± 0.4	87.5±1.1	25.5±0.4/48.4±1.6	62.0/39.1
gp054c	92.3 ± 0.8	90.8±0.3	23.2±0.8/51.7±1.3	67.6/39.1
gp054d	91.5 ± 0.1	90.7±0.3	29.8±0.8/71.3±2.6	60.9/19.4
gp054e	91.7 ± 0.6	87.5±0.5	23.7±1.2/58.0±0.8	63.8/29.5
gp054f	88.1 ± 0.1	88.0±0.2	25.2±0.5/51.9±1.4	62.8/36.1
un1	nd	nd	40.8±9.8	nd
un2	> 95	> 95	50.3±0.9	> 44.7
un3	64.06 ± 0.68, >95	65.3±1.2, >95	34.7±4.7	30.6/ > 60.3

Table 10 Stability of HSV-1 G-quadruplex folding sequences measured by UV and CD, and in the presence/absence of K^+.

Because of the very low solubility of *un1* in the presence of K^+, T_m values for this sequence were not obtained. T_m values obtained by UV thermal unfolding analysis were in very close accordance with those obtained by CD (Table 10). In the absence of K^+, CD-monitored unfolding of *gp054* oligonucleotides showed two transitions: the first one with a maximum at around 290 nm displayed T_m below 30°C; the second one, with a positive peak at 260 nm with T_m around 50°C. The only exception was *gp054d* which reported a second T_m of 71.3°C. In the absence of K^+, *un2* was the most stable sequence, followed by *un1* and *un3* (Table 10).

The ability of the HSV-1 QGRS to fold into G-quadruplex was further assessed by EMSA analysis. After folding in the absence or in the presence of K^+, oligonucleotides were loaded onto native gels lacking or containing K^+ 100 mM, respectively. Even in the absence of K^+, all *gp054* sequences run markedly faster than their 22 bp-length control marker, indicating folding in these conditions (compare lanes a-f with lane M, Figure 4.1.4a). In particular, *gp054d* displayed the fastest mobility. This oligonucleotide also exhibited the highest T_m value (second transition) in the absence of K^+ (Table 10), confirming its inherent best aptitude to fold into G-quadruplex in the absence of K^+.

The 29 bp- and 28 bp-long sequences *un1* and *un2*, respectively, also migrated faster than the 22-long control marker (compare lanes 1-2 with lane M, Figure 4.1.4a), indicating effective folding. In the case of *un1*, its low solubility was responsible for the lower signal. In contrast, the 23 bp-long *un3* migrated as an unfolded oligonucleotide (compare lane 3 with lane M, Figure 4.1.4a), confirming its lower tendency to fold in the absence of K^+ (see lower G-score, Table 8, and lower stability, Table 10). In the presence of K^+ (Figure 4.1.4b), the *gp054* sequences maintained their G-quadruplex conformation as monomolecular species. In addition, lower migrating species, ascribable to intermolecular dimeric G-quadruplex forms, were also observable (lanes a-f, Figure 4.1.4b). *Un1* and *un2* remained essentially unvaried with respect to no K^+ conditions (lanes 1-2, Figure 4.1.4b), while *un3* in this case run faster than the 22 bp-long marker (lane 3, Figure 4.1.4b), indicating effective folding in the presence of the monovalent cation.

The ability of the HSV-1 GQRS to form intermolecular multimeric G-quadruplexes was further evaluated by EMSA with increasing concentrations of unlabelled oligonucleotide. As shown in Figure 4.1.5, the *gp054* sequences only were able to efficiently form dimer tetraplexes (Figure 4.1.5a), while *un2* and *un3* essentially did not fold into dimers even at high oligonucleotide concentration (Figure 4.1.5b,c).

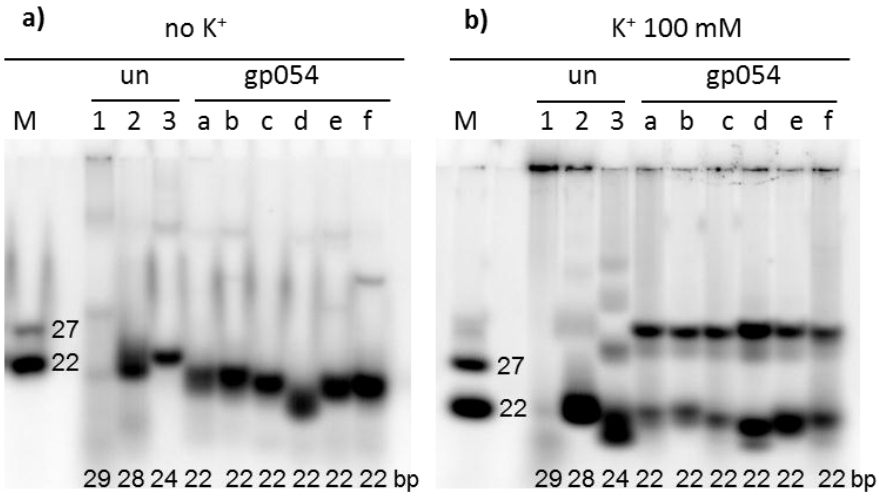

Figure 4.1.4 Electrophoresis mobility shift analysis (EMSA) of HSV-1 oligonucleotides. Oligonucleotides were folded a) in the absence or b) presence of K^+ and loaded on native gels lacking or containing K^+, respectively. The identity and length of each oligonucleotide are shown above and below the gel image, respectively. M indicate a marker lane loaded with two oligonucleotides with known length and unable to fold into secondary structure.

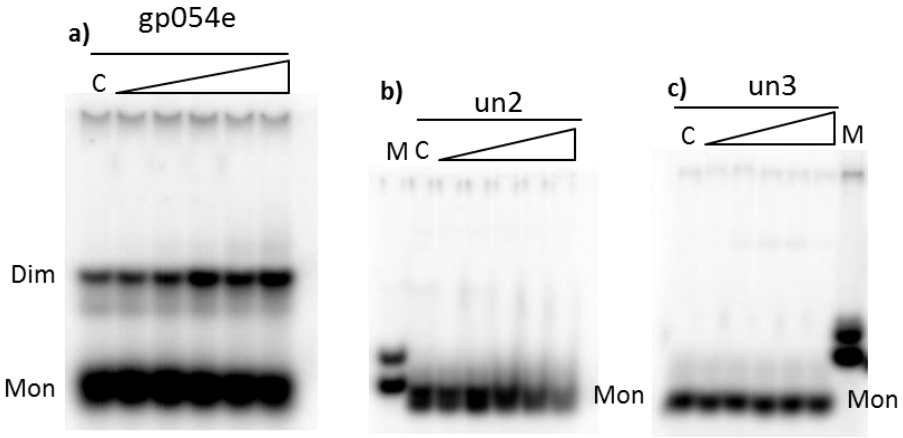

Figure 4.1.5 EMSA analysis of HSV-1 oligonucleotides. Each labelled oligonucleotide was incubated with increasing concentrations of the same unlabelled oligonucleotide and loaded on a native polyacrylamide gel. The identity of each oligonucleotide is shown above the gel image. M indicate a marker lane, loaded with two oligonucleotides with known length and unable to fold into secondary structure. C is a control lane, lacking the unlabelled oligonucleotide. The monomeric and dimeric forms are indicated as Mon and Dim.

4.1.3 Stabilization of HSV-1 G-4 forming sequences by G-quadruplex ligands

Given the capability of all the HSV-1 selected sequences to form highly stable G-quadruplex structures at several conditions, the G-quadruplex ligands BRACO-19 and TMPyP4 were next tested by CD analysis for their ability to bind the HSV-1 GQRS in the presence of K^+.

BRACO-19 converted the shoulder at 260 nm of the *gp054* oligonucleotides into a negative peak, therefore shifting the initial hybrid G-quadruplex towards an antiparallel-like

conformation (Figure 4.1.6a,b). Differently, a similar peak conversion is induced by TMPyP4 only in *gp054a*, *gp054b*, *gp054d* and *gp054e* (Figure 4.1.6b), but not in *gp054c* (Figure 4.1.6a) and *gp054b*.

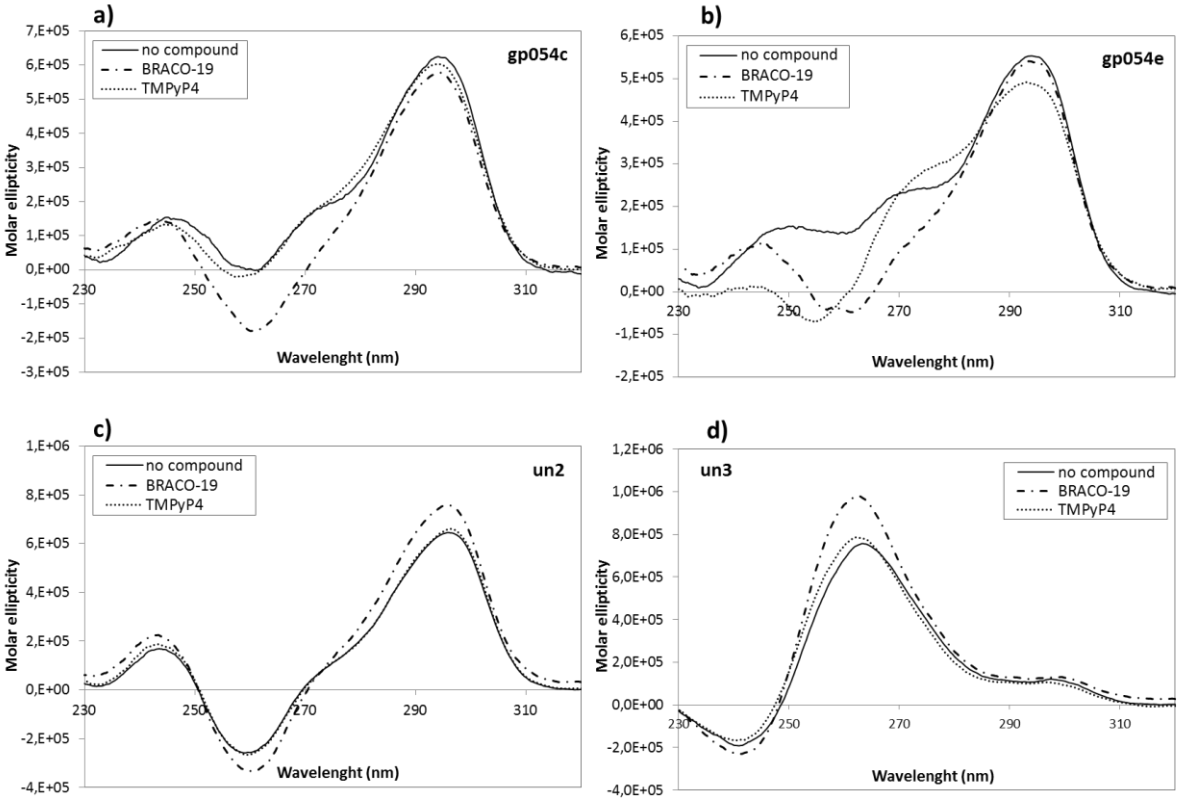

Figure 4.1.6 Biophysical analysis of HSV-1 G-quadruplex forming oligonucleotides in the presence of two G-quadruplex ligands: spectra of the a) *gp054c*, b) *gp054e*, c) *un2* and d) *un3* oligonucleotides (4 µM) in the presence or absence of BRACO-19 or TMPyP4 (16 µM) are shown.

During thermal unfolding, different conformations were sequentially stabilized by both BRACO-19 and TMPyP4. The initial antiparallel conformation of *gp054* oligonucleotides in the presence of both ligands was shifted to a parallel conformation at higher temperatures (Figure 4.1.7a,d). In contrast, *un2* and *un3* maintained their innate antiparallel and parallel, topologies, respectively in the presence of the compounds (Figure 4.1.6c,d) and during thermal unfolding (*un2* in Figure 4.1.7b,e; *un3* in Figure 4.1.7c,f). BRACO-19 further stabilized all HSV-1 oligonucleotides, increasing T_m to above 95°C.

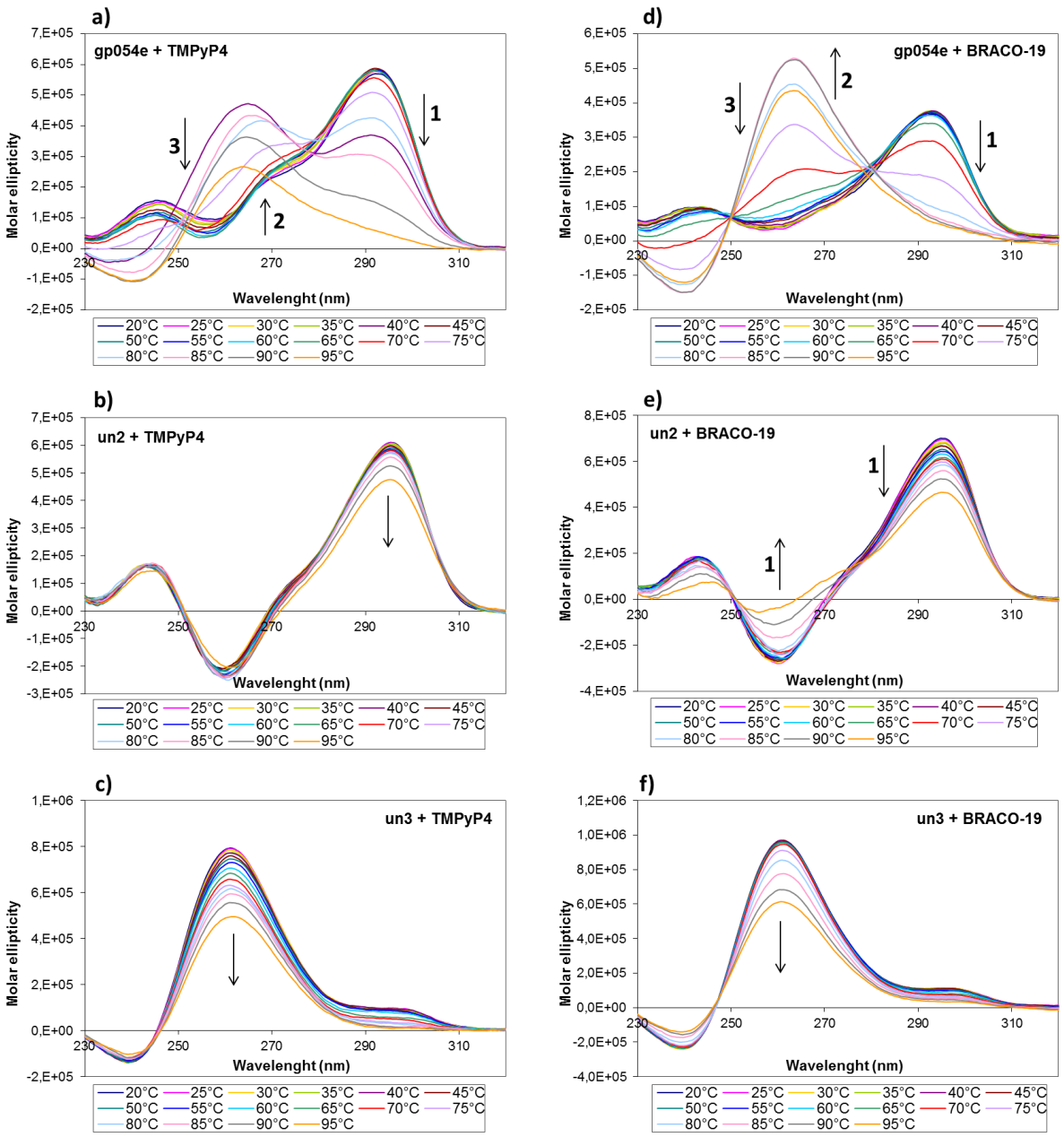

Figure 4.1.7 CD thermal denaturation analysis in the presence of TMPyP4 (a, b, c) or BRACO-19 (d, e, f): spectra of the indicated oligonucleotides (4 µM) during thermal unfolding, in the presence of the two G-quadruplex ligands (16 µM), are shown. Arrows indicate spectra progression during temperature increasing. Numbers indicate temporal sequence of spectra variation.

Additional evidence of the intrinsic stability of the identified HSV-1 G-quadruplexes and on the possibility of strongly stabilizing them with BRACO-19 was provided by the Taq polymerase stop assay. Extended *un2*, *un3*, *gp054a* and *g054d* sequence templates (Table 4) were designed to contain a primer-annealing region. Following primer annealing, the templates were treated with Taq polymerase in the absence/presence of K^+ and with increasing concentrations of BRACO-19. As shown in Figure 4.1.8, all G-quadruplex forming sequences except *un3* did stop the polymerase at the first G-rich region encountered by the

enzyme even in the absence of K^+ (lanes 1, *un2*, *gp054a*, *gp054d*, Figure 4.1.8). When the cation was added, a strong stop was observed in all G-quadruplex templates (lanes 2, *un2*, *un3*, *gp054a*, *gp054d*, Figure 4.1.8). Upon addition of BRACO-19 the intensity of the initial stop site dramatically increased (see lanes 3-4, *un2*, *un3*, *gp054a*, *gp054d*, Figure 4.1.8). Moreover, an additional stop site corresponding to a second G-rich region was observed in the *un2* template, possibly indicating the presence of multiple G-quadruplex structures. In contrast, a control sequence devoid of G-tracts that could fold into tetraplex did not show any stop site in the presence of K^+ and BRACO-19 (lanes 1-4, *non-G4*, Figure 4.1.8), indicating that the observed polymerase inhibition was G-quadruplex dependent and specific.

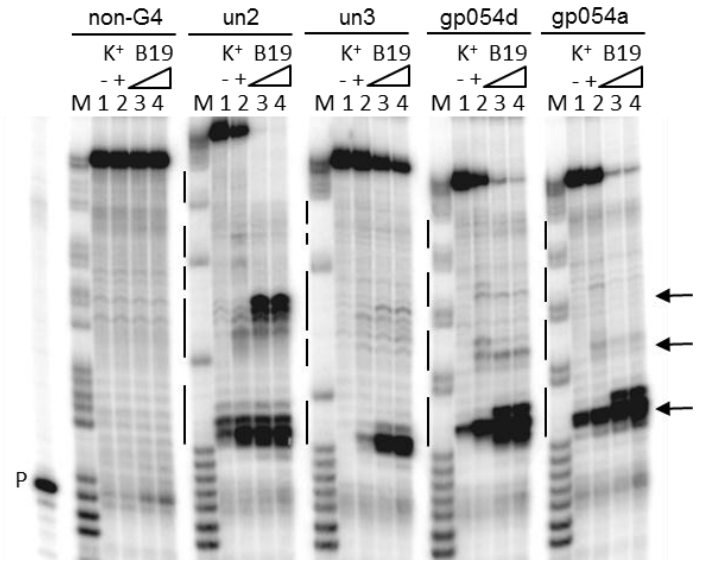

Figure 4.1.8 Taq polymerase stop assay on *un2*, *un3*, *gp054d* and *gp054a* DNA templates in the absence and presence of K^+ 10 mM (- and + lanes, respectively) and in the presence of increasing concentration of BRACO-19 (0.5 µM, 1 µM) (B19 lanes). A non-G-quadruplex template (non-G4 lanes) was also used as negative control. P indicates primer. RT pausing sites are indicated by arrows. G clusters are shown aside each gel image.

4.1.4 Antiviral property of G-quadruplex ligands against HSV-1

Once demonstrated that selected putative HSV-1 G-quadruplex forming sequences can effectively fold into stable G-quadruplex structures, which are further stabilized by K^+ and G-quadruplex ligands, we next assayed the commercially available compounds, BRACO-19 and TMPyP4, for antiviral activity. Given the differential effect on HSV-1 replication cycle, the two G-quadruplex ligands are discussed individually.

TMPyP2, a porphyrin derivative which shares chemical features, i.e. a large aromatic surface and cationic moieties, with BRACO-19 and TMPyP4, but displays a different G-quadruplex

binding mode and markedly lower G-quadruplex binding affinity (Han, et al., 2001), (Le, et al., 2013), was used as a negative control.

4.1.5 Antiviral activity of BRACO-19 on HSV-1

Given the ability of BRACO-19 to recognize and stabilize HSV-1 G-quadruplexes, we tested the possibility that it displayed antiviral activity.

Cytotoxicity of BRACO-19 was assessed on Vero cells, a monkey kidney epithelial cell line which sustains HSV-1 infection (Figure 4.1.9).

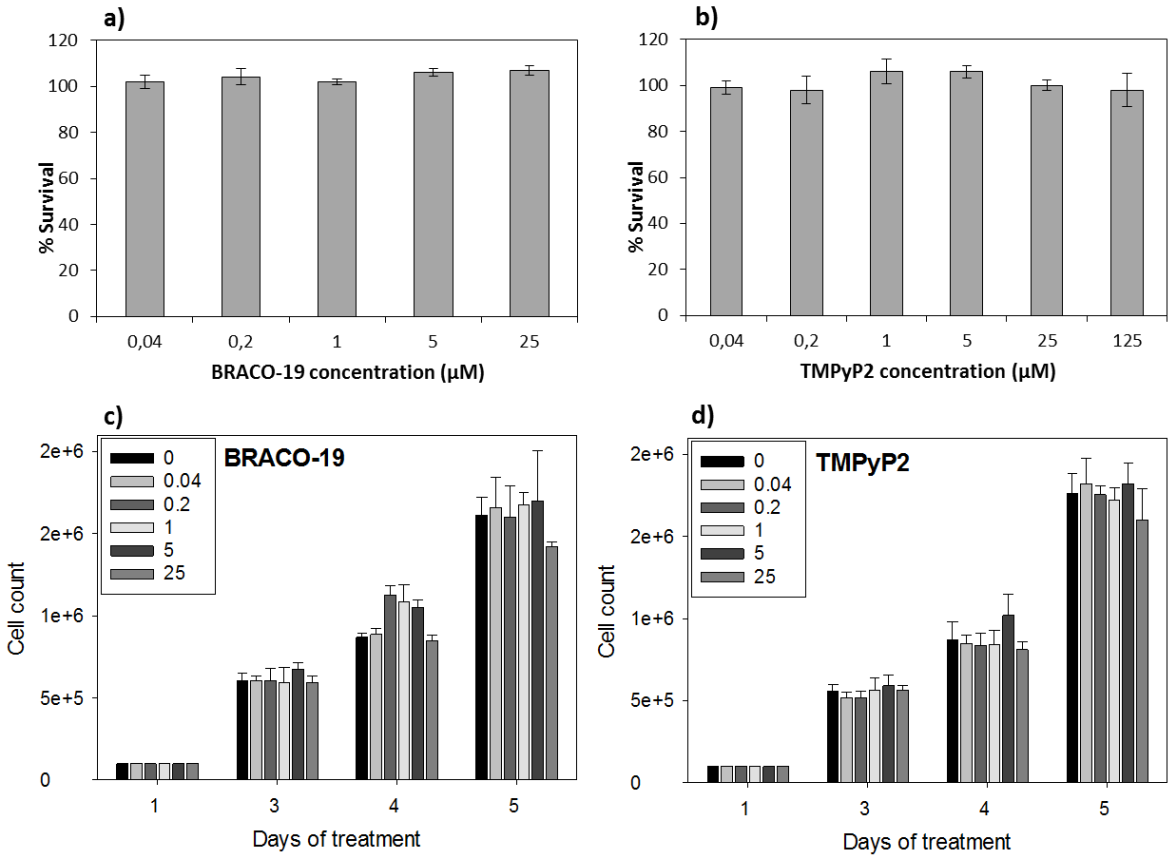

Figure 4.1.9 Cytotoxicity of BRACO-19 and TMPyP2 (µM). MTT assay with a) BRACO-19 (0.04-25 µM) or b) TMPyP2 (0.04-125 µM). b), Growth curve analysis, obtained by treating Vero cells with c) BRACO-19 or d) TMPyP2 (0.04-25 µM).

BRACO-19 was non-cytotoxic up to 25 µM, the highest tested dose, (cytotoxic concentration required to reduce the cell number by 50%, CC_{50} > 25 µM) (Figure 4.1.9a), whereas TMPyP2 was non-cytotoxic up to 125 µM (CC_{50} > 125 µM) (Figure 4.1.9b). In addition, they did not impair cell growth up to 5 days of daily-treatments (Figure 4.1.9c,d). Increasing concentrations of BRACO-19 or TMPyP2 were added to Vero cells infected with HSV-1

strain F (MOI 1), and supernatants were collected at 24 h.p.i. Infectious viruses present in the supernatants were quantified by plaque assay.

As shown in Figure 4.1.10, BRACO-19 demonstrated an effect at 200 nM and its antiviral activity increased up to 70% at 25 μM (EC_{50} = 10 μM). The compound TMPyP2, used as reference, was inactive up to 1 μM, while it showed 50% inhibition at the highest concentration (EC_{50} = 25 μM) (Figure 4.1.10).

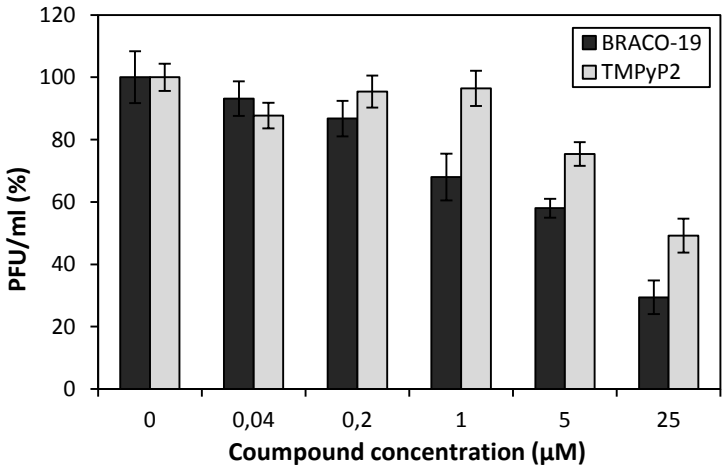

Figure 4.1.10 Plaque assay: infected cells (MOI 1) were treated with increasing concentrations (0.04 μM – 25 μM) of BRACO-19 and TMPyP2; supernatants were collected at 24 h.p.i. and the number of plaque forming units was determined.

4.1.5.1 Effect of BRACO-19 on viral entry

It has been shown that HSV-1 fusion to the cells is mediated by interaction of several viral glycoproteins, most importantly gB and gC (Herold, et al., 1991), with heparan sulfate, a polysaccharide present on the cell surface (Reske, et al., 2007). BRACO-19, as most G-quadruplex binding molecules, is a polycationic agent, the observed antiviral activity might be mediated by the interaction of BRACO-19 with the negatively charged heparin sulfate, thus preventing virus attachment to the cells.

To test this hypothesis, BRACO-19 was added at different times post-infection until the virus had completed its fusion to the cell and entry (i.e. 1 h.p.i.) (Sodeik, et al., 1997). In this time range we did not observe any difference to the activity obtained by treating the cells 1 h pre-infection (Figure 4.1.11), indicating that, despite its polycationic nature, BRACO-19 does not act by inhibiting virus fusion to the cells.

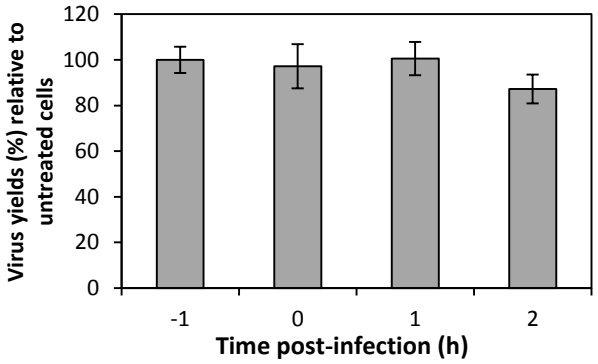

Figure 4.1.11 Effect of BRACO-19 on virus entry into the cells. Cells were treated with BRACO-19 (25 μM) at various time points (-1, 0, 1, 2 h) relative to infection with HSV-1 strain F at a MOI of 1. After an infection of 1 h at 37°C, cells were washed and maintained in culture medium. At 30 h.p.i. supernatants were collected and titrated by plaque assay. Virus yields are given as % relative to the untreated control.

4.1.5.2 Mechanism of action of BRACO-19 against HSV-1

Because large portions of the viral genome could fold into G-quadruplex structures and could be stabilized by BRACO-19, we investigated if compound treatment impaired polymerase processing at the viral genome. To test this hypothesis, we extracted HSV-1 DNA from a viral stock and treated it with increasing concentrations of BRACO-19 and TMPyP2. The *gp054* sequences (within the UL36 coding region) and the *un* G-rich tracts (in the TR_L region) were amplified by standard PCR using Taq polymerase and primers (Table 4) that annealed to the relevant G-rich flanking regions. A non-G-rich/non-G-quadruplex forming region (in the UL36 coding region) was also amplified as negative control sequence.

Amplified DNA corresponding to *gp054* and *un* G-quadruplex forming regions decreased in a concentration-dependent manner in the presence of BRACO-19 (Figure 4.1.12a, *un* and *gp054* with BRACO-19). In contrast, BRACO-19 was not able to disrupt polymerase processing in the non-G-quadruplex forming region (Figure 4.1.12a, non-G4 with BRACO-19) and TMPyP2 had no effect on enzymatic activity both in the G-quadruplex and non-G-quadruplex forming regions (Figure 4.1.12a, *un*, *gp054* and non-G4 with TMPyP2). For quantification purposes, HSV-1 DNA extracted from infected cells treated with increasing amounts of BRACO-19 and TMPyP2 were amplified by real-time PCR and quantified by SYBR® green. As shown in Figure 4.1.12b, amplification of the G-quadruplex forming region (*gp054*) was inhibited up to 40% (with respect to the non-treated control, 100%) in the presence of BRACO-19 (4 μM), while no effect was detected in the non-G-quadruplex forming region, confirming lack of activity of the compound against the polymerase enzyme.

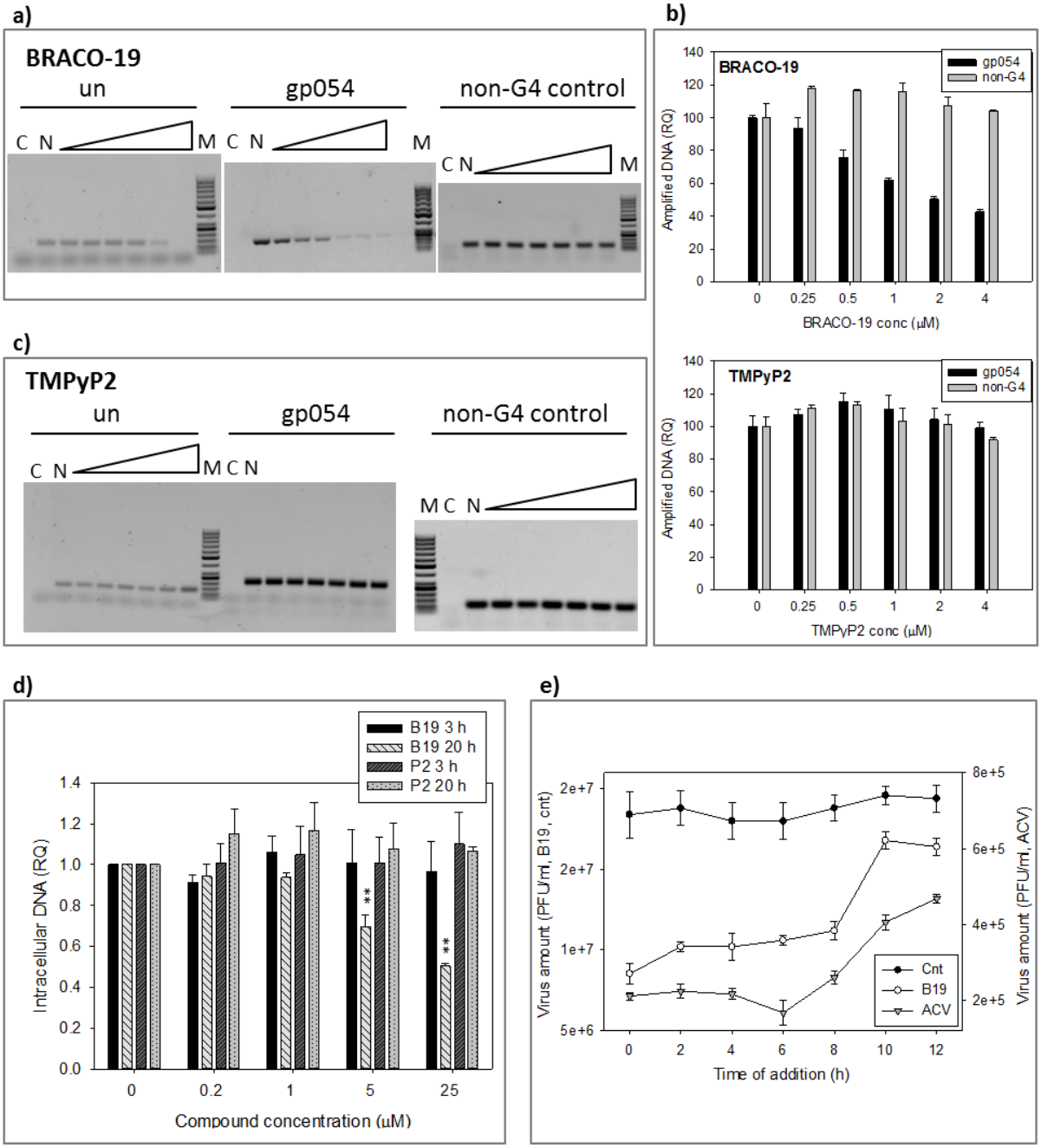

Figure 4.1.12 Inhibition of HSV-1 DNA replication by BRACO-19. a), b), c) Inhibition of DNA replication in G-quadruplex regions *in vitro*. *gp054* and *un* G-quadruplex regions were elongated using the Taq polymerase stop assay, in the presence of increasing concentration of a) BRACO-19 or c) TMPyP2 (2-fold dilutions from 16 μM to 0.25 μM). A non-treated sample (lane N) and a sample without DNA (lane C) were used as negative controls. M indicates the marker. b) Real-time PCR on a *gp054* G-quadruplex sequence and a control non-G-quadruplex region was performed in the presence of BRACO-19 or TMPyP2 (2-fold dilutions from 4 μM to 0.25 μM). Quantification of amplified products was obtained by SYBR® green detection. HSV-1 DNA was extracted from HSV-1-infected Vero cells. In all cases, HSV-1 DNA was extracted from HSV-1-infected Vero cells.
d) Quantification of intracellular DNA amounts obtained from infected cells at 3 h and 20 h.p.i., treated with increasing concentration of BRACO-19 (B19) and TMPyP2 (P2), with $n \geq 3$, mean ± s.d., Student's t-test, $^{**}P < 0.01$. RQ are Relative Quantities. DNA was detected using specific IE-gene, E-gene or L-gene primers sequences (Table 3). e) Time-of-addition assay of BRACO-19. Vero cells were infected with HSV-1 strain F and BRACO-19 was added at different time points after infection. Virus was collected at 30 h.p.i. and quantified by plaque assay. The activity of BRACO-19 was compared with that of the negative control (non-treated infected cells) and of ACV as reference drugs. Data representative of two independent experiments.

As expected, TMPyP2 was also inactive against both G-quadruplex and non-G-quadruplex forming sequences. This data demonstrate that BRACO-19 specifically interact with G-quadruplex forming regions in the HSV-1 genome *in vitro* and inhibit polymerase processing likely due to the steric hindrance caused by multiple tetraplex structures stabilized by the ligand.

We therefore tested whether viral DNA replication was impaired by BRACO-19 in infected cells. HSV-1 infected cells (MOI 1) were treated with different amounts of BRACO-19 or TMPyP2 and intracellular viral DNA was extracted post-infection and quantified by real-time PCR. DNA extraction was performed at three different time points likely before (3 h.p.i.), during (8 h.p.i.) and after (20 h.p.i.) the viral DNA was replicated in cells by the viral replication machinery. As shown in Figure 4.1.12d, BRACO-19 reduced intracellular viral DNA levels to 50% of the untreated control (100%) at the highest concentration only at 8 h.p.i. and 20 h.p.i. (Figure 4.1.12d). In contrast, BRACO-19 at 3 h.p.i. and TMPyP2 did not affect viral DNA amounts. In addition, BRACO-19 at 8 and 20 h.p.i. did not modify DNA amounts of a control cellular gene (Figure 4.1.12d). These results indicate that BRACO-19 exerts its antiviral activity by acting specifically at the viral DNA level.

To further define the viral step affected by the compound, a time-of-addition experiment was set up (Daelemans, et al., 2011). This experiment determines how long the addition of a compound can be postponed before its antiviral activity is lost in a single replication cycle. Thus, HSV-1 replication is blocked up to a time point corresponding to the occurrence of the last viral step targeted by the drug, which can be revealed comparing the antiviral effect of the test compound with that of a reference compound with established mode of action in the time frame of replication events. Cells were infected at an MOI of 1, and BRACO-19 was added each 2 hours, over 12 h after infection, as indicated in Figure 4.1.12e. Supernatants were collected at 30 h.p.i. and virus replication was monitored by plaque assay. ACV was used as reference compound targeting viral DNA replication (James & Prichard, 2014). When treating infected cells with BRACO-19, a sharp increase in virus amounts (PFU/ml) was observed between 8 and 10 h.p.i., indicating that the compound is active at events that occur in this time range. Interestingly, ACV showed a similar increase between 8-12 h.p.i.

Since ACV acts by inhibiting the viral DNA polymerase during DNA replication, these data confirm the activity of BRACO-19 during early events of the virus life cycle, including direct inhibition of the replication machinery or reduction of functions in trans, such as the activity of promoters/genes that are involved in virus DNA replication (Figure 4.1.12e and Figure 4.1.13).

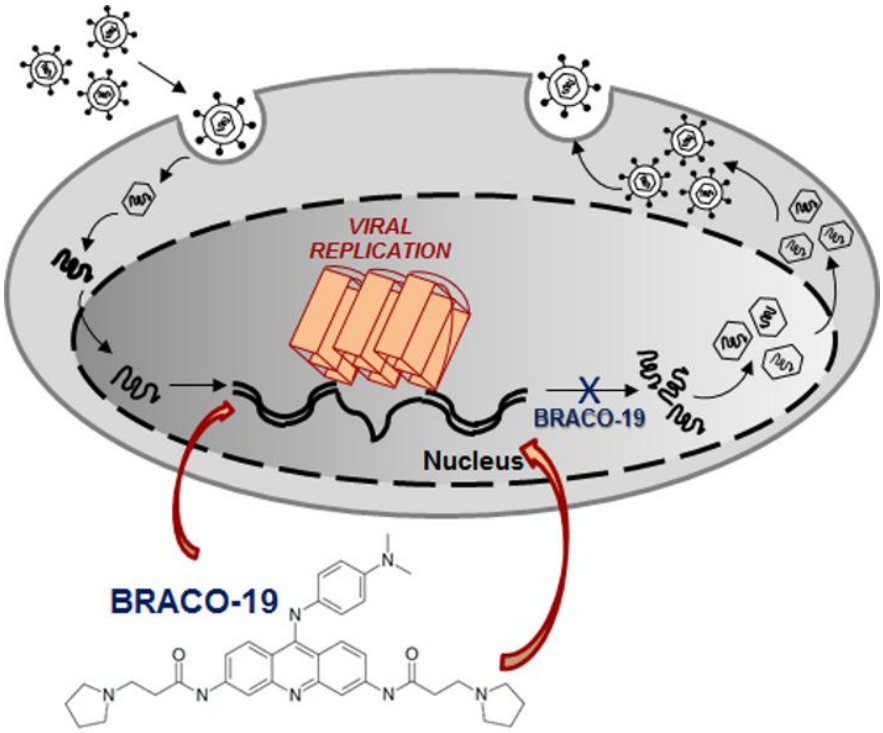

Figure 4.1.13 Scheme of the site of action of BRACO-19 on HSV-1 infected cell.

4.1.6 Antiviral activity of TMPyP4 on HSV-1

We investigated the possibility that a second G-quadruplex ligand, TMPyP4, displayed antiviral activity against HSV-1.

Cytotoxicity of TMPyP4 was first assessed on Vero cells with MTT assay. The compound did not affect cell viability up to 100 μM, the highest tested dose (CC_{50} > 100 μM) (Figure 4.1.14a). Moreover, cell growth was not impaired by this compound up to 5 days, following daily-treatment (Figure 4.1.14b). Increasing concentrations of TMPyP4, or TMPyP2, were added to Vero cells infected with HSV-1 strain F (MOI 1). Supernatants were collected at 24 h.p.i. Infectious viruses present in the supernatants were quantified by plaque assay.

Interestingly, the antiviral activity of TMPyP4 was even higher than that of BRACO-19. Similarly to BRACO-19, TMPyP4 demonstrated an effect of 22% at 200 nM (Figure 4.1.14c), but its antiviral activity increased up to 90-100% at 1 μM (EC_{50} = 600 nM). A complete inhibition was observed at higher concentrations (5 μM, 25 μM) (Figure 4.1.14c, 4.1.18a).

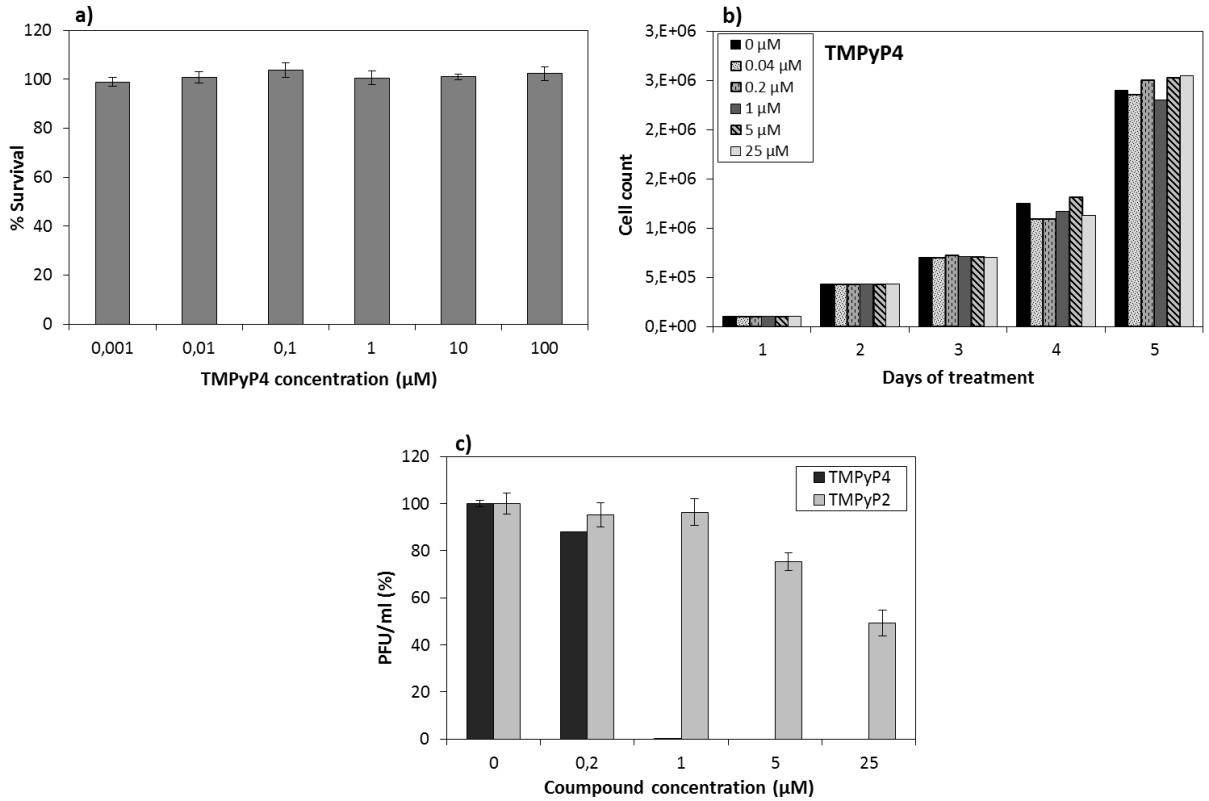

Figure 4.1.14 a) Cytotoxicity of TMPyP4 assayed using MTT assay (0.001-100 μM). b) Growth curve analysis, obtained by treating Vero cells with TMPyP4 (0.04-25 μM). c) Plaque assay: infected cells (MOI 1) were treated with increasing concentrations (0.2 μM – 25 μM) of TMPyP4 and TMPyP2; supernatants were collected at 24 h.p.i. and the number of plaque forming units was determined.

4.1.6.1 Entry and viral replication as possible TMPyP4-mediated mechanisms of action

Once proved the antiviral property of TMPyP4 on HSV-1, a number of additional assays were carried out to study the mechanism of action exploited by this porphyrin.

To test whether TMPyP4 influence viral entry, HSV-1 (strain F) infected Vero cells were treated with the compound (5, 25 μM) at different times post-infection until the virus had completed its fusion to the cell and entry. Similarly to BRACO-19, in this time range we did not observe any difference to the activity obtained by treating the cells 1 h pre-infection (Figure 4.1.15). The result indicates that TMPyP4 does not affect the attachment of the virus to the host cells.

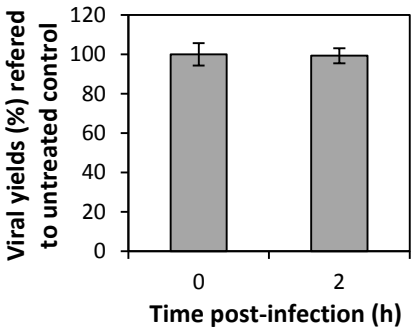

Figure 4.1.15 Effect of TMPyP4 on virus entry into the cells. Cells were treated with TMPyP4 (5 μM) at various time points (0, 2 h) relative to infection with HSV-1 strain F at a MOI of 1. After an infection of 1 h at 37°C, cells were washed and maintained in culture medium. At 30 h.p.i. supernatants were collected and titrated by plaque assay. Virus yields are given as % relative to the untreated control.

Second, the hypothesis that TMPyP4 impaired viral replication was examined. As described above, HSV-1 DNA was isolated from a viral stock and treated with increasing concentrations of TMPyP4 (0.1-3.2 μM). Using Taq polymerase stop assay, we demonstrated that TMPyP4 was able to prevent the amplification of G-rich regions in a dose-dependent manner *in vitro* (Figure 4.1.16a). The primer sequences used to amplify by standard PCR these regions, *gp054* sequences (within the UL36 coding region) and the non-G-rich/non-G-quadruplex forming region (in the UL36 coding region), are listed in Table 4.

Similarly to the effect observed treating HSV-1 DNA with increasing concentrations of BRACO-19 (Figure 4.1.12a,b), TMPyP4 was proved to strongly affect the activity of the Taq enzyme in a concentration-dependent manner, during the elongation of the G-4 containing regions *gp054* (Figure 4.1.16a). A non-G-rich/non-G-quadruplex forming sequence was also treated with TMPyP4 and amplified, as a negative control sequence. As previously observed with BRACO-19 and TMPyP2 (Figure 4.1.12a,b), TMPyP4 was not capable to disrupt polymerase processing in the non-G-quadruplex region (Figure 4.1.16b).

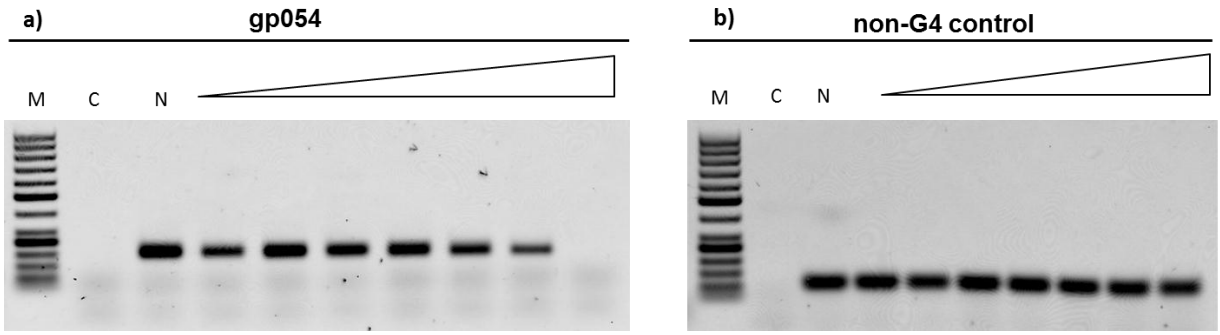

Figure 4.1.16 Taq polymerase stop assays on HSV-1 DNA treated with increasing concentrations of TMPyP4 (0.1-3.2 µM). a) Gradual TMPyP4-induced inhibition of the Taq-enzyme processing. b) Defective amplification of a non G-4 region, within the HSV-1 genome, previously treated with increasing concentration of TMPyP4 (0.1-3.2 µM).

We next tested if viral DNA replication was impaired by TMPyP4 in infected cells, as observed with BRACO-19. To assess this hypothesis, HSV-1 infected cells (MOI 1) were treated with increasing concentration of TMPyP4 (0.04-25 µM), subsequently intracellular viral DNA was extracted at 3, 8, 20 h.p.i. and quantified by real-time PCR. In comparison with non-treated infected cells used as control, no decrease of viral DNA was detected after TMPyP4 treatment (Figure 4.1.17), thus suggesting that viral DNA replication is not affected by TMPyP4.

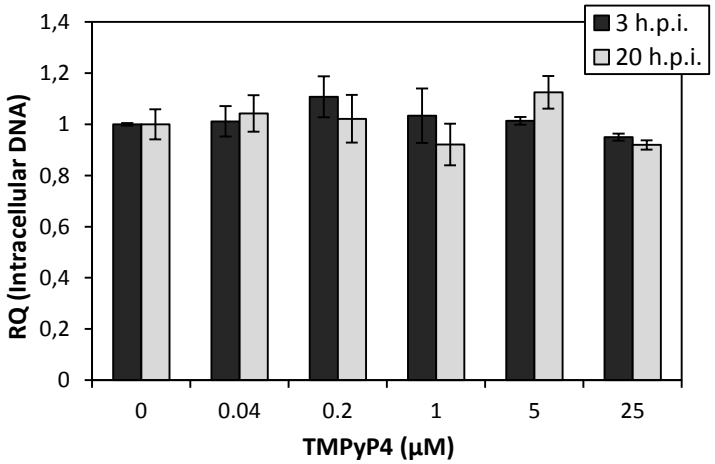

Figure 4.1.17 Quantification of intracellular DNA amounts obtained from infected cells at 3 h and 20 h.p.i., treated with increasing concentration of TMPyP4 (0.04-25 µM), with $n \geq 3$, mean ± s.d., Student's t-test, $^{**}P < 0.01$. RQ are Relative Quantities.

4.1.6.2 Mechanism of action of TMPyP4 against HSV-1

Although the extraordinary inhibitory capability displayed by TMPyP4 on HSV-1, viral entry and DNA replication were demonstrated not to be affected by the compound. We, therefore, hypothesized that the intracellular HSV-1 DNA was not fully infectious or included in mature

virions still entrapped within the cytoplasm of cells. To test this hypothesis, we carried out two different types of experiments.

First, Vero cells were infected with HSV-1 (F strain) at a MOI of 1 PFU/ml, treated with increasing concentrations of TMPyP4, as described above. At 24 h.p.i., both supernatants and cell content were conserved and analysed in parallel. Cells were lysed with repeated freeze/thaw cycles to be tested by plaque assay along with the supernatants (Figure 4.1.18).

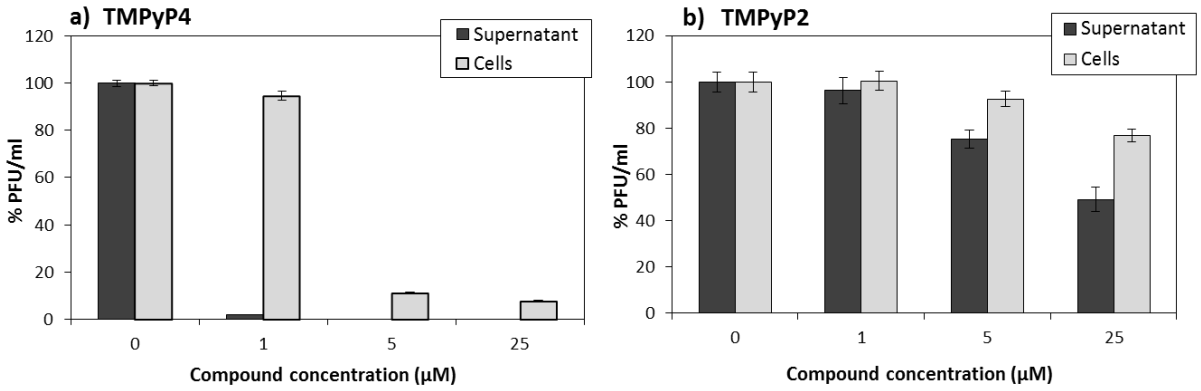

Figure 4.1.18 Plaque assay: infected cells (MOI 1) were treated with increasing concentrations (1 μM – 25 μM) of a) TMPyP4 and b) TMPyP2, as negative control. Supernatants were collected at 24 h.p.i. and the number of plaque forming units was determined (dark grey). In parallel**,** infected and treated Vero cells were lysed with repeated freeze/thaw cycles, and intracellular HSV-1 was titrated (light grey).

As previously mentioned, plaque assay from supernatants showed a TMPyP4-induced inhibitory effect of up to 90% at 1 μM, whereas the virus was completely knocked down at higher concentrations (Figure 4.1.18a). At the same TMPyP4 concentration (1 μM), on the contrary, intracellular HSV-1 levels were approximately equal to untreated cells, used as a control (Figure 4.1.18a). However, HSV-1 inhibition within the cells was observed at higher concentrations (5, 25 μM), thus suggesting that multiple sites of action on the virus are affected by TMPyP4. Moreover, these data suggest that TMPyP4 induced trapping of fully infectious HSV-1 particles in the cytoplasm of cells.

TMPyP2 did not display a pronounced activity on the intracellular HSV-1, in comparison with the supernatants in which, once again, it was inactive up to 1 μM but it showed a 50% HSV-1 inhibition at 25 μM (Figure 4.1.18b).

We next performed transmission electron microscopy (TEM) experiments to observe the precise location of HSV-1, after the treatment with TMPyP4. Following the standard protocol, Vero cells were infected with HSV-1 strain F (MOI 1) and treated with TMPyP4 (0 μM as a control, and 1, 5, 25 μM). At 24 h.p.i., cells were fixed in 2.5% glutaraldehyde and pellets were appropriately processed for TEM analysis.

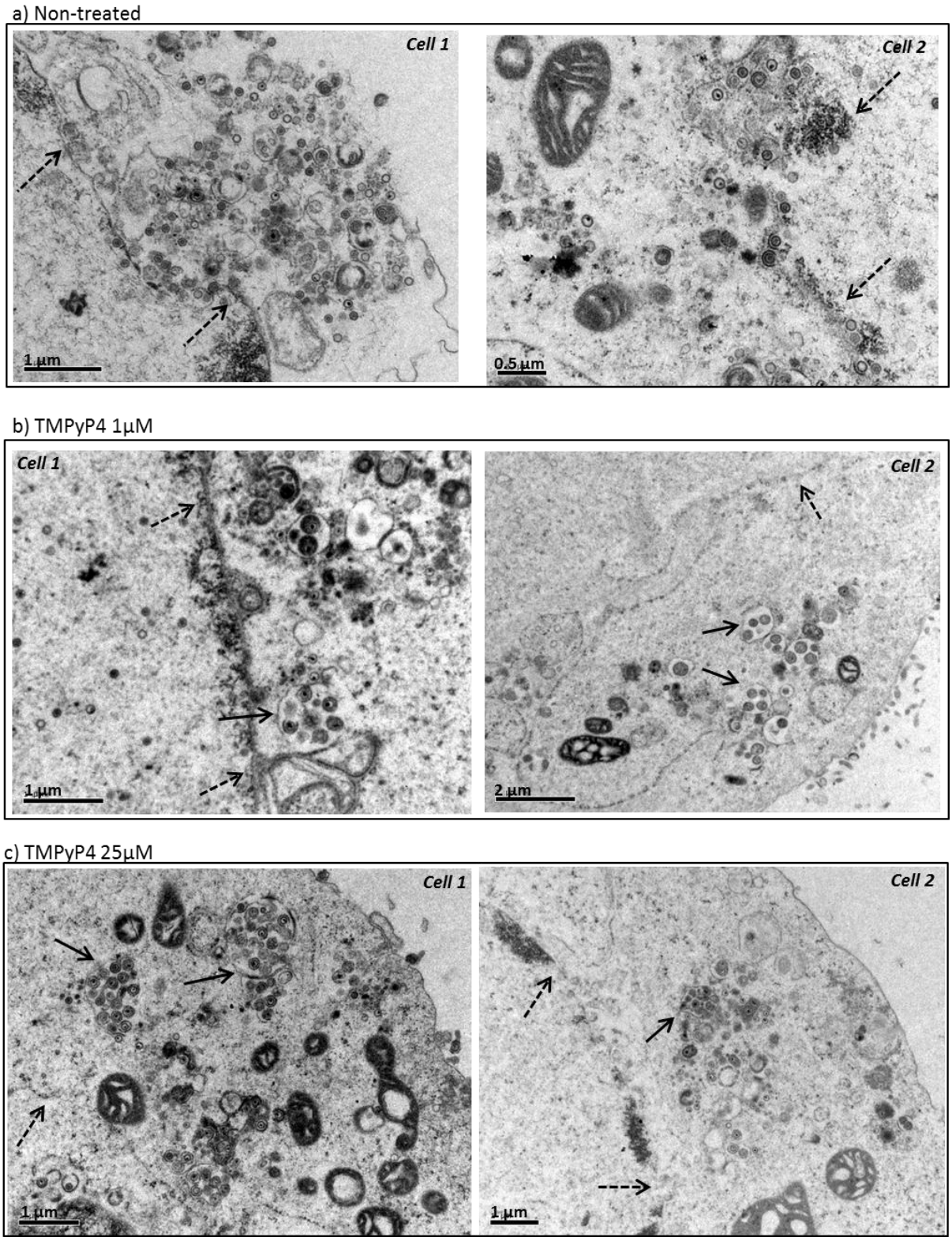

Figure 4.1.19 Transmission electron microscopy analysis. a) Non-treated/infected Vero cells, and infected cells treated with b) 1 µM or c) 25 µM of TMPyP4 are shown. In the cytoplasm of infected/treated cells, HSV-1-containing vesicles are indicated with solid black arrows. Dashed black arrows indicate the nuclear membrane. Two cells for each condition are shown.

Compared to non-treated infected sample used as a control (Figure 4.1.19a), large vesicles enclosing groups of HSV-1 particles were observed within the cytoplasm of infected/treated cells (1 µM in Figure 4.1.19b, 25 µM in Figure 4.1.19c). All these vesicles, characterized by their own membrane, were located nearby the nuclear membrane.

Interestingly, HSV-1 particles appeared properly assembled, a DNA-containing dark was is visible as well as capsid and tegument in the nucleus and/or the cytosol area. Nevertheless, several immature HSV-1 virions were also observed, some of them with an empty core (Figure 4.1.19).

An analogous experimental approach was employed for TMPyP2 and even BRACO-19, to verify whether these compounds were also capable to form such particular vesicular formations.

At 1 µM, TMPyP2 was unable to induce the formation of such HSV-1 aggregates. In addition, the principal steps of the viral cycle appeared in compliance with the literature, and both extensive nuclear egress and cell egress of mature virions were observed (Figure 4.1.20a). However, very few HSV-1 containing-vesicles appeared at 25 µM of TMPyP2. This behavior could be ascribable to the partial G-quadruplex binding capability of TMPyP2 (Figure 4.1.20b). Indeed, as mentioned above, TMPyP2 is a porphyrin derivative, conformational isomer of TMPyP4, thus sharing a number of chemical features with BRACO-19 and TMPyP4 (Han, et al., 2001), (Le, et al., 2013).

In 1999, for example, the team of Prof. Lawrence Hurley investigated the interactions of TMPyP4 and TMPyP2 with an antiparallel quadruplex DNA ($[GGGTTA]_4$). It was discovered that both compounds can bind to G-quadruplex with a differential binding mode. TMPyP4 binds to the intramolecular quadruplex DNA by stacking externally to the guanine tetrad at the GT step, while TMPyP2 binds predominantly to the same G-4 DNA structure via external binding to the TTA loop (Han, et al., 1999). Therefore, even if TMPyP2 acts as a G-quadruplex ligand, its extremely lower binding affinity towards the G-quadruplex still makes it the compound of choice to be used as negative control. However, it must be kept in mind that some of the observed effects might be due to the residual G-quadruplex binding activity.

As a further proof of the differential mechanism of action displayed by TMPyP4 and BRACO-19, TEM analysis was performed on infected Vero cells treated with several concentration of BRACO-19 (5, 25 µM). BRACO-19 did not showed HSV-1 containing vesicles (infected/untreated cells as control in Figure 4.1.21a; infected/treated cells with BRACO-19 at 5 µM in Figure 4.1.21b and 25 µM in Figure 4.1.21c).

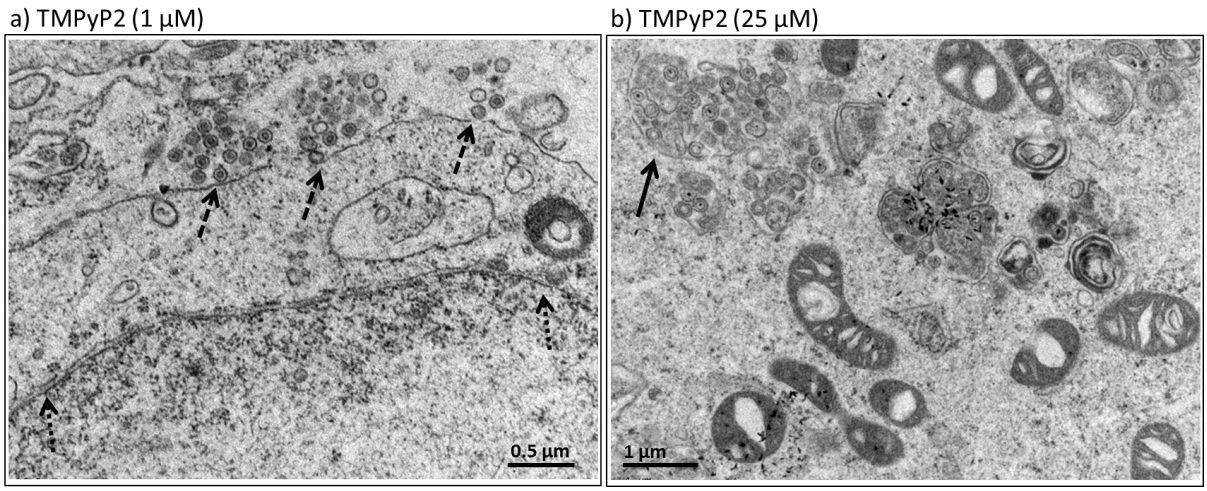

Figure 4.1.20 Transmission electron microscopy analysis. TMPyP2-treated/infected Vero cells, at a concentration of a) 1 µM or b) 25 µM, are shown. HSV-1-containing vesicles are indicated with solid black arrows (b). Dashed black arrows indicate cell egress, dotted black arrows indicate the nuclear membrane (a).

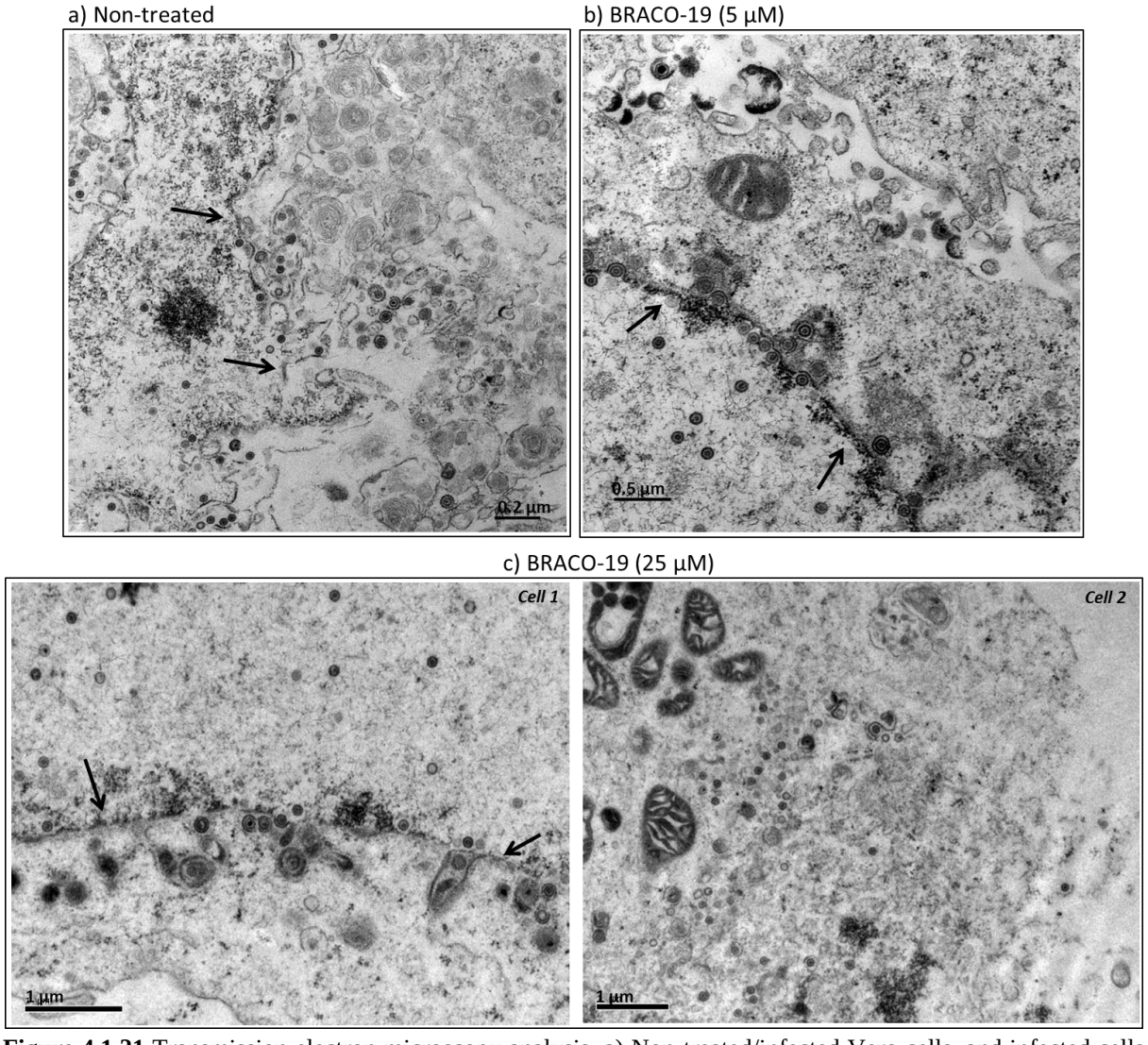

Figure 4.1.21 Transmission electron microscopy analysis. a) Non-treated/infected Vero cells, and infected cells treated with b) 5 µM or c) 25 µM of BRACO-19 are shown. Solid black arrows indicate the nuclear membrane.

Overall, we proved that TEM data are in accordance to plaque assay experiments, for both TMPyP4 and TMPyP2. Given the 80-90% HSV-1 inhibition in the supernatants (Figure 4.1.18a), the treatment of infected cells with TMPyP4 (1 μM) impaired the release of mature HSV-1 virions from the cytoplasm of Vero cells. TEM revealed that HSV-1 is detectable within multivesicular bodies in the cells (Figure 4.1.19b,c, solid arrows). Consequently, these data suggest that TMPyP4 could have a role in the HSV-1 maturation and/or egress (Brown, et al., 1994). The similarities of the HSV-1 including vesicles to lysosomal vesicles made us further hypothesis the involvement of a defensive cellular mechanism, better known as autophagy, which is likely TMPyP4-induced.

Autophagy is postulated to play a role in antiviral innate immunity. It is an evolutionarily conserved process in which the cell packages cytosolic constituents in double-membrane vesicles and delivers them to the lysosome for degradation (Orvedahl, et al., 2007). So far, herpesviruses have developed strategies to downregulate autophagy, although the varicella-zoster virus does not seem to encode any autophagy inhibitors (Takahashi, et al., 2009).

HSV-1-encoded neurovirulence protein ICP34.5, the viral homologs of *bcl-2* of Kaposi's sarcoma herpesvirus, murine gammaherpesvirus 68 (γHV-68) (Sinha, et al., 2008) (Pattingre, et al., 2005), and the human cytomegalovirus (HCMV) TRS1 protein have all been shown to block the formation of autophagosomes through their interactions with the autophagy protein Beclin 1.

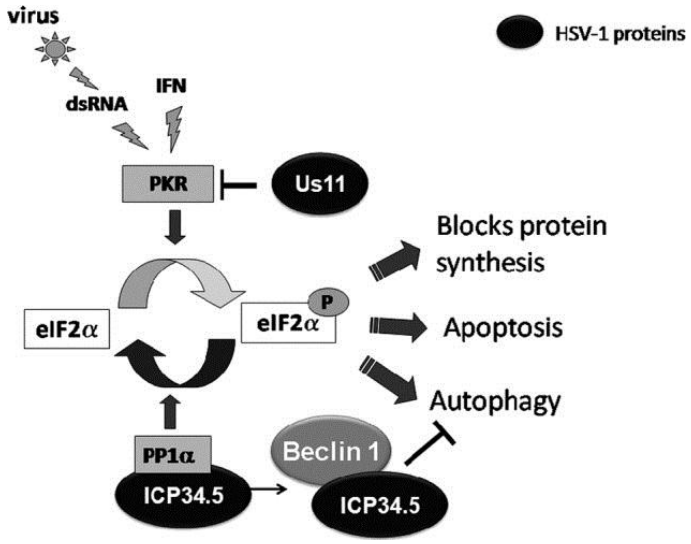

Figure 4.1.22 Schematic representation of PKR/eIF2α pathway in HSV-1 **(Lussignol, et al., 2012)**.

Beclin 1 is a critical component of several highly regulated complexes that control the formation and maturation of autophagosomes (Lussignol, et al., 2012). Moreover, the protein

kinase RNA activated (PKR) is also known to be activated by many viruses because dsRNA is a frequent by-product of viral replication or a product of overlapping transcription from the compact genomes of DNA viruses. PKR activation blocks viral protein synthesis and, consequently, stifles viral production. HSV-1 protein ICP34.5 interacts with the cellular phosphatase-1α (PP1α) to mediate the dephosphorylation of the eukaryotic initiation factor 2α (eIF2α), thus antagonizing the PKR signaling pathway and inhibiting its autophagy function (Figure 4.1.22) (Orvedahl, et al., 2007), (Radtke, et al., 2013), (Lussignol, et al., 2012). As a consequence, lack of the HSV-1 protein ICP34.5 can stimulate autophagy.

Importantly, the *un3* cluster corresponds to the promoter of the gene $\gamma_1$34.5 that encodes the ICP34.5 protein (Chou & Roizman, 1986). The $\gamma_1$34.5 gene itself is located in the inverted repeats of the *b* sequence of the L component and it is present in two copies per genome (Ackermann, et al., 1986). HSV-1 mutants that fail to express the $\gamma_1$34.5 protein are incapable of multiplying and causing encephalitis in experimental animal models (Chou, et al., 1990). On the contrary HSV-1 mutants, lacking both copies of the $\gamma_1$34.5 gene, can normally replicate in some permissive cell lines as Vero cells (Chou & Roizman, 1994).

Very interestingly, the DR2 segment present in the *a* region, which overlaps exactly with our *un3* sequence, has been shown to form an unwound, nuclease sensitive conformation of non-B DNA, called anisomorphic DNA (Sarisky & Weber, 1994), that entirely matches with the G-quadruplex structure presented in this work. Notably, this region has been shown to mediate transcriptional repression only in its anisomorphic DNA conformation (i.e. the G-quadruplex), which perfectly correlates with the notion that G-quadruplex act as transcriptional silencers. Many examples of transcriptional repressors have been provided in human cells (Cogoi & Xodo, 2006), (McLuckie, et al., 2011), (Qin, et al., 2010).

In addition, the DR2 segment (*un3*) has been shown to be bound by the eukaryotic transcription factor SP1 (Chung, et al., 1995), which again has been involved in G-quadruplex-mediated regulation of transcription in human cells (Todd & Neidle, 2008).

We have recently demonstrated a G-quadruplex-mediated transcriptional silencing activity in a SP1 binding region of the HIV-1 long terminal repeat promoter (Perrone, et al., 2013a). It is also interesting to note that the *un3* G-quadruplex was inherently less stable than the other tested sequences (Table 8, 9). This fact raises the possibility that the DNA in this region is processed by proteins that alternately stabilize the G-quadruplex and B-form, which in turn function as a switch to activate or turn off transcription. A similar behavior has been reported for *c-myc* and KRAS oncogene promoters where different proteins recognize and stabilize the

folded and unfolded sequence (Brooks, et al., 2010), (Paramasivam, et al., 2009), (Cogoi, et al., 2008).

To test the autophagy hypothesis, we infected Vero cells with HSV-1 strain F (MOI 1) and co-treated the cells with 3-MA, which is reported as an autophagy inhibitor by inhibiting phosphoinositide 3-kinase (PI3K) (Le Sage & Banfield, 2012), (Wu & Brosh, 2010). Supernatants were collected as 24 h.p.i. and assayed by plaque assay. As shown in Figure 4.1.23, the co-treatment of infected Vero cells with TMPyP4 (1-25 µM) and 3-MA (1 mM) was able to counteract the antiviral effect of TMPyP4 (at 1 µM) of 20%, thus limiting the autophagy process. Due to the total HSV-1 inhibition, an almost undetectable differential effect was noticed at the highest TMPyP4 concentrations (5 and 25 µM). The lack of a total abolishment of TMPyP4 antiviral effect by co-treating with 3-MA is in accord with the hypothesis of a multiple site of action of TMPyP4, which is mainly evident at the highest concentrations.

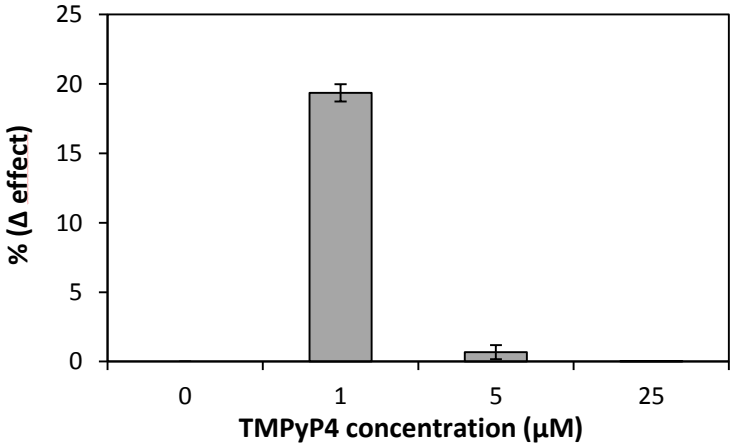

Figure 4.1.23 Plaque assay of infected Vero cells treated with both TMPyP4 (1-25 µM) and 3-MA (1 mM). The differential effect of TMPyP4/3-MA co-treated and infected cells is given as % relative to the TMPyP4-only treated/infected cells (% Δ effect).

Further studies are ongoing to confirm the involvement of autophagy in TMPyP4-mediated antiviral effect against HSV-1: quantification of a specific autophagy marker (LC3) and the effect of TMPyP4 on Vero cells infected with the ICP34.5 mutant R3616 (Chou, et al., 1990).

4.1.7 Effect of G-quadruplex ligands on HSV-1 gene expression

The HSV-1 QGRS are embedded in genes encoding essential viral proteins (*gp054* for UL36 and ICP0). We thus investigated whether the transcription of HSV-1 late genes was impaired by G-quadruplex ligand treatment. We designed primers for the transcripts of two γ genes (UL36, UL37) (Table 3). Upon treatment of infected cells (MOI 1) with BRACO-19, both UL36 and UL37 transcripts were markedly decreased at 24 h.p.i. up to 50% and 60% respectively (Figure 4.1.24, BRACO-19). This effect was specific for HSV-1 transcripts since no variation in the control ß-actin transcript was observed (Figure 4.1.25), as well as following TMPyP4 or TMPyP2 treatment (Figure 4.1.25).

The treatment with TMPyP4 caused an even higher inhibition up 90% for UL37 and 80% for UL36 (Figure 4.1.24, TMPyP4).

In contrast, TMPyP2 reduced HSV-1 transcript levels to a much lower extent (100-70%).

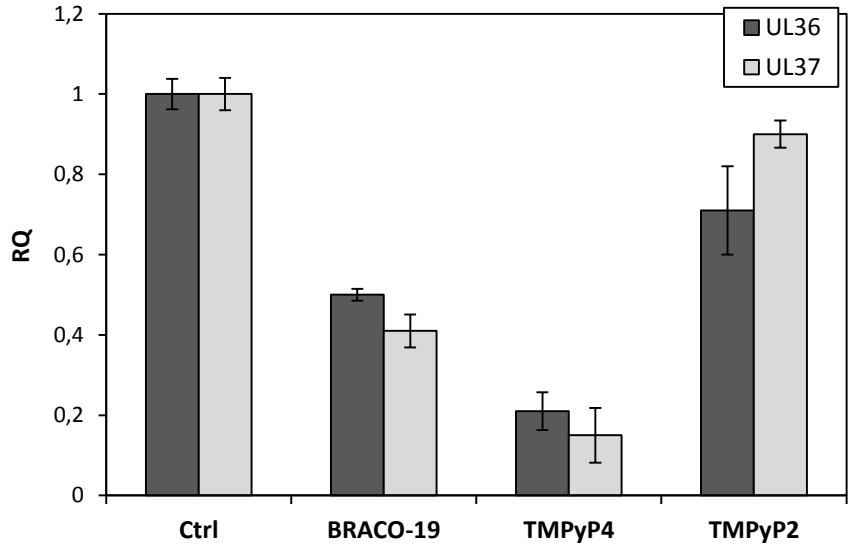

Figure 4.1.24 mRNA levels of selected HSV-1 late genes: infected cells were treated with BRACO-19, TMPyP4 or TMPyP2 (5µM). At 24 h.p.i. total RNA was isolated, retrotranscribed into cDNA, and expression of specific genes determined by RT-PCR. Ctrl indicates the non-treated Control, RQ are Relative Quantities. In all data sets: $n \geq 3$, mean ± s.d., Student's t-test, $^{**}P < 0.01$.

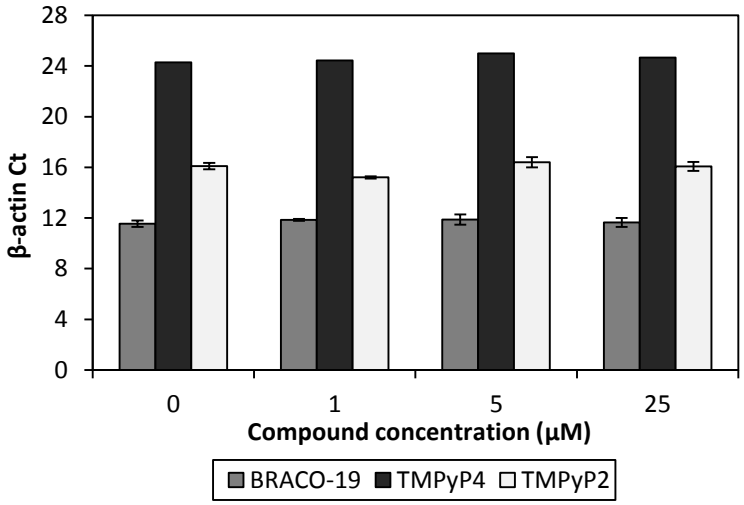

Figure 4.1.25 cDNA levels of the cellular gene ß-actin, indicated as Ct. Infected cells were treated with BRACO-19, TMPyP4 or TMPyP2 (1-25 µM); 24 h post infection total RNA was isolated, retrotranscribed into cDNA and expression of ß-actin gene determined by RT-PCR.

4.2 HHV-6: RESULTS AND DISCUSSION

4.2.1 Analysis of human herpes virus-6 genome

The genomic architecture shared by HHV-6A and HHV-6B is unique among herpesviruses (Figure 1.2.10) (Braun, et al., 1997). For the present study, the most interesting feature showed by the HHV-6 genome is the presence of several reiterations of the hexanucleotide $(TTAGGG)_n$. These reiterations are located nearby the *pac1* and *pac2* domains within the direct repeats DR_L and DR_R. More specifically, adjacent to the *pac2* sequences are serial TTAGGG motifs that are identical to the human telomeric repeat sequence (TRS), while those adjacent to *pac1* are imperfect and are referred to as het$(TTAGGG)_n$ sequences. As described above, it is presumed that through homologous recombination between the TRS present within the HHV-6 genome and the telomeres, the HHV-6 genome, or part of it, gets integrated within human chromosomes (Morissette & Flamand, 2010). Although these hexanucleotides are present in both HHV-6A and HHV-6B, the context of the reiterated sequences within the DR in HHV-6A and HHV-6B differs (Braun, et al., 1997).

The genome of the main HHV-6A (GS and U1102) and HHV-6B (Z29 and HST) strains was analyzed to determine the precise telomeric motif repeat number at the terminal ends of these viruses (Figure 4.2.1). Moreover, following the parameters previously used to analyze HSV-1 genome, an extensive analysis of both the leading and lagging strands was achieved to investigate the presence of additional putative G-quadruplex forming sequences.

The highest G-quadruplex folding propensity was observed in correspondence with the DRs in the lagging strand (G-score of 42), in which the telomeric motifs are repeated as $(TTAGGG)_n$ (Figure 4.2.1). However, in HHV-6 the G+C content is ~43%, much lower than G+C amount in the HSV-1 genome (~68%) (Gompels & Macaulay, 1995) (Braun, et al., 1997), therefore no other interesting clusters of repeated putative G-quadruplex forming sequences were identified. Considering the leading strand, the strain Z29 of HHV-6B displayed the greatest number of TTAGGG units (Figure 4.2.1). In all HHV-6 strains, a single TTAGGG repeat was also identified between the two telomeric clusters in both DRs, whereas repeated and isolated TTAGGG sequences were identified in the unique region of genomes. Although the great number of repeats (33 repeats in the strain Z29, 25 in the strain U1102, 19 and 18 repeats in GS and HST respectively) (Figure 4.2.1), the presence of wide loop regions between them prevents the folding into G-quadruplex.

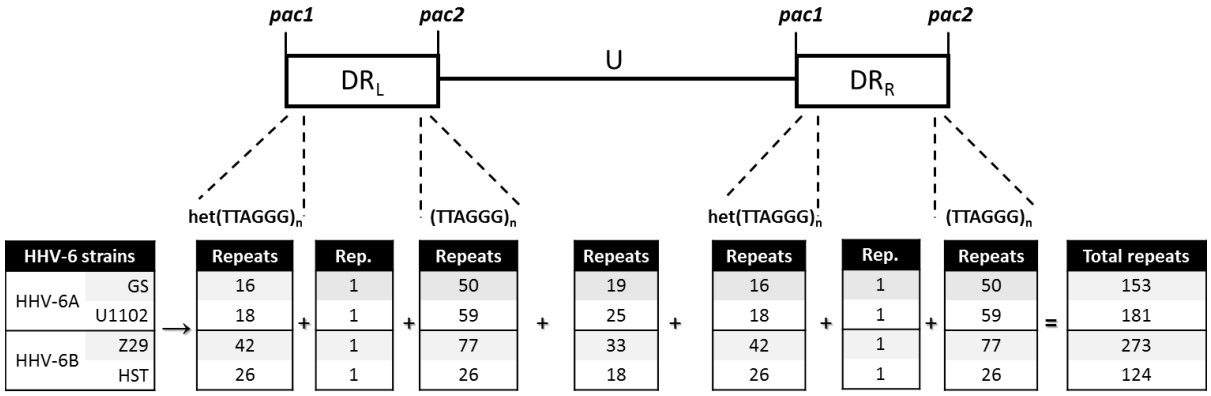

HHV-6 strains		Repeats	Rep.	Repeats	Repeats	Repeats	Rep.	Repeats	Total repeats
HHV-6A	GS	16	1	50	19	16	1	50	153
	U1102	18	1	59	25	18	1	59	181
HHV-6B	Z29	42	1	77	33	42	1	77	273
	HST	26	1	26	18	26	1	26	124

Figure 4.2.1 HHV-6 genome analysis. The number of the telomeric motif (TTAGGG) in the genome of the main strains of HHV-6A/6B is shown. U indicates the unique long region of the viral genome, het(TTAGGG)$_n$ are imperfect telomeric repeated sequences. The scheme refers to as the leading strand (5'→3').

4.2.2 Antiviral activity of G-quadruplex ligands against HHV-6

The G-quadruplex folding ability of the telomeric sequence has been extensively studied and its hybrid G-quadruplex structure has been fully characterized by circular dichroism, UV spectroscopy, NMR or mass spectrometry (Parkinson, et al., 2002), (Phan, et al., 2007).

Therefore, we tested the possibility that the two G-quadruplex ligands BRACO-19 and TMPyP4 displayed antiviral activity against HHV-6. The antiviral activity of BRACO-19 and TMPyP4 was assayed on the T-lymphoblastic cell line Molt-3, which is permissive to HHV-6B infection. Differently, TMPyP4 was the only G-quadruplex ligand tested on HSB-2 cells, which sustain HHV-6A infection, due to the high cytotoxicity of BRACO-19 on these T-lymphoblasts. PBMCs were also isolated from blood samples of donors and tested for both compounds, following the infection with HHV-6A (GS strain) and B (Z29 strain). In all cases, TMPyP2 was used as a negative control.

Cytotoxicity of the compounds was first assessed on Molt-3, HSB-2 and PBMC with MTT assay. Compared to Vero cells, TMPyP4 and BRACO-19, tested from 0.01 µM up to 50 µM, revealed very high toxicity on Molt-3 and HSB-2 cells, which constituted the most susceptible cell line (Table 11). TMPyP2 cytotoxicity on both these cell lines was almost equal to TMPyP4 cytotoxicity (Table 11). PBMCs, on the contrary, were generally less affected by all compounds.

The cytotoxicity critically increased after HHV-6 infection. For this reason, cell growth of infected cells treated every 48 h with the small molecules was carefully monitored by cell count (Figure 4.2.2), and subsequently the concentration range to test the compounds was selected.

	BRACO-19	TMPyP4	TMPyP2
HSB-2	CC_{50} ~ 2 µM	CC_{50} ~ 10 µM	CC_{50} ~ 10 µM
Molt-3	CC_{50} ~ 6.9 µM	CC_{50} ~ 10 µM	CC_{50} ~ 10 µM
PBMC	CC_{50} ~ 9.5 µM	CC_{50} > 50 µM	CC_{50} > 50 µM

Table 11 CC_{50} values of BRACO-19, TMPyP4 and TMPyP2 on the cell lines HSB-2, Molt-3 and PBMC, determined with MTT assay.

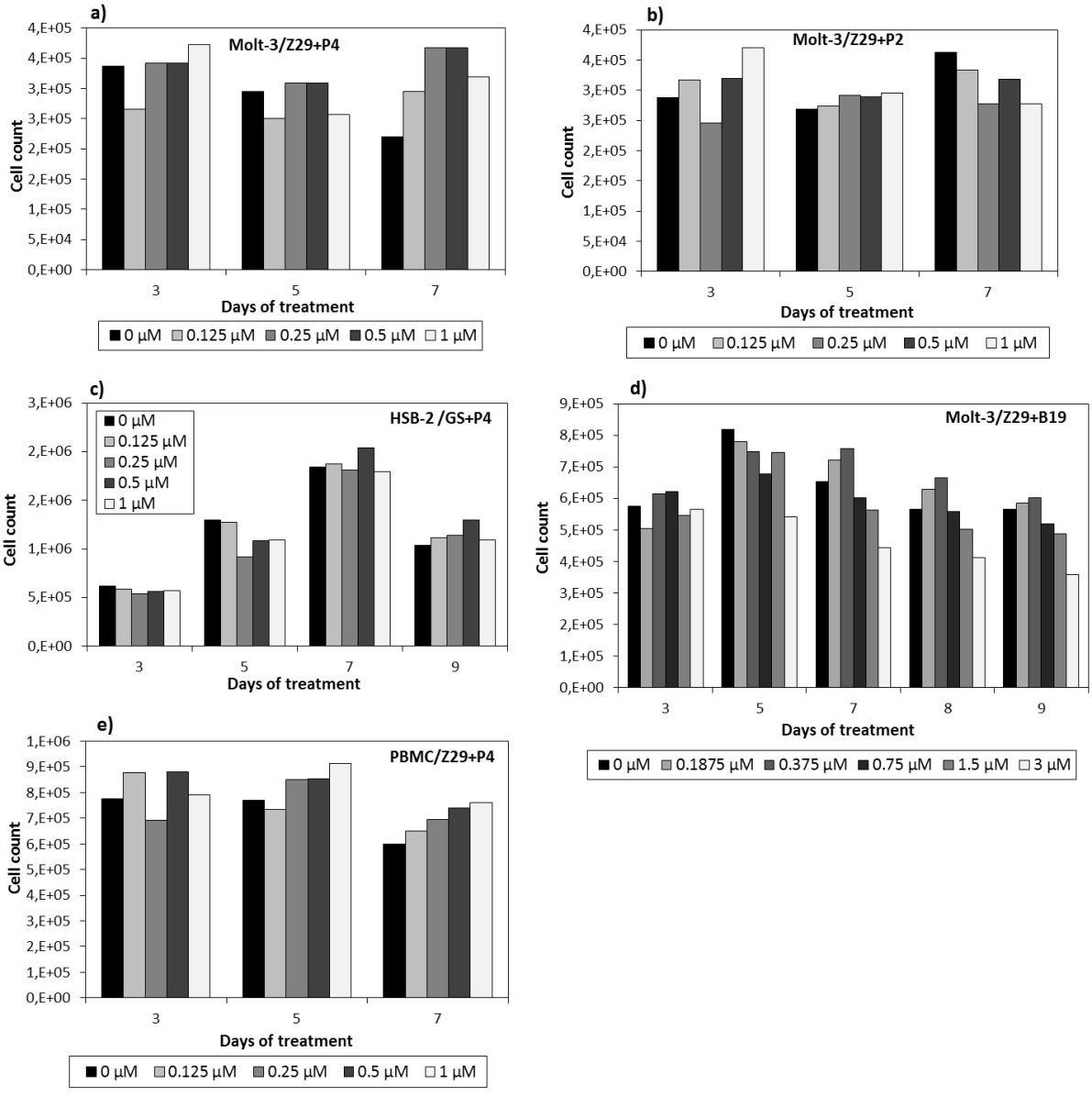

Figure 4.2.2 Cell growth of infected Molt-3, HSB-2 and PBMCs monitored by count, after the treatment with TMPyP4, BRACO-19 or TMPyP2. For Molt-3 and PBMCs, compounds were added every 48 h at 4 h.p.i. (day 1), 48 h.p.i. (day 3 p.i.) and 96 h.p.i. (day 5 p.i.); differently, for HSB-2, TMPyP4 was added at 48 h.p.i. (day 3 p.i.), 96 h.p.i. (day 5 p.i.) and 144 h.p.i. (day 7 p.i.). Cells were counted at 48 h.p.i. (day 3 p.i.), 96 h.p.i. (day 5 p.i.), 144 h.p.i. (day 7 p.i.), and also 192 h.p.i. (day 9 p.i.) for HSB-2. Cell count of Molt-3 infected with HHV-6B (Z29 strain, MOI of 0.5) treated with a) TMPyP4, b) TMPyP2 or d) BRACO-19 is shown. c) HSB-2 infected with HHV-6A (GS strain, MOI of 0.5) and treated with TMPyP4. e) PBMCs infected with HHV-6B (Z29 strain, MOI of 0.5) and treated with TMPyP4. P4 and P2 mean TMPyP4 and TMPyP2, respectively. B19 is BRACO-19.

Molt-3 cells, as well as PBMCs first isolated from blood samples, were infected with HHV-6 strain Z29 (MOI 0.2 and 0.5) and, subsequently, increasing concentrations of TMPyP4 (2-fold dilutions from 1 μM to 0.125 μM or 10-fold dilutions from 1 μM to 0.01 μM), BRACO-19 (2-fold dilutions from 2 μM to 0.25 μM) or TMPyP2 (2-fold dilutions from 1 μM to 0.125 μM) were added every 48 h. Aliquots of supernatant and/or cells were collected every 48 h, from 48 h.p.i (day 3, post infection) up to 144 h.p.i. (day 7, post infection). HHV-6 DNA was isolated from both supernatant and cell collected samples and assayed with RT-PCR. Non-treated infected cells were used as control, the housekeeping GAPDH was used as reference.
Differently, HSB-2 cells were infected with HHV-6A strain GS at a MOI of 0.5 (or 1), grown at 37°C, 5% CO_2 for 48 h, then treated with TMPyP4 or TMPyP2 (2-fold dilutions from 1 μM to 0.125 μM or 10-fold dilutions from 1 μM to 0.01 μM). The differential procedure was due to the lower rate of infection.

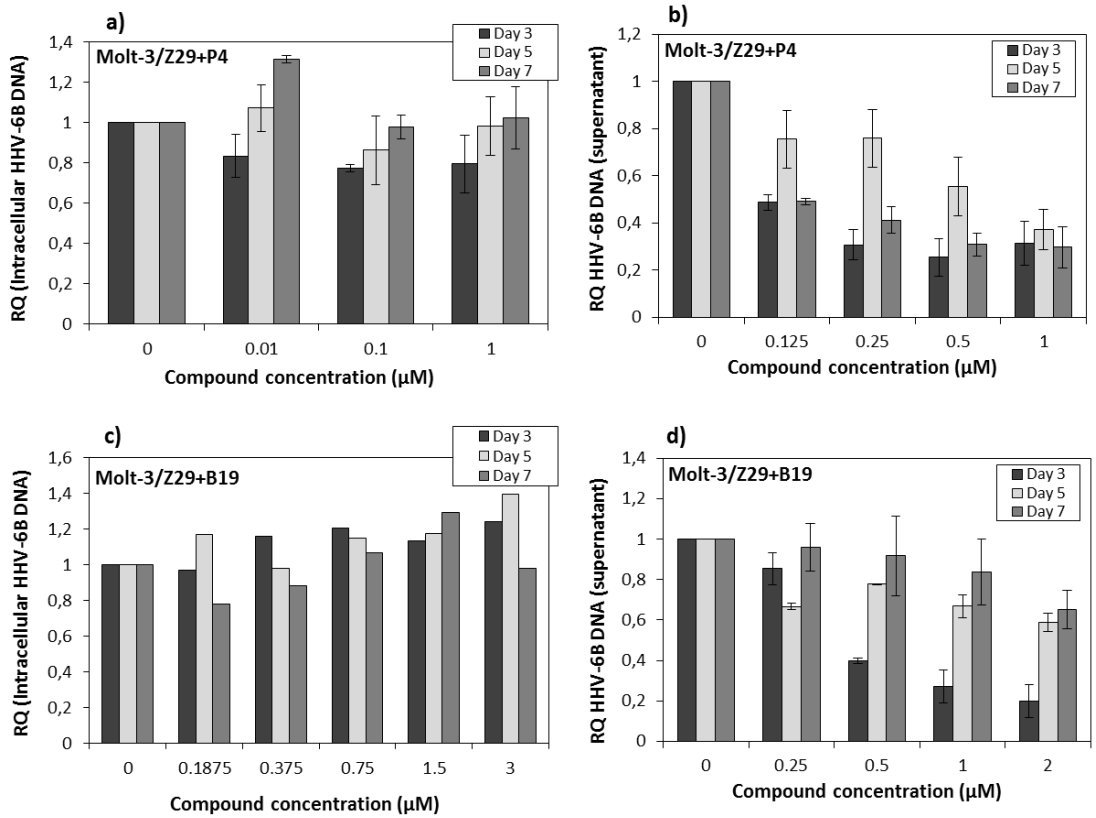

Figure 4.2.3 Antiviral effect determined on Molt-3 cells infected with HHV-6B strain Z29 (MOI of 0.5) and treated with TMPyP4 or BRACO-19 every 48 h, from 4 h.p.i. up to 96 h.p.i. (day 5 p.i.). Aliquots of supernatant and cell were collected at 48 h.p.i. (day 3 p.i.), 96 h.p.i. (day 5 p.i.) and 144 h.p.i. (day 7 p.i.); DNA was extracted and quantified by SYBR® green detection. Non-treated infected cells are used as control, GAPDH as reference to normalize data. Intracellular viral DNA levels after treatment with a) TMPyP4 (10-fold dilutions from 1 μM to 0.01 μM) or c) BRACO-19 (2-fold dilutions from 3 μM to 0.1875 μM) are shown. Viral DNA levels from supernatant after treatment with b) TMPyP4 (2-fold dilutions from 1 μM to 0.125 μM) or d) BRACO-19 (2-fold dilutions from 2 μM to 0.25 μM) are also shown. RQ are Relative Quantities, B19 means BRACO-19, whereas P4 indicates TMPyP4.

Similarly to HSV-1 study, TMPyP4 displayed the most interesting antiviral effect against both HHV-6A and HHV-6B.

As shown in Figure 4.2.3b, TMPyP4 inhibited HHV-6B of 60% at 0.125 µM up to 70% at 0.5-1 µM at 48 and 144 h.p.i. (day 3, 7 p.i. respectively) (EC_{50} ~ 0.125 µM). At 96 h (day 5), the antiviral effect of TMPyP4 was up to 60%, at the highest tested concentration 1 µM.

A stronger TMPyP4 effect was observed on PBMCs infected with HHV-6B: the viral inhibition was up to 70% at 1 µM at 48 h.p.i. (day 3 p.i.), whereas up to 80-90% at 0.125 µM at 96 and 144 h.p.i. (Figure 4.2.4).

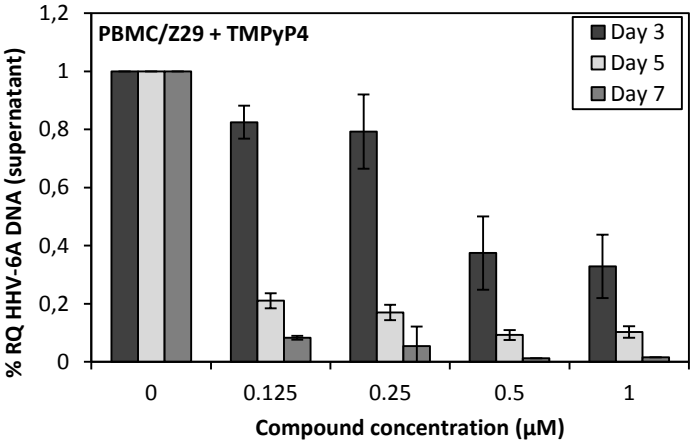

Figure 4.2.4 Antiviral effect of TMPyP4 (2-fold dilutions from 1 µM to 0.125 µM) determined on PBMCs infected with HHV-6B strain Z29 (MOI of 0.5). Cells were treated every 48 h, from 4 h.p.i. (day 1 p.i.) up to 96 h.p.i. (day 5 p.i.). Aliquots of supernatant were collected at 48 h.p.i. (day 3 p.i.), 96 h.p.i. (day 5 p.i.) and 144 h.p.i. (day 7 p.i.); DNA was extracted and quantified by SYBR® green detection. Non-treated infected cells are used as control, GAPDH as reference to normalize data. RQ are Relative Quantities.

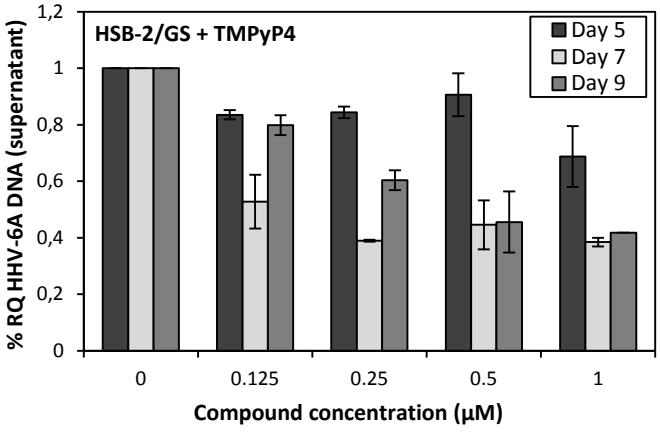

Figure 4.2.5 Antiviral effect of TMPyP4 (2-fold dilutions from 1 µM to 0.125 µM) determined on HSB-2 cells infected with HHV-6A strain GS (MOI of 0.5). Cells were treated every 48 h, from 48 h.p.i. (day 3 p.i.) up to 144 h.p.i. (day 7 p.i.). Aliquots of supernatant were collected at 96 h.p.i. (day 5 p.i.), 144 h.p.i. (day 7 p.i.) and 192 h.p.i. (day 9 p.i.); DNA was extracted and quantified by SYBR® green detection. Non-treated infected cells are used as control, GAPDH as reference to normalize data. RQ are Relative Quantities.

As shown in Figure 4.2.5, on HHV-6A the treatment with TMPyP4 showed a maximal antiviral effect of 60% at 144 and 192 h.p.i. (day 7 or 9, respectively) (EC_{50} ~ 0.125-300 μM). As mentioned above, BRACO-19 was tested only on HHV-6B, due to the high cytotoxicity of this G-quadruplex ligand on HSB-2. BRACO-19 inhibited HHV-6B up to 80% at 48 h.p.i. (day 3 p.i.) (EC_{50} ~ 0.450 μM). However, although its inhibitory effect was also maintained at 96 and 144 h.p.i (day 5 and 7, respectively), the progressive increasing rate of infection reduced the antiviral property of this acridine derivative up to 40% at the highest tested dose 2 μM (Figure 4.2.3d). In fact, after the infection with HHV-6 and simultaneously to an increase of virus in the cells, cell growth is temporarily reduced within the first 48 h.p.i., followed by a further increase of the cell growth up to a predominant cytopathic effect induced by the virus, which normally leads to cell death. To follow whether an adequate progression of the infection was occurring all along the assay, Ct and/or HHV-6 copies were monitored at the increasing time points after infection (Figure 4.2.7).

The compound TMPyP2, used as reference, was almost inactive up to 1 μM on both HHV-6A (Figure 4.2.6b) and HHV-6B (Figure 4.2.6a), indeed it displayed an inhibition of 20% maximum at 1 μM).

Interestingly, no decreased intracellular HHV-6A (not shown) and HHV-6B (TMPyP4 in Figure 4.2.3a and BRACO-19 in Figure 4.2.3c) DNA amounts were observed at the investigated time points.

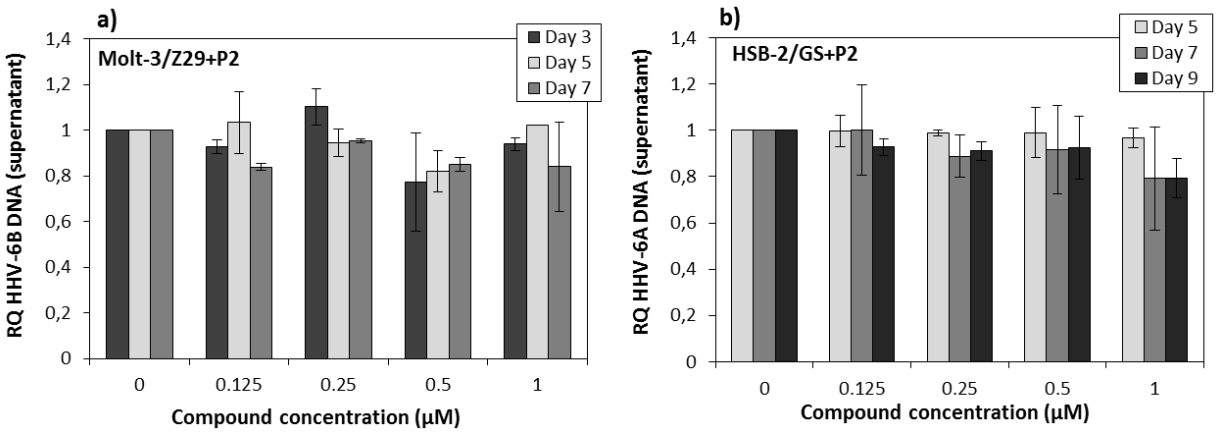

Figure 4.2.6 Activity of TMPyP2 (2-fold dilutions from 1 μM to 0.125 μM) determined on a) Molt-3 infected with HHV-6B strain Z29 (MOI of 0.5) and b) HSB-2 cells infected with HHV-6A strain GS (MOI of 0.5) is shown. Molt-3 cells were treated with the compound every 48 h, from 4 h.p.i. up to 96 h.p.i. (day 5, p.i.), aliquots of supernatant were collected at 48 h.p.i. (day 3, p.i.), 96 h.p.i. (day 5, p.i.) and 144 h.p.i. (day 7, p.i.). Differently, HSB-2 cells were treated every 48 h, from 48 h.p.i. up to 144 h.p.i. (day 7, p.i.), aliquots of supernatant were collected at 96 h.p.i. (day 5, p.i.), 144 h.p.i. (day 7, p.i.) and 192 h.p.i. (day 9, p.i.). In both cases, viral DNA contained in the collected supernatants was isolated and quantified by SYBR® green detection. Non-treated infected cells are used as control, GAPDH as reference to normalize data. RQ are Relative Quantities, whereas P2 indicates TMPyP2.

The function of $(TTAGGG)_n$ is not known, but it has been hypothesized to play a role in DNA packaging and in the maintenance of viral chromosome as a self-replicating episome in latently infected cells. The conserved terminal *cis*-acting herpesvirus packaging signals, *pac1* and *pac2*, are present in HHV-6A and HHV-6B, flanked by imperfect and perfect iterations of TTAGGG. During DNA replication, a head-to-tail arrangement probably occurs, juxtaposing the *pac1* and *pac2* signals in the correct orientation, creating a favored cleavage site for unit-length molecules (Braun, et al., 1997).

Further studies are ongoing to confirm this hypothesis and a role of G-quadruplex in the packaging of the virus.

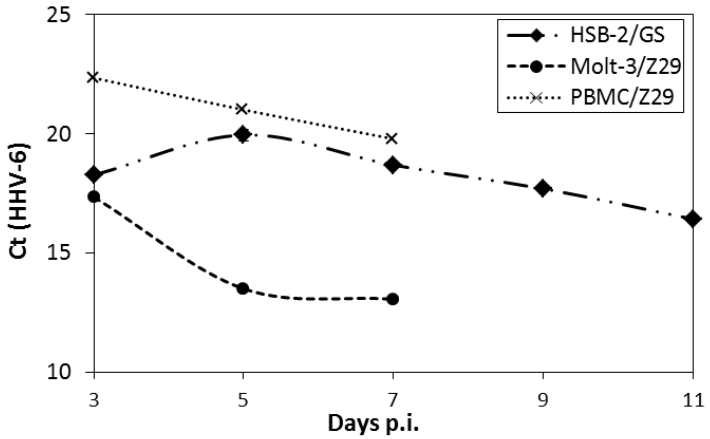

Figure 4.2.7 Progression of HHV-6 infection. Ct referred to infected/non-treated cells (control) at increasing days post infection. Figure shows the infection of Molt-3 and PBMCs with HHV-6b (Z29 strain), and HSB-2 with HHB-6A (GS strain)

4.3 VIRAL G-QUADRUPLEX VISUALIZATION IN INFECTED CELLS: RESULTS AND DISCUSSION

As extensively discussed above, comprehensive biophysical and structural studies proved that G-rich DNA (or RNA) sequences can spontaneously fold into G-quadruplex *in vitro*. Moreover, the additional G-quadruplex stabilization under near-physiological conditions (K^+) suggests that this non-canonical secondary structure may form in genomic DNA *in vivo*, although this is a topic of some debate (Lipps & Rhodes, 2009). In fact, the visualization of G-quadruplex in human cells has always represented a big challenge, and only recently the first evidences have started to accumulate for its presence and function *in vivo*.

DNA G-quadruplex structures are associated with a number of important aspects of genome function, which include transcription, recombination and replication (Figure 4.3.1). Therefore, the replication of DNA G-quadruplex motifs requires their unfolding by helicases, such as BLM (Sun, et al., 1998), FANCJ (Wu, et al., 2008), WRN, REV1 and ATRX (alpha-thalassaemia/mental retardation syndrome X-linked) (Law, et al., 2010).

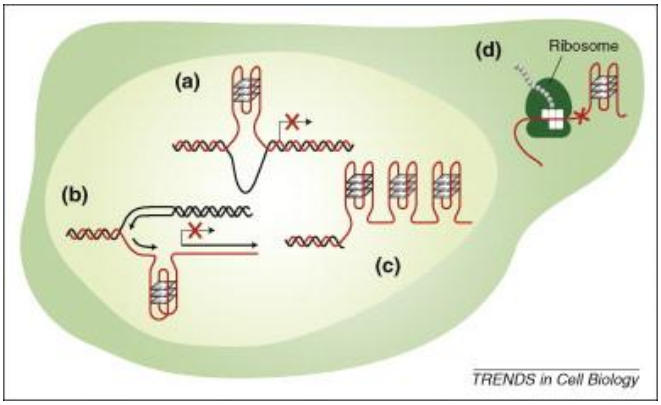

Figure 4.3.1 Possible locations of G-quadruplex structures in cells. G-quadruplex formation could occur in G-rich regions of double-stranded DNA, such as at promoter regions of genes (a) and during replication (b) when DNA becomes transiently single-stranded. Telomeric G-overhangs are single-stranded, favoring G-quadruplex formation (c). (d) Outside the nucleus, G-quadruplexes could form in mRNA and indeed the 5'-UTRs of mRNAs, rich in G-quadruplex forming potential. The red crosses indicate possible impediments caused by G-quadruplexes to replication, transcription and translation (Lipps & Rhodes, 2009).

In 2012, the research team of Prof. Shankar Balasubramanian was the first to provide important evidences for the formation of G-quadruplex structures in the genome of human cells, using a G-quadruplex selective antibody named BG4. They also proved that G-quadruplex formation in DNA is modulated during cell-cycle progression and further stabilized by the small-molecule ligand pyridostatin (PDS) (Biffi, et al., 2013).

In 2013, following the development of a G-quadruplex selective monoclonal antibody named 1H6, an additional proof of G-quadruplex formation in mammalian cells was provided by the team of Prof. Peter M. Lansdorp (Henderson, et al., 2013).

We have successfully demonstrated the presence of putative G-quadruplex forming sequences in both HSV-1 and HHV-6, their capability to effectively form highly stable G-quadruplex structures, which are further stabilized by the addition of K^+ and G-quadruplex ligands, as well as the very promising antiviral activity of some of these G-quadruplex ligands such as TMPyP4 and BRACO-19. As a further step, we wondered whether it was possible to visualize viral G-quadruplex structures in infected cell lines. To this end, we tested both BG4 and 1H6 antibodies on HSV-1 infected Vero cells (MOI 0.5) and HHV-6B infected Molt-3 (MOI 1), through immunofluorescence.

4.3.1 G-quadruplex structure affinity of BG4 and 1H6

To evaluate the binding affinity of BG4 and 1H6 for viral G-quadruplex forming sequences (Table 7) and their different structural conformations, we performed ELISA assay.

BG4 was first produced in highly competent cells (BL21DE3-RIL) and cells were next sonicated to release the protein. Subsequently, BG4 was purified using an imidazole gradient (from 20 mM to 500 mM), dialysized in PBS 1X to remove salts and finally quantified through the Bradford assay and a BSA curve.

Briefly, to perform ELISA 96-well plates were coated with avidin and biotinylated G-quadruplex folding oligonucleotides (2 pmoles/60 µl) (Table 7), previously denatured by heating at 95°C for 10 minutes to favor the folding into G-quadruplex, were bound to the plate using the interaction avidin-biotin. Following incubation with BG4 (2-fold dilution from 6.25 to 200 nM) or 1H6 (2-fold dilution from 0.02 to 40 ng/µl), the binding was detected with anti-mouse HRP antibody and TMB solution. Before the incubation with HRP, BG4 required a further incubation with an anti-mouse α-flag secondary antibody. Non-treated biotinylated oligonucleotides were used as control, *ss-DNA* as negative control to normalize data (Biffi, et al., 2013). Absorbance was determined at λ=450 nm, using a reference wavelength of λ=570 nm.

The binding between BG4 and HSV-1 G-quadruplex sequences (*gp054a*, *un2* and *un3*) is shown in Figure 4.3.2, whereas the binding between BG4 and HIV-1 G-quadruplex sequences (LTR II+III+IV, LTR III+IV, LTR III+IV M5 and LTR III+IV M4+5) (used as positive controls) is shown in Figure 4.3.3. As an additional control of the BG4 specificity for G-

quadruplex DNA, we also tested several non-G4 forming sequences (Table 7). Non-G4 folding/G-rich sequences (*ss-DNA high G-content*), non-G4 folding sequences (*ss-DNA*, *ss-DNA long*), C-rich sequences (TERC DNA, H6 TR_S), all used as negative controls, are shown in Figure 4.3.4.

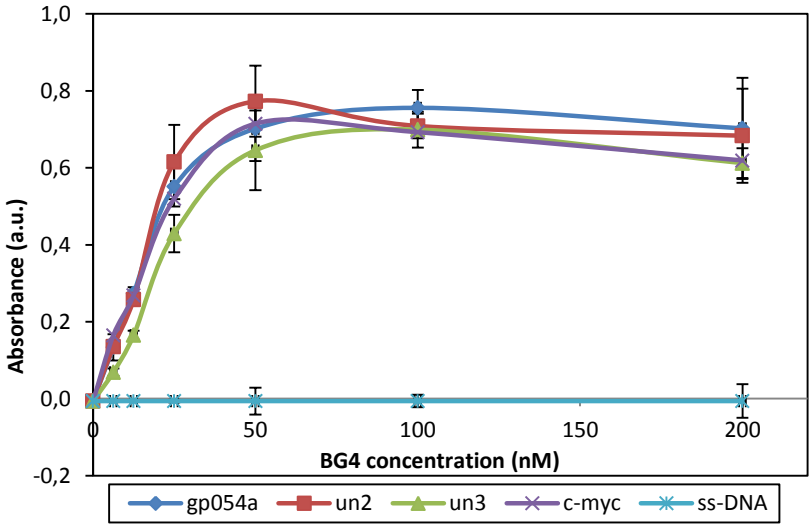

Figure 4.3.2 BG4 (2-fold dilution from 6.25 to 200 nM) binding affinity for G-quadruplex structures determined with ELISA assay on the biotinylated HSV-1 sequences *gp054a*, *un2* and *un3* (2 pmoles/60 µl); a non-G4-forming/non G-rich sequence named ss-DNA was used as negative control, whereas *c-myc* sequence as reference. Plates were read at λ=450 nm, using a reference wavelength of λ=570 nm.

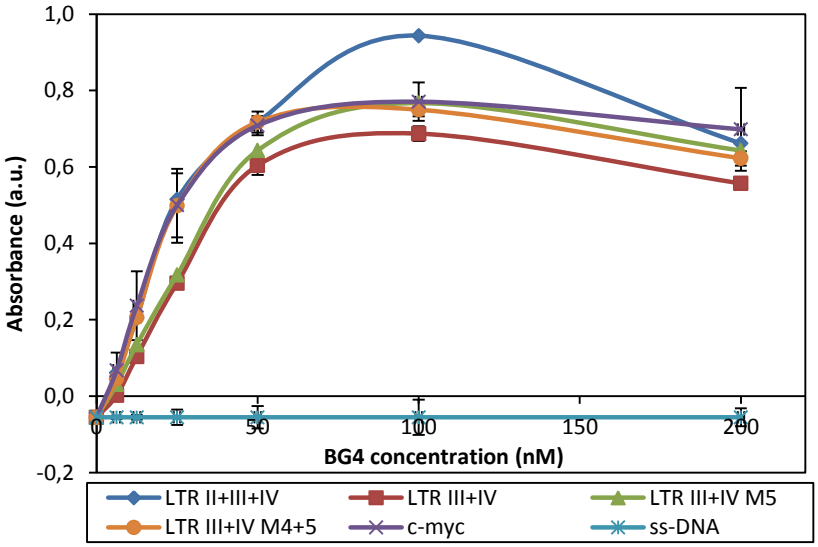

Figure 4.3.3 BG4 (6.25-200 nM, 2-fold dilutions) affinity for the biotinylated HIV G4-forming sequences determined with ELISA assay (LTR II+III+IV, LTR III+IV, LTR III+IV M5 and LTR III+IV M4+5; all 2 pmoles/60 µl); ss-DNA was used as negative control and *c-myc* sequence as reference. Plates were read at λ=450 nm, using a reference wavelength of λ=570 nm.

BG4 showed high affinity for all tested G-quadruplex forming sequences located in the HSV-1 and HIV-1 genome, despite their different G-quadruplex topology. In fact, BG4 interacted

with parallel G-quadruplexes, such as *un3* and the reference sequence *c-myc (*Figure 4.3.2), with anti-parallel topologies, such as *un2 (*Figure 4.3.2), and with mixed-type G-quadruplex sequences, such as *gp054a (*Figure 4.3.2), LTR II+III+IV and LTR III+IV *(*Figure 4.3.3). Surprisingly, BG4 displayed affinity also for the mutated HIV sequences LTR III+IV M5 and LTR III+IV M4+5, which were proved to fail the folding into G-quadruplex (Perrone, et al., 2013a). In addition, it bound non-G4-forming/G-rich sequences, long sequences, a C-rich sequence (TERC DNA) and a complementary telomeric sequence (H6 TR_S) as well.

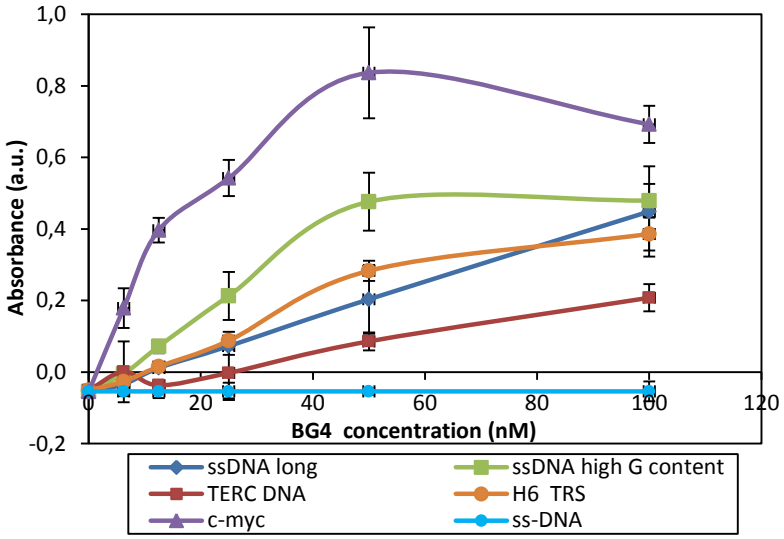

Figure 4.3.4 BG4 (6.25-100 nM, 2-fold dilutions) affinity for biotinylated non-G4 forming sequences determined with ELISA assay (2 pmoles/60 µl); ss-DNA was used as negative control and *c-myc* sequence as reference. Plates were read at λ=450 nm, using a reference wavelength of λ=570 nm.

All the non-G4-forming sequences were analyzed by circular dichroism to confirm that the folding into G-quadruplex did not occur in the test conditions (Figure 4.3.5).

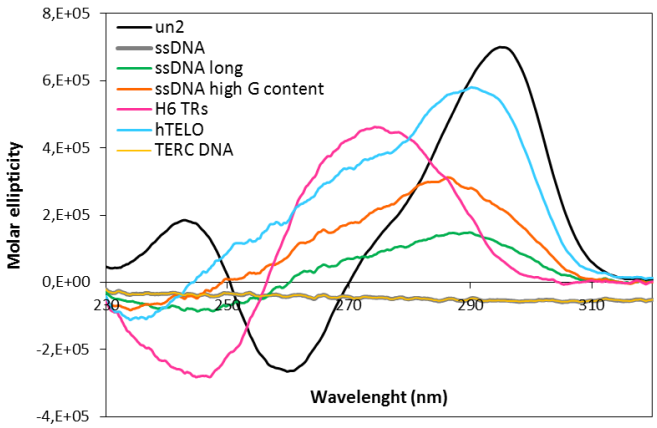

Figure 4.3.5 CD spectra of negative control sequences (4 µM) in the presence of K^+ 100 mM. *un2* was included ad positive control. Molar ellipticity has been plotted against wavelength.

In comparison to G-quadruplex folding sequences, such as *un2* and hTELO, the control sequences did not display folding into G-quadruplex (Figure 4.3.5).

Therefore our data suggested that, apart from G-quadruplex DNA structures, BG4 does not efficiently discriminate between a wide range of DNA structures. The binding is influenced by several factors such as the length of the DNA sequences, the G-content independently of the G4-folding ability, and the presence of alternative DNA secondary conformations, most likely random coil conformation.

Very promising results were obtained with 1H6 antibody. Due to the limited antibody availability and the high 1H6 concentration required to carry out ELISA assay, only two G-quadruplex forming sequences could be tested (*gp054a* and *hTELO*), and the negative control *ss-DNA*. As shown in Figure 4.3.6, 1H6 displayed differential affinity depending on the G-quadruplex topology. This monoclonal antibody showed high affinity especially for the telomeric sequence (hTELO) and a lower affinity for *gp054a*. As expected, no binding was observed between 1H6 and *ss-DNA*.

Interestingly, during the development and characterization of 1H6 antibody, it showed a high selectivity also for the sequence GGGGTTGGGGTTGGGGTTGGGG (i.e. *gp054b*).

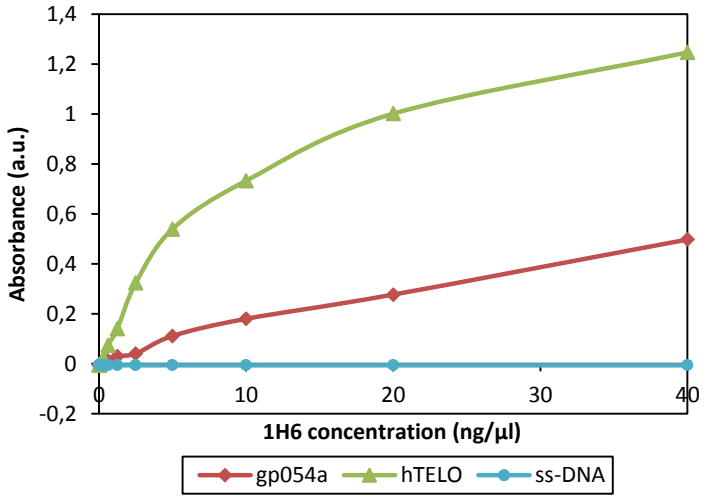

Figure 4.3.6 1H6 (0.020-40 ng/µl, 2-fold dilutions) affinity for biotinylated G-quadruplex forming sequences gp054a (HSV-1) and hTELO (HHV-6), determined with ELISA assay (2 pmoles/60 µl); ss-DNA was used as negative control. Plates were read at λ=450 nm, using a reference wavelength of λ=570 nm.

4.3.2 Visualization of viral G-quadruplex DNA structures

BG4 and 1H6 were tested on HSV-1 infected Vero cells (MOI 1 or 0.5) and HHV-6 infected Molt-3 cells (MOI 1) with immunofluorescence. Briefly, Vero and Molt-3 were infected with HSV-1 (F strain or mutant) or HHV-6 (Z29 strain) respectively and incubated at 37°C, 5% CO_2. At selected time points (2-20 h.p.i.), cells were fixed with 4% paraformaldehyde (Vero) or 100% acetone (Molt-3), and eventually permeabilized with 0.5% tween-20. The blocking step occurred in 5% FBS at 4°C, for 12 h. Cells were then incubated with BG4 (dilution 1/100, from a stock concentration of 520 ng/µl) or 1H6 (1 µg/ml). BG4 required a further incubation with an anti-mouse α-flag secondary antibody. The detection was achieved by incubating with alexa Fluor-488 or 594 for BG4, or alexa Fluor-546 for 1H6. Moreover, nuclear staining for DNA was achieved with DAPI (BG4 experiments) or DRAQ5® (1H6 experiments).

Although the solvent used to fix the cells did not affect the interaction between antibody and G-quadruplex DNA structures, BG4 did not display promising results.

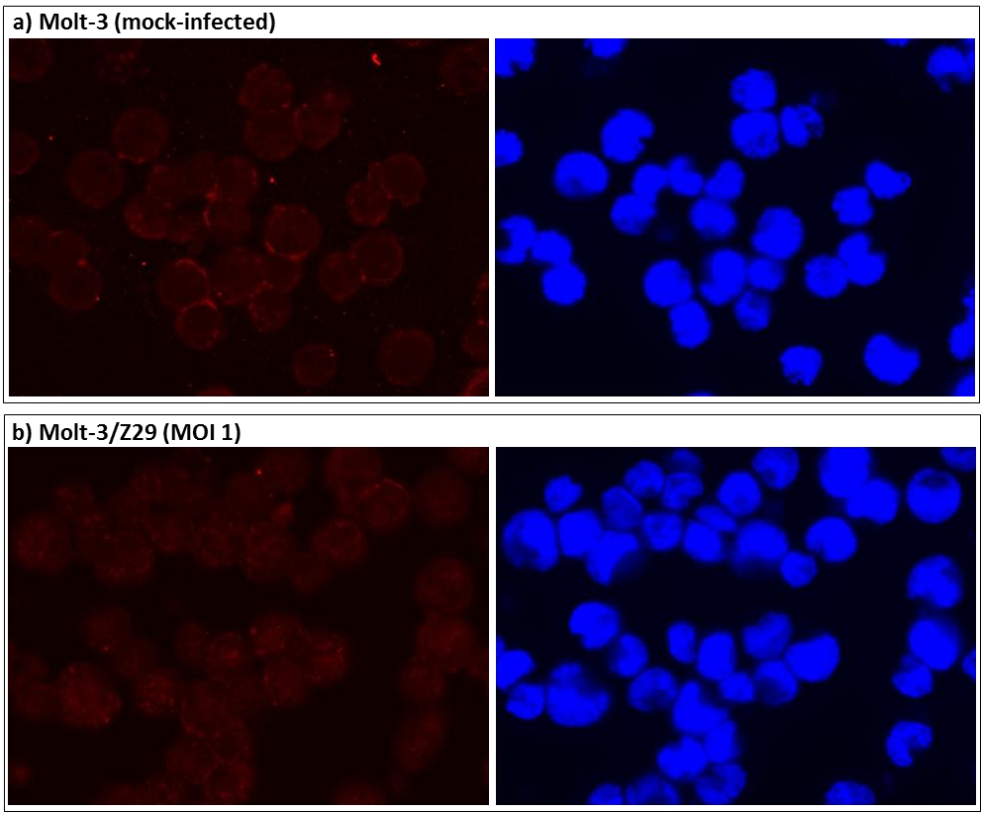

Figure 4.3.7 Immunofluorescence assay with BG4. a) mock-infected Molt-3 and b) infected Molt-3 cells (MOI of 1) were incubated with BG4 (~5.2 ng/µl), α-flag (1 µg/µl) and subsequently with Alexa-546 1/500 (red signal). Nuclear staining for DNA (blue signal) was achieved by incubating with DAPI.

A very high background signal was detected using alexa Fluor-488, whereas alexa Fluor-594 abolished aspecific fluorescence but also highlighted that BG4 is unable to completely cross the nuclear membrane. Despite increasing MOI or different time points of investigation, the red fluorescence, referred to the binding of BG4 with G-4, was comparable among uninfected and infected cells (Figure 4.3.7).

In contrast, visualization of viral G-quadruplex DNA structures was achieved using the 1H6 antibody. To carry out immunofluorescence, Vero cells were infected with a recombinant HSV-1 (F strain) named V41, expressing VP16 linked to the green fluorescent protein (GFP). Infected Vero cells were fixed with 4% paraformaldehyde, crucial solvent for a good execution of immunofluorescence with 1H6, at several time points depending on the viral cycle step. Given that the folding into G-quadruplex depends on separation of the two complementary strands by helicases during important physiological processes, such as replication or transcription, the selected time points for investigation are strictly related to the HSV-1 replication cycle.

Therefore, we chose two time points preceding viral replication (2 and 4 h.p.i.), two time points corresponding to HSV-1 replication (6 and 9 h.p.i.), and a number of time points consecutive to viral replication (14 h.p.i., or 18-20 h.p.i.).

VP16, product of the UL48 gene, is one of the most-abundant tegument proteins. VP16 is essential for HSV-1, because it regulates IE-genes transcription, assembly and egress of infectious virions. Moreover, it modulates the activity of several viral components, and it is assembled in approximately 1000 to 1500 copies per virion (La Boissière, et al., 2004). This recombinant virus replicates with virtually normal kinetics and yields and incorporate the fusion protein into the virion, resulting in autofluorescent particles.

As reported by the group of Prof. Peter O'Hare, no significant fluorescence is visible at the earliest stages of infection (up to 3 h.p.i.), whereas between 3 and 5-6 h.p.i VP16-GFP is detectable as bright punctate foci, mostly as a diffuse pattern within the nucleus. At intermediate times from 7 to 12 h after infection, in which VP16-GFP is observable in a homogeneous diffuse cytoplasmic pattern, these nuclear foci expand and coalesce into large globular domains within the nucleus, likely representing replication compartments. After 12 h.p.i., VP16-GFP accumulates in vesicular-like foci mainly in the cytoplasm. Moreover increasing in intensity and additional accumulation at the boundaries between cells occur at late stages (La Boissière, et al., 2004).

Recombinant HSV-1 V41, therefore, allowed monitoring of the cell infection state and locating HSV-1 within infected cells.

Interestingly, a very consistent increase of foci (in red), specific for the binding between G-quadruplex DNA structures and 1H6, following detection with alexa Fluor-546, was observed at the two HSV-1 replication-related time points, 6 and 9 h.p.i. (Figure 4.3.8d,e respectively), in comparison with mock-infected Vero cells (Figure 4.3.8a). The highest intensity of red fluorescence was recorded at 6 h.p.i., corresponding to the beginning of HSV-1 replication. Moreover, in comparison with both mock-infected and infected cells, the red fluorescence decreased when treating infected cells with PAA (400 μg/ml) (Zhou & Knipe, 2002), which is an inhibitor of viral replication (Figure 4.3.9a, PAA treatment). These evidences suggested that 1H6 specifically recognized and interacted with viral DNA G-quadruplexes over cellular G-quadruplex structures.

At the earliest stages of infection, 2 and 4 h.p.i. (Figure 4.3.8b,c respectively), 1H6-related signal was comparable to the red fluorescence of uninfected Vero cells (Figure 4.3.8a). In fact, between 0-1 h.p.i. and 4-5 h.p.i. earlier steps of the replication cycle, such as HSV-1 attachment and entry and IE-gene transcription, occur and likely no unfolding of viral DNA, from double-stranded DNA to single-stranded DNA, takes place. In accordance with literature, GFP-VP16 was barely visible at 2 h.p.i., whereas GFP foci became clearer from 4 h.p.i.

At later stages (14 h.p.i. and after), once HSV-1 replication occurred, the fluorescence determined by 1H6 binding to G-quadruplex structures gradually decreased (Figure 4.3.8f). However, between 14 and 16 h.p.i., red foci mainly localized at the nuclear membrane, most likely due to the nuclear egress of nucleocapsids to the cytoplasm of cells. This peculiar behavior was not detectable after 16 h.p.i. (Figure 4.3.8f).

No background was recorded by incubating mock-infected/infected cells with alexa-546 (1/500) and DRAQ5® 1/1000 only, in the absence of the primary antibody 1H6 (Figure 4.3.9b,c, background).

The different procedure, used to fix HHV-6B infected Molt-3, made impossible a good execution of immunofluorescence in the presence of 1H6, while pure acetone is not suitable for this antibody.

Taken together, data suggested a highly specific interaction between 1H6 and viral G-quadruplex DNA structures. In fact, the increase of fluorescence occurred at viral replication fundamental steps (6-9 h.p.i.), whereas it was inhibited by treating infected cells with replication inhibitors. Interestingly, these data constitute the first evidence of virus-related G-quadruplex formation in infected cells.

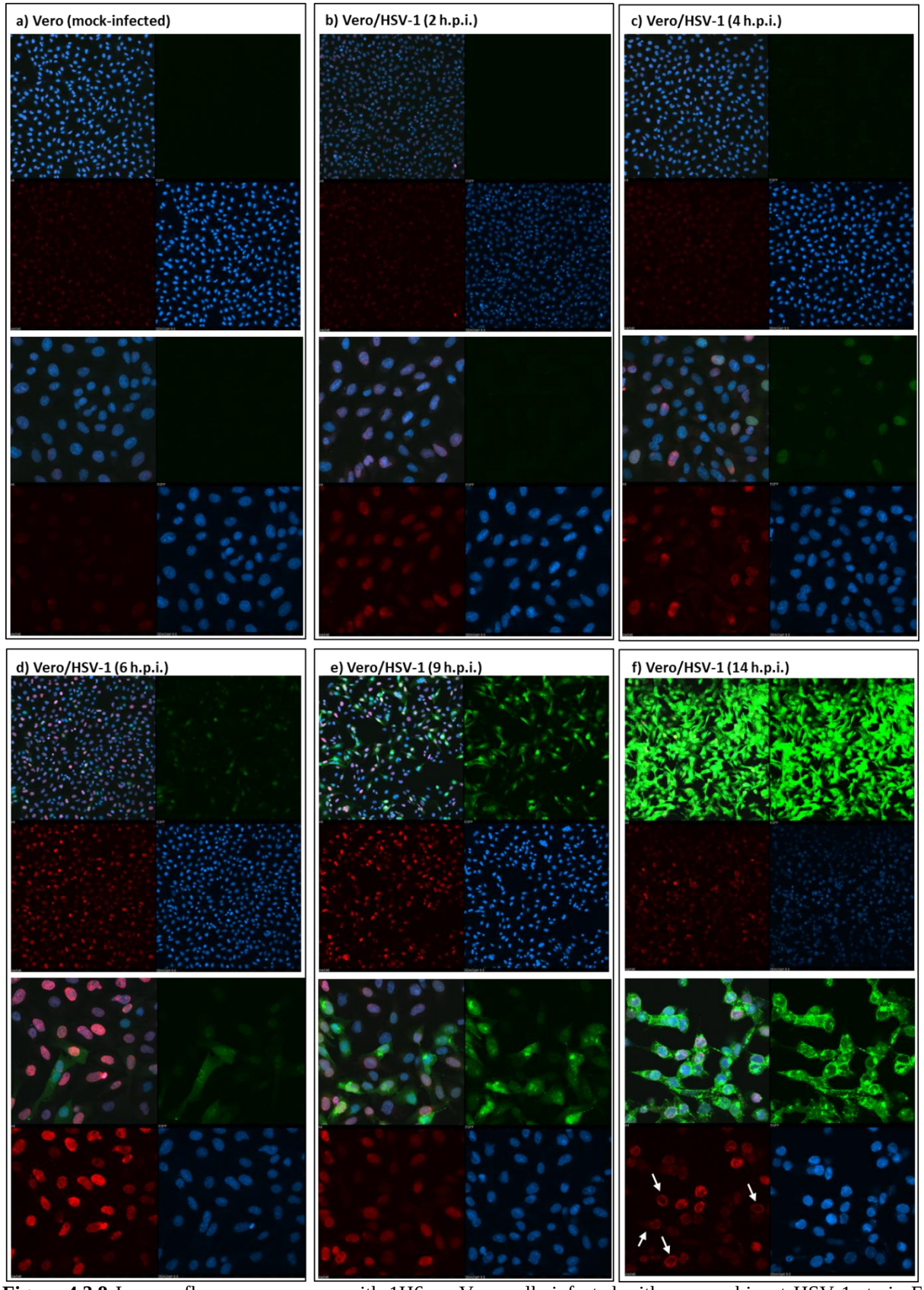

Figure 4.3.8 Immunofluorescence assay with 1H6 on Vero cells infected with a recombinant HSV-1 strain F (MOI 0.5), the GFP-expressing recombinant virus V41, which promotes the release of the GFP-fused VP16. Cells were fixed and analyzed at different time points: b) 2 h.p.i., c) 4 h.p.i., d) 6 h.p.i., e) 9 h.p.i., f) 14 h.p.i., whereas a) mock-infected Vero cells were used as control. Green fluorescence is the signal of GFP-fused VP16;

red fluorescence was achieved by incubating infected and fixed cells with 1H6 antibody (1µg/ml) and, subsequently, with an anti-mouse alexa Fluor-546 secondary antibody (1/500). Nuclear staining for DNA, highlighted as a blue signal, was achieved by incubating Vero cells with DRAQ5® (1/1000). At the top of each figure, merge of signals is on the left side and GFP signal on the right side; at the bottom of each figure, red 1H6/alexa-546-derived signal is on the left side, while DRAQ5® fluorescence is on the right. e) White arrows indicate 1H6 mainly localized at the nuclear membrane. In each panel, pictures at 20X (at the top) and 60X (at the bottom) are shown.

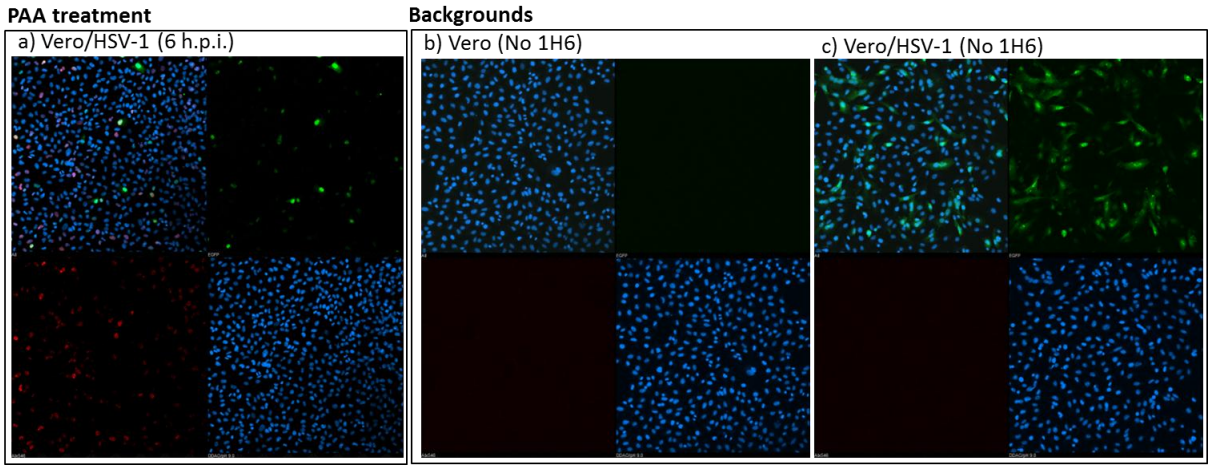

Figure 4.3.9 Immunofluorescence assay on a) infected Vero cells treated with PAA to block viral replication; b) mock-infected or c) infected Vero cells to test the background of the reagents used to perform experiments. Fort the infection, the recombinant V41 HSV-1 was used at a MOI of 0.5. Cells were fixed at 6 h.p.i. and incubated with alexa Fluor-546 (1/500) and DRAQ5® (1/1000) only to test a background signal (b, c), or also with the primary antibody 1H6 (a). At the top of each figure, merge of signals is on the left side and GFP signal on the right side; at the bottom of each figure, alexa-546 signal (referred to 1H6) is on the left side, while DRAQ5® fluorescence is on the right. In each panel, pictures at 20X are shown.

4.4 ANALYSIS OF VIRAL PACKAGING SEQUENCES BY CIRCULAR DICHROISM

In the present study, we demonstrated the presence of extensive clusters of G-4 forming sequences that are able to form highly stable G-quadruplex structures. More specifically, some of these clusters, *un3* sequences in HSV-1 and tandem repeats of the human telomeric sequence in HHV-6, are located nearby the domains *pac1* and *pac2* needed for viral cleavage and packaging.

HSV-1 encodes six proteins (UL6, UL15, UL17, UL28, UL32, UL33), which are necessary for DNA cleavage and packaging, as previously described in detail, and homologs of these proteins are also present in HHV-6 (U12, U36, U50, U60, U66).

For HSV-1, the protein UL28 is required for the cleavage of concatameric DNA into viral procapsids. In 2001, it was reported by the group of Prof. Joel D. Baines that G-rich DNA fragments, containing the *pac1* DNA packaging motif, can be induced by heat treatment to adopt "novel" DNA conformations, able to migrate faster than the corresponding duplex in non-denaturing gels. Interestingly, it was proved that UL28 protein displayed a very high binding-affinity for these novel DNA structures, whereas double-stranded DNA of identical sequence composition is not recognized by the protein. They also demonstrated that only one strand of the *pac1* motif (G-rich strand) is responsible for the formation of these unusual DNA structures (Adelman, et al., 2001).

We hypothesized that these novel conformations are indeed G-quadruplex structures and, therefore, we analyzed these reported wild-type (wt) and mutated HSV-1 packaging sequences (Table 2) with circular dichroism, in order to verify whether the "novel" reported DNA conformations are effectively G-quadruplex structures. In fact, published evidences showed that the folding into this particular DNA conformation appears crucial for viral cleavage/packaging (Adelman, et al., 2001). For this reason, whether a folding into G-quadruplex occurs, targeting the viral genome at this level could actually constitute a promising G4-related site of action in innovative antiviral strategies.

We also tested the *pac1* motif of HHV-6, which differs in HHV-6A and HHV-6B (Table 6) (Thomson, et al., 1994).

Given the high number of guanosines in HSV-1 packaging sequences, we recorded CD spectra in the absence or presence of KCl 50 mM. In the case of HHV-6, pac1 sequences are characterized by a lower amount of G bases, therefore CD spectra were recorded in the

absence or presence of KCl 100 mM. HSV-1 packaging sequences were also tested in the presence of BRACO-19 (16 µM).

All wt and mutated HSV-1 packaging sequences showed a parallel conformation in the absence of K^+, in physiological conditions and also after the addition of BRACO-19 (Figure 4.4.1, 4.4.2). However, mutations of some bases strongly affected the stability of these sequences during thermal unfolding, especially for *mut L-poly G* and *mut T-rich* (Figure 4.4.2).

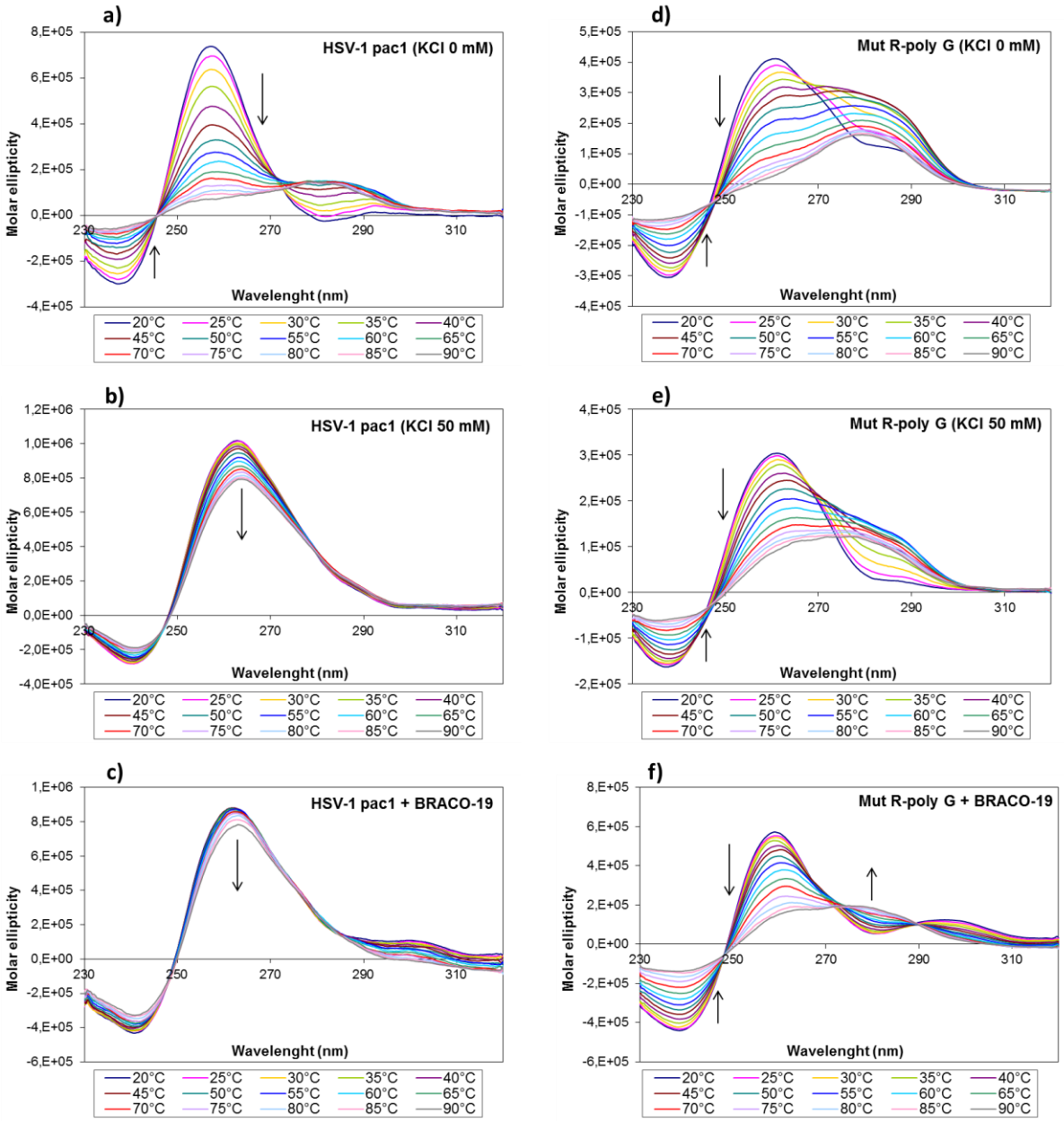

Figure 4.4.1 CD thermal denaturation analysis in the presence of the wild-type *HSV-1 pac1* sequence and a mutated form (*mut R-poly G* sequence). CD spectra of the indicated oligonucleotides (4 µM) were recorded in the absence of K^+ (a, d), in the presence of K^+ 50 mM (b, e), or in the co-presence of K^+ 50 mM and the G-quadruplex ligand BRACO-19 (16 µM) (c, f). Arrows indicate spectra progression during temperature increasing.

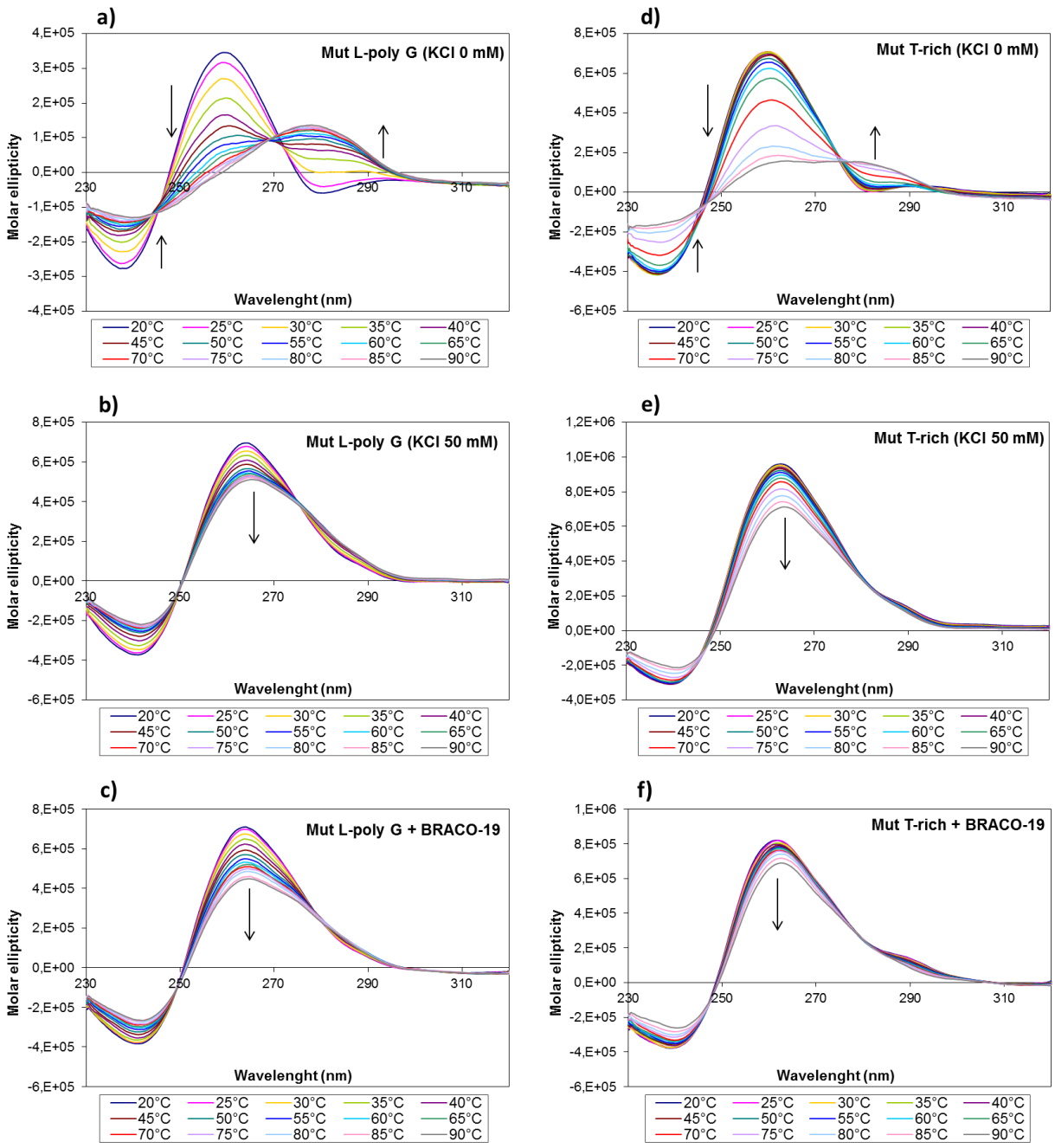

Figure 4.4.2 CD thermal denaturation analysis in the presence of two mutated HSV-1 packaging sequences, *mut L-poly G* and *mut T-rich*. CD spectra of the indicated oligonucleotides (4 µM) were recorded in the absence of K^+ (a, d), in the presence of K^+ 50 mM (b, e), or in the co-presence of K^+ 50 mM and the G-quadruplex ligand BRACO-19 (16 µM) (c, f). Arrows indicate spectra progression during temperature increasing.

In the absence of K^+, *mut L-poly G* displayed the highest Tm (72.11°C) (Figure 4.4.2a), and it was further stabilized by K^+ 50 mM and BRACO-19 (Figure 4.4.2b,c) (Table 12). *HSV-1 pac1* showed a Tm of ~41°C, but an incredibly high stabilization was determined by adding BRACO-19 (over 60°C) (Table 12). The less stable oligonucleotide is *mut L-poly G*, thus indicating a crucial role of two cytosines followed by four guanines in the first G-tract of the *HSV-1 pac1* sequence during the folding into G-quadruplex. Given the lower stabilization of

mut T-rich induced by K^+ or BRACO-19 (Figure 4.4.2d,e,f and Table 12), also the T-rich tract appeared indispensable for G-quadruplex formation and stability.

HSV-1 (wt/mutated) packaging sequences					
Oligo	**K^+ 0 mM**	**K^+ 50 mM**	**K^+ 50 mM+B19**	**ΔTm (K^+ 50mM/no K^+)**	**ΔTm (K^+ 50 mM+B19/no K+)**
HSV-1 pac1	40,99 ± 0,94	60,48 ± 0,5	>100	19,5	>59,01
Mut. L-poly G	32,76 ± 1,7	35,55 ± 1,64	39,42 ± 8,58	2,8	6,7
Mut. T-rich	53,99 ± 0,76	56,22 ± 0,3	67,07 ± 1,2	2,23	13,1
Mut. R-poly G	72,11 ± 0,47	91,15 ± 6,9	>100°C	19,04	>27,9
HHV-6 packaging sequences					
Oligo	**K^+ 0 mM**	**K^+ 100 mM**		**ΔTm (K^+ 100mM/no K^+)**	
HHV-6A pac1	67,31 ± 2,79	>100	-	>32,9	-
HHV-6B pac1	55,67 ± 0,94	67,24 ± 3,26	-	11,57	-

Table 12 Stability of HSV-1 and HHV-6 G-quadruplex folding packaging sequences measured by CD, in the presence/absence of K^+ (50 or 100 mM), and BRACO-19 (B19, 16 μM) in the case of HSV-1 sequences. Values are indicated as Tm (°C).

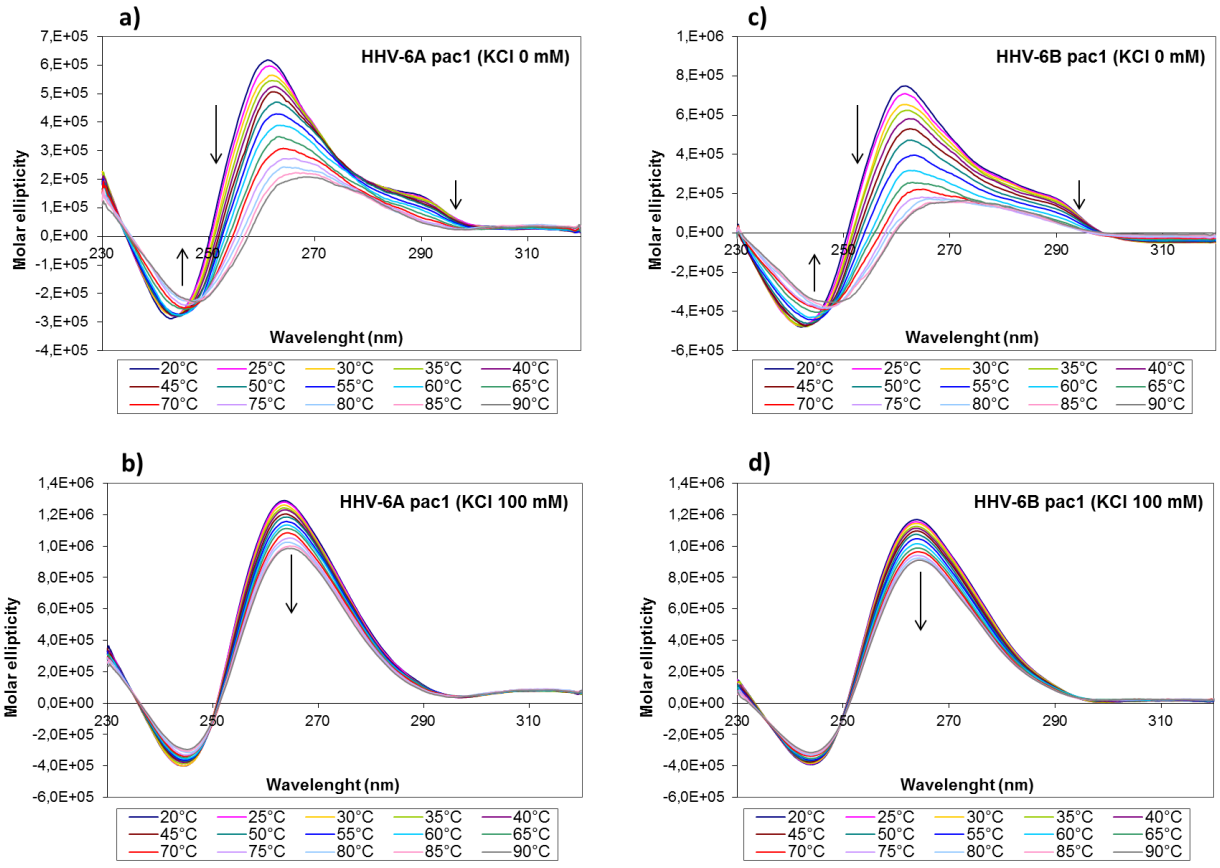

Figure 4.4.3 CD thermal denaturation analysis in the presence of *HHV-6A pac1* and *HHV-6B pac1* sequences. CD spectra of the indicated oligonucleotides (4 μM) were recorded in the absence of K^+ (a, c) and in the presence of K^+ 100 mM (b, d). Arrows indicate spectra progression during temperature increasing.

Similarly to HSV-1 packaging sequences, *HHV-6A pac1* and *HHV-6B pac1* sequences exhibited a parallel G-quadruplex topology, characterized by very high molar ellipticities (Figure 4.4.3). Although the major stability displayed by the *pac1* sequence of HHV-6A (U1102 strain), both sequences were very stable in the absence of K^+, with Tm between 56-68°C, whereas the addition of K^+ (100 mM) further stabilized the G-quadruplex structures of ~12°C for HHV-6B *pac1* and over 33°C for HHV-6A *pac1* (Figure 4.4.3 and Table12).

5 CONCLUSIONS

In this work we have found that the GC-rich HSV-1 genome presents 6 extended repeated clusters of G-quadruplex forming sequences, covering 1100 bp on the leading strand and 920 bp on the lagging strand (Figure 4.1.1 and Table 9). The *a* sequence, which embedded the *un3* G-quadruplex forming tract, has been shown to sustain multiple essential viral functions: it supports recombination with high efficiency (Smiley, et al., 1990), despite being dispensable for isomerization (Martin & Weber, 1996); it contains the packaging signal and the cleavage site of concatemeric DNA (Smiley, et al., 1992). Importantly, the *un3* cluster corresponds to the promoter of the gene that encodes the $\gamma_1$34.5 protein (Chou & Roizman, 1986). The $\gamma_1$34.5 gene itself is located in the inverted repeats of the *b* sequence of the L component and it is present in two copies per genome (Ackermann, et al., 1986). This protein has initially been shown to contribute to HSV neurovirulence *in vivo*. Indeed, HSV-1 mutants that fail to express the $\gamma_1$34.5 protein are incapable of multiplying and causing encephalitis in experimental animal models (Chou, et al., 1990), (Chou & Roizman, 1994). However, collecting evidence suggests that the $\gamma_1$34.5 protein is a multifunctional protein. Among other roles, the $\gamma_1$34.5 protein is implicated in HSV-1 DNA replication since its carboxyl-terminal domain complexes with PCNA (proliferating cell nuclear antigen), a nuclear protein involved in DNA replication and cell cycle regulation (Harland, et al., 2003). In addition, the $\gamma_1$34.5 protein has been shown to facilitate the initiation of protein translation in infected cells by bridging eukaryotic initiation factor eIF2α and protein phosphatase PP1α (He, et al., 1997), mechanism by which it blocks autophagy in cascade signal pathway (Lussignol, et al., 2012), (Orvedahl, et al., 2007).

Very interestingly, the DR2 segment present in the *a* region, which overlaps exactly with our *un3* sequence, has been shown to form an unwound, nuclease sensitive conformation of non-B DNA, called anisomorphic DNA (Sarisky & Weber, 1994), that entirely matches with the G-quadruplex structure presented here. Notably, this region has been shown to mediate transcriptional repression only in its anisomorphic DNA conformation (i.e. the G-quadruplex). This conformation perfectly correlates with the notion that G-quadruplex acts as transcriptional silencers, in addition it has been shown to be bound by the eukaryotic transcription factor SP1 (Chung, et al., 1995), which again has been involved in G-quadruplex-mediated regulation of transcription in human cells (Todd & Neidle, 2008).

The viral functional role of the remaining repeat regions possessing the ability to fold into G-quadruplex has been less extensively studied than the *a* sequence. Their complexity and importance is however evident: the inverted repeats of the L and S component contain the α genes 0 and 4, respectively, in their entirety (Chou & Roizman, 1986), (Perry & McGeoch, 1988). These genes encode ICP0 and ICP4 proteins, which are fundamental transcriptional activators. In addition, two HSV-1 origins of DNA replication (*Ori*$_S$) are localized in the TR$_S$/IR$_S$ repeated region of the viral genome (Stow, 1982). To note, however, that the identified G-quadruplex forming regions were close but not embedded in these functional sequences.

The analyzed G-quadruplex forming sequences in the HSV-1 genome displayed distinctive features: for example, the *gp054* oligonucleotide series only formed dimers. G-quadruplex dimer formation is required in HIV to promote virus recombination by strand transfer (Piekna-Przybylska, et al., 2013). Among the *gp054* oligonucleotides, *gp054d* stands out for its improved stability. Interestingly, this is the only sequence that presents one C base in the loop and displays identical CT loops. It has been reported that C can also be involved in G-quartet formation (Lim, et al., 2009), therefore it is possible that C bases augment the folding stability of this sequence.

The general remarkably high stability of the HSV-1 G-quadruplex forming sequence is an intriguing aspect: in physiological conditions all but one sequence (*un3*) displayed T_m around 90°C and were capable of folding into tetraplex even in the absence of K^+. Therefore, during temporary DNA unfolding which occurs in replication and transcription, these sequences in their single-stranded form are very likely to fold into G-quadruplex. In eukaryotes and prokaryotes, G-quadruplex have been implicated in genetic instability (Ribeyre, et al., 2009), genome rearrangements (Cahoon & Seifert, 2009), chromosome end capping (De Cian, et al., 2008) and control of gene expression. In promoter and gene coding sequences, G-quadruplexes were proposed to serve as loading platforms for gene regulatory factors enabling, for example, rapid activation of gene transcription under stress conditions (Helmrich, et al., 2013). In addition, G-quadruplex motifs have been associated with over 90% of DNA replication origins (Besnard, et al., 2012). It is therefore plausible that the G-quadruplex forming regions in the HSV-1 genome display multiple yet non-identified functions required for the viral biology.

The porphyrin TMPyP4 (Shi, et al., 2001), (Yamashita, et al., 2005) and BRACO-19, a tri-substituted acridine (Harrison, et al., 2003) (Read, et al., 2001), both characterized by

excellent G-quadruplex binding properties (Phatak & Burger, 2007), have been employed here to check the effect of the stabilization of HSV-1 G-quadruplex forming regions.

We have shown that TMPyP4 and BRACO-19 stabilized all tested sequences. In particular, BRACO-19 was able to arrest viral DNA processing by Taq polymerase *in vitro*, while in infected cells this activity resulted in early inhibition of viral replication (less viral DNA was synthesized in treated cells), generalized shut down of late viral mRNA levels and overall, in inhibition of viral production. The time of addition assay indicated an early time range of activity (within 8 h.p.i.), similarly to ACV which targets viral DNA polymerase. Altogether these data indicate that BRACO-19 targets early viral mechanisms, such as viral replication by directly inhibiting the replication machinery or by inhibiting functions in trans, like the $\gamma_1$34.5 promoter activity. In contrast, no specific inhibition of the UL36 protein was observed (Figure 4.1.10, 4.1.12e).

Very promising results were further provided by TMPyP4, tested on HSV-1 infected Vero cells. Data suggested that TMPyP4 exploits its antiviral activity by interfering with the $\gamma_1$34.5 promoter thought alternative mechanisms of action, in comparison to those of BRACO-19. TMPyP4 displayed a strongly significant antiviral activity against HSV-1 in collected supernatants, even higher than the inhibitory effect of BRACO-19. However, plaque assay showed the presence of infectious HSV-1 particles within treated cells (Figure 4.1.18). TEM analysis proved that HSV-1 remains entrapped in vesicles located in the cytoplasm of cells, nearby the nucleus. Given the high similarities of these HSV-1-containing vesicles to autophagosomes, two TMPyP4-induced mechanisms of action were hypothesized to occur: 1) TMPyP4 affects HSV-1 maturation/egress and 2) TMPyP4 acts by stabilizing *un3* G-quadruplex forming sequences, which results in an altered expression of the $\gamma_1$34.5 protein and thus in autophagy induction. Indeed, these two mechanism may converge in just one common mechanism, since the presence of *un3* cluster within the promoter of $\gamma_1$34.5 gene can impact on the $\gamma_1$34.5 protein expression, which has been related to HSV-1 maturation/ egress regulation (Brown, et al., 1994), and autophagy regulation (Lussignol, et al., 2012), (Orvedahl, et al., 2007), (Le Sage & Banfield, 2012). To this end, the co-treatment of HSV-1 infected Vero cells with both TMPyP4 and 3-MA counteract the antiviral efficacy of TMPyP4 of up to 20%, by specifically reducing autophagy process (Le Sage & Banfield, 2012). Further experiments, such as the use of a ICP34.5-deleted HSV-1 mutant and quantification of ICP34.5 after treatment with TMPyP4, are ongoing to confirm these hypothesis.

Interestingly, these differential mechanisms of action of BRACO-19 and TMPyP4 could be ascribable to a different interaction between G-quadruplex ligands and G-quadruplex topologies.

The antiviral activity of TMPyP4 and BRACO-19 was compared to that of TMPyP2, a molecule which shares similar chemical features but shows a much lower binding affinity towards G-quadruplexes (Han, et al., 2001). At the highest concentrations, TMPyP2 displayed a moderate HSV-1 inhibitory capability, which might be mediated by G-quadruplex interaction as well (Le, et al., 2013). However, based on the observation that TMPyP2 was essentially inactive in other assays, it cannot be excluded that TMPyP2 at high doses displays anti-HSV-1 activity via a non-G-quadruplex related mechanism, or that the instability of the porphyrin derivatives might contribute to the observed differences.

It has to be noted that only large clusters of G-quadruplex sequences have been considered in this work: additional single tetraplexes in key regions of the HSV-1 genome (i.e. promoters of early key genes) may be present and participate to the antiviral activity of the compound. Since its first introduction in the 1980s, ACV has been the antiviral drug of choice for the treatment of HSV-1 infections (Vere Hodge & Field, 2013). However, the emergence of resistance to ACV has created an obstacle for the treatment of HSV-1 (Bacon, et al., 2003).

Moreover, because of the inherent different mechanism of action, G-quadruplex ligands could be envisaged as therapeutic options against HSV-1 strains resistant to current anti-herpetic drugs.

This work has provided the first evidence of 1) large clusters of repeated G-quadruplex folding sequences in the HSV-1 genome; 2) the possibility to target them with G-quadruplex ligands; 3) BRACO-19-mediated antiviral effects during early events of the viral life cycle, such as DNA replication or promoter activity/expression of genes that control viral replication and transcription (Figure 4.1.10, 4.1.24); 4) TMPyP4-mediated antiviral effects during HSV-1 maturation/egress events by stimulating autophagy process, due to a minor expression of $\gamma_1$34.5 protein as a consequence of the G-quadruplex presence in the promoter of $\gamma_1$34.5 gene.

The great capacity of TMPyP4 and BRACO-19 to also inhibit both HHV-6A and HHV-6B indicates that G-quadruplex can be considered a promising innovative anti-herpetic target.

The visualization of G-quadruplex structures in cells, which has always constituted an ambitious challenge, was recently achieved using specific antibodies able to selectively binds to G-quadruplex DNA structures (Biffi, et al., 2013), (Henderson, et al., 2013).

For the present study, detection of viral DNA G-quadruplexes in infected cells is strongly necessary to support and confirm the presence of this particular secondary conformation of

DNA in the genome of viruses, as HSV-1. The visualization of viral G-quadruplex, in addition, can prove the role of G-quadruplex itself during essential events of the viral replication cycle, therefore the importance of targeting it in successful novel antiviral therapy, which could be capable to potentially eradicate the virus from the host. As shown, the use of the monoclonal antibody 1H6, showing high selectivity for G-quadruplex structures, for the first time allowed us to reach this very ambitious goal. A strong increase of red foci, relative to the binding of 1H6 with DNA G-quadruplex structures, were observed between 6 and 9 h.p.i., in which viral DNA is locally unwound to facilitate the replication of HSV-1. The increasing fluorescence in such a crucial time point, in comparison with mock-infected cells, suggested a specific interaction between the antibody and viral G-quadruplexes, over cellular G-quadruplex structures. An additional proof a specific interaction between 1H6 and viral G-quadruplex structures was provided by treating infected cells with PAA, known to specifically improve viral replication. In fact, the treatment reduced the fluorescence raising.

Therefore, this work provides a proof of concept for the development of selective anti-herpetic agents with an innovative mechanism of action which could prove useful also in the treatment of viral strains resistant to current anti-herpetic drugs. Although data successfully propose G-quadruplex as a very promising antiviral strategy, rational design of small molecules, able to selectively recognize viral G-quadruplexes versus the eukaryotic structures and improve this binding, is undoubtedly necessary.

6 REFERENCES

Ablashi, D. et al., 2014. Classification of HHV-6A and HHV-6B as distinct viruses. *Arch Virol.,* 159(5), pp. 863-870.

Ablashi, D. et al., 1987. HBLV (or HHV-6) in human cell lines Nature. *Nature,* Volume 329, p. 207.

Ackermann, M., Chou, J., Sarmiento, M. & Roizman, B., 1986. Identification by antibody to a synthetic peptide of a protein specified by a diploid gene located in the terminal repeats of the L component of herpes simplex virus genome. *Journal of Virology,* 58(3), pp. 843-850.

Adelman, K., Salmon, B. & Baines, J., 2001. Herpes simplex virus DNA packaging sequences adopt novel structures that are specifically recognized by a component of the cleavage and packaging machinery. *Proc Natl Acad Sci USA,* 98(6), p. 3086–3091.

Ahlqvist, J. et al., 2006. Complete replication cycle and acquisition of tegument in nucleus of human herpesvirus 6A in astrocytes and in T-Cells. *Journal of Medical Virology,* Volume 78, p. 1542–1553.

Akhtar, J. & Shukla, D., 2009. Viral entry mechanisms: cellular and viral mediators of herpes simplex virus entry. *FEBS Journal,* 276(24), p. 7228–7236.

Arvin, A. et al., 2007. *Human Herpesviruses. Biology, Therapy, and Immunoprophylaxis.*. Cambridge: Cambridge University Press.

Bacon, T., Levin, M. & Leary, J., 2003. Herpes simplex virus resistance to acyclovir and penciclovir after two decades of antiviral therapy. *Clinical Microbiology,* 16(1), pp. 114-128.

Bailey, S. & Murnane, J., 2006. Telomeres, chromosome instability and cancer. *Nucleic Acids Research,* 34(8), p. 2408–2417.

Baines, J. & Weller, S., 2005. Cleavage and packaging of herpes simplex virus 1 DNA. In: *Viral genome packaging machines: genetics, structure, and mechanism.* s.l.:C.E. Catalano (Ed.), pp. 135-150.

Balasubramanian, S., Hurley, L. & Neidle, S., 2011. Targeting G-quadruplexes in gene promoters: a novel anticancer strategy?. *Nat Rev Drug Discov.,* 10(4), pp. 261-275.

Balasubramanian, S. & Neidle, S., 2009. G-quadruplex nucleic acids as therapeutic targets. *Curr Opin Chem Biol.,* 13(3), pp. 345-353.

Bang, I., 1910. Untersuchungen über die Guanylsäure. *Biochemische Zeitschrift,* Volume 26, pp. 293-311.

Bedadala, G., Pinnoji, R., Palem, J. & Hsia, S., 2010. Thyroid hormone controls the gene expression of HSV-1 LAT and ICP0 in neuronal cells. *Cell Research,* Volume 20, p. 587–598.

Besnard, E. et al., 2012. Unraveling cell type-specific and reprogrammable human replication origin signatures associated with G-quadruplex consensus motifs. *Nature Structural & Molecular Biology,* 19(8), pp. 837-844.

Biffi, G., Tannahill, D., McCafferty, J. & Balasubramanian, S., 2013. Quantitative visualization of DNA G-quadruplex structures in human cells. *Nature Chemistry,* Volume 5, pp. 182-186.

Blackburn, E., 1991. Structure and function of telomeres. *Nature,* Volume 350, pp. 569-573.

Braun, D., Dominguez, G. & Pellet, P., 1997. Human Herpesvirus 6. *Clinical Microbiology Reviews,* 10(3), pp. 521-567.

Brooks, T., Kendrick, S. & Hurley, L., 2010. Making sense of G-quadruplex and i-motif functions in oncogene promoters. *FEBS J.,* Volume 277, p. 3459–3469.

Brown, S., Alasdair, R., James, D. & Harland, J., 1994. ICP34.5 influences herpes simplex virus type 1 maturation and egress from infected cells in vitro. *Journal of General Virology,* Volume 75, pp. 3679-3686.

Bugaut, A. & Balasubramanian, S., 2008. A sequence-independent study of the influence of short loop lengths on the stability and topology of intramolecular DNA G-quadruplexes. *Biochemistry*, Volume 47, p. 689–697.

Burger, A. et al., 2005. The G-quadruplex-interactive molecule BRACO-19 inhibits tumor growth, consistent with telomere targeting and interference with telomerase function. *Cancer Research,* Volume 65, pp. 1489-1496.

Burge, S. et al., 2006. Quadruplex DNA: sequence, topology and structure. *Nucleic Acid Research,* Volume 34, p. 5402–5415.

Cahoon, L. & Seifert, H., 2009. An alternative DNA structure is necessary for pilin antigenic variation in Neisseria gonorrhoeae. *Science,* 325(5941), pp. 764-767.

Carbone, I. et al., 2014. Herpes virus in Alzheimer's disease: relation to progression of the disease. *Neurobiol Aging,* 35(1), pp. 122-129.

Cardinali, G. et al., 1998. Viral glycoproteins accumulate in newly formed annulate lamellae following infection of lymphoid cells by human herpesvirus 6. *Journal of Virology,* 72(12), pp. 9738-9746.

Caselli, E. et al., 2012. Virologic and immunologic evidence supporting an association between HHV-6 and Hashimoto's thyroiditis. *PLoS Pathog.,* 8(10), p. e1002951.

Challberg, M., 1996. *Herpesvirus DNA replication.* Cold Spring Harbor, N.Y.: Cold Spring Harbor Press.

Chou, J., Kern, E., Whitley, R. & Roizman, B., 1990. Mapping of herpes simplex virus-1 neurovirulence to gamma 134.5, a gene nonessential for growth in culture. *Science,* 250(4985), pp. 1262-1266.

Chou, J. & Roizman, B., 1986. The terminal a sequence of the herpes simplex virus genome contains the promoter of a gene located in the repeat sequences of the L component. *Journal of Virology,* 57(2), pp. 629-637.

Chou, J. & Roizman, B., 1994. Herpes simplex virus 1 y134.5 gene function, which blocks the host response to infection, maps in the homologous domain of the genes expressed during growth arrest and DNA damage. *Proc. Natl. Acad. Sci. USA,* Volume 91, pp. 5247-5251.

Chung, I., Soisson, S. & Muller, M., 1995. Clustering of Sp1 sites near the promoter region of ICP34.5 in herpes simplex virus type 1. *Journal of Biochemistry,* 117(1), pp. 19-22.

Cogoi, S., Paramasivam, M., Spolaore, B. & Xodo, L., 2008. Structural polymorphism within a regulatory element of the human KRAS promoter: formation of G4-DNA recognized by nuclear proteins. *Nucleic Acids Research,* Volume 36, pp. 3765-3780.

Cogoi, S. & Xodo, L., 2006. G-quadruplex formation within the promoter of the KRAS proto-oncogene and its effect on transcription. *Nucleic Acids Research,* Volume 34, pp. 2536-2549.

Copeland, A., Newcomb, W. & Brown, J., 2009. Herpes simplex virus replication: roles of viral proteins and nucleoporins in capsid-nucleus attachment. *Journal of Virology,* 83(4), pp. 1660-1668.

Cuenca, F. et al., 2008. Tri- and tetra-substituted naphthalene diimides as potent G-quadruplex ligands. *Bioorganic & Medicinal Chemistry Letters,* Volume 18, pp. 1668-1673.

Daelemans, D., Pauwels, R., De Clercq, E. & Pannecouque, C., 2011. A time-of-drug addition approach to target identification of antiviral compounds. *Nat Protoc,* Volume 6, pp. 925-933.

De Bolle, L., Naesens, L. & De Clercq, E., 2005. Update on Human Herpesvirus 6 Biology, Clinical Features, and Therapy. *Clinical Microbiology Reviews,* 18(1), p. 217–245.

De Cian, A. et al., 2008. Targeting telomeres and telomerase. *Biochimie,* 90(1), pp. 131-155.

Deng, H. & Dewhurst, S., 1998. Functional identification and analysis of cis-acting sequences which mediate genome cleavage and packaging in human herpesvirus 6.. *Journal of Virology,* 72(1), pp. 320-329.

Dexheimer, T., Sun, D. & Hurley, L., 2006. Deconvoluting the structural and drug-recognition complexity of the G-quadruplex-forming region upstream of the bcl-2 P1 promoter. *Journal of the American Chemical Society,* Volume 128, pp. 5404-5415.

Di Antonio, M., Rodriguez, R. & Balasubramanian, S., 2012. Experimental approaches to identify cellular G-quadruplex structures and functions. *Methods,* 57(1), pp. 84-92.

Doi, T., Yoshida, M., Shin-ya, K. & Takahashi, T., 2006. Total synthesis of (R)-telomestatin. *Organic Letters,* Volume 8, pp. 4165-4167.

Donati, D. et al., 2003. Detection of human herpesvirus-6 in mesial temporal lobe epilepsy surgical brain resections. *Neurology,* 61(10), pp. 1405-1411.

Doria, F. et al., 2012. Water soluble extended naphthalene diimides as pH fluorescent sensors and G-quadruplex ligands. *Organic & Biomolecular Chemistry,* Volume 10, pp. 3830-3840.

Everett, R., 1984. A detailed analysis of an HSV-1 early promoter: sequences involved in trans-activation by viral immediate-early gene products are not early-gene specific. *Nucleic Acids Research,* 12(7), pp. 3037-3056.

Flint, S., Enquist, L., Racaniello, V. & Skalka, A., 2003. *Principles of Virology: Molecular Biology, Pathogenesis, and Control of Animal Viruses.* 2nd Edition ed. Washington, DC: ASM Press.

Gellert, M., Lipsett, M. & Davies, D., 1962. Helix formation by guanylic acid. *Proceedings of the National Academy of Sciences of the United States of America,* Volume 48, pp. 2013-2018.

Gompels, U. & Macaulay, H., 1995. Characterization of human telomeric repeat sequences from human herpesvirus 6 and relationship to replication. *J Gen Virol.,* 76(2), pp. 451-458.

Granzow, H. et al., 2001. Egress of alphaherpesviruses: comparative ultrastructural study. *Journal of Virology,* 75(8), p. 3675–3684.

Greider, C. & Blackburn, E., 1985. Identification of a specific telomere terminal transferase activity in tetrahymena extracts. *Cell,* 43(2), p. 405–413.

Hanahan, D. & Weinberg, R., 2000. The hallmarks of cancer. *Cell,* Volume 100, pp. 57-70.

Han, F., Wheelhouse, R. & Hurley, L., 1999. Interactions of TMPyP4 and TMPyP2 with Quadruplex DNA. Structural basis for the differential effects on telomerase inhibition. *J. Am. Chem. Soc.,* 121(15), p. 3561–3570.

Han, H. & Hurley, L., 2000. G-quadruplex DNA: a potential target for anti-cancer drug design. *Trends in Pharmacological Sciences,* Volume 21, p. 136–142.

Han, H., Langley, D., Rangan, A. & Hurley, L., 2001. Selective interactions of cationic porphyrins with G-quadruplex structures. *J Am Chem Soc,* 123(37), pp. 8902-8913.

Harland, J. et al., 2003. The herpes simplex virus (HSV) protein ICP34.5 is a virion component that forms a DNA-binding complex with proliferating cell nuclear antigen and HSV replication proteins. *Journal of Neurovirology,* 9(4), pp. 477-488.

Harrison, R. et al., 2003. Trisubstituted acridine derivatives as potent and selective telomerase inhibitors. *Journal of Medicinal Chemistry,* 46(21), pp. 4463-4476.

He, B., Gross, M. & Roizman, B., 1997. The gamma(1)34.5 protein of HSV-1 complexes with protein phosphatase 1alpha to dephosphorylate the alpha subunit of the eukaryotic translation initiation factor 2 and preclude the shutoff of protein synthesis by double-stranded RNA-activated. *Proc Natl Acad Sci USA,* 94(3), pp. 843-848.

Helmrich, A. et al., 2013. Transcription-replication encounters, consequences and genomic instability. *Nature structural & Molecular Biology,* 20(4), pp. 412-418.

Henderson, A. et al., 2013. Detection of G-quadruplex DNA in mammalian cells. *Nucleic Acids Research,* 42(2), pp. 860-869.

Herold, B., WuDunn, D., Soltys, N. & Spear, P., 1991. Glycoprotein C of herpes simplex virus type 1 plays a principal role in the adsorption of virus to cells and in infectivity. *Journal of Virology,* Volume 65, pp. 1090-1098.

Hershman, S. et al., 2008. Genomic distribution and functional analyses of potential G-quadruplex-forming sequences in Saccharomyces cerevisiae. *Nucleic Acids Research,* Volume 36, pp. 144-156.

Huppert, J. & Balasubramanian, S., 2005. Prevalence of quadruplexes in the human genome. *Nucleic Acids Research,* 33(9), pp. 2908-2016.

Hurley, L., 2000. G-quadruplexes as targets for drug design. *Pharmacology & Therapeutics,* 85(3), p. 141–158.

Igarashi, K., Fawl, R., Roller, R. & Roizman, B., 1993. Construction and properties of a recombinant herpes simplex virus 1 lacking both S-component origins of DNA synthesis. *Journal of Virology,* 67(4), pp. 2123-2132.

Itzhaki, R. et al., 1997. Herpes simplex virus type 1 in brain and risk of Alzheimer's disease. *The Lancet,* 349(9047), pp. 241-244.

Jackson, S. & DeLuca, N., 2003. Relationship of herpes simplex virus genome configuration to productive and persistent infections. *PNAS,* 100(13), p. 7871–7876.

James, S. & Prichard, M., 2014. Current and future therapies for herpes simplex virus infections: mechanism of action and drug resistance. *Current Opinion in Virology,* Volume 8C, pp. 54-61.

Kikin, O., D'Antonio, L. & Bagga, P., 2006. QGRS Mapper: a web-based server for predicting G-quadruplexes in nucleotide sequences. *Nucleic Acids Research,* Volume 34, pp. 676-682.

Kim, N. et al., 1994. Specific association of human telomerase activity with immortal cells and cancer. *Science,* Volume 266, pp. 2011-2015.

Kramer, M. et al., 2003. Latent herpes simplex virus infection of sensory neurons alters neuronal gene expression. *Journal of Virology,* 77(17), p. 9533–9541.

La Boissière, S., Izeta, A., Malcomber, S. & O'Hare, P., 2004. Compartmentalization of VP16 in cells infected with recombinant herpes simplex virus expressing VP16-green fluorescent protein fusion proteins. *Journal of Virology,* 78(15), pp. 8002-8014.

Lacroix, A. et al., 2007. HHV-6 and EBV DNA quantitation in lymph nodes of 86 patients with Hodgkin's lymphoma. *J Med Virol.,* 79(9), pp. 1349-1356.

Law, M. et al., 2010. ATR-X syndrome protein targets tandem repeats and influences allele-specific expression in a size-dependent manner. *Cell,* Volume 143, pp. 367-378.

Le Sage, V. & Banfield, B., 2012. Dysregulation of autophagy in murine fibroblasts resistant to HSV-1 infection. *Plos One,* 7(8), p. e42636.

Lehman, I. & Boehmer, P., 1999. Replication of herpes simplex Virus DNA. *The Journal of Biological Chemistry,* Volume 274, pp. 28059-28062.

Le, V., Nagesh, N. & Lewis, E., 2013. Bcl-2 promoter sequence G-quadruplex interactions with three planar and non-planar cationic porphyrins: TMPyP4, TMPyP3, and TMPyP2. *PloS One,* 8(8), p. e72462.

Levy, M. et al., 1991. Telomer end-replication problem and cell aging. *J. Mol. Biol.,* Volume 225, pp. 951-960.

Li, G., Eller, M., Firoozabadi, R. & Gilchrest, B., 2003. Evidence that exposure of the telomere 3' overhang sequence induces senescence. *Proc. Natl. Acad. Sci. USA,* 100(2), pp. 527- 531.

Lim, K. et al., 2009. Sequence variant (CTAGGG)n in the human telomere favors a G-quadruplex structure containing a G.C.G.C tetrad. *Nucleic Acids Research,* 37(18), pp. 6239-6248.

Lipps, H. & Rhodes, D., 2009. G-quadruplex structures: in vivo evidence and function. *Trends in Cell Biology,* 19(8), p. 414–422.

Lockshon, D. & Galloway, D., 1988. Sequence and structural requirements of a herpes simplex viral DNA replication origin. *Mol. Cell. Biol.,* Volume 8, pp. 4018-4027.

Lopes, J. et al., 2011. G-quadruplex-induced instability during leading-strand replication. *EMBO J.,* 30(19), p. 4033–4046.

Lussignol, M. et al., 2012. The herpes simplex virus 1 Us11 protein inhibits autophagy through its interaction with the protein kinase PKR. *Journal of Virology,* 87(2), pp. 859-871.

Lusso, P. & Gallo, R., 1995. Human herpesvirus 6. *Baillière's Clinical Haematology,* 8(1), pp. 201-223.

Lusso, P. & Gallo, R., 1995. Human herpesvirus 6 in AIDS. *Immunol Today,* 16(2), pp. 67-71.

Maizels, N., 2006. Dynamic roles for G4 DNA in the biology of eukaryotic cells. *Nature Structural & Molecular Biology,* Volume 13, pp. 1055-1059.

Marsden, H. et al., 1996. The herpes simplex virus type 1 UL8 protein influences the intracellular localization of the UL52 but not the ICP8 or POL replication proteins in virus-infected cells. *J Gen Virol.,* Volume 77, pp. 2241-2249.

Martin, D. & Weber, P., 1996. The a sequence is dispensable for isomerization of the herpes simplex virus type 1 genome. *Journal of Virology,* 70(12), pp. 8801-8812.

Martin, M. et al., 1991. The genome of human herpesvirus 6: maps of unit-length and concatemeric genomes for nine restriction endonucleases. *J Gen Virol.,* 72(1), pp. 157-168.

McLuckie, K. et al., 2011. G-quadruplex-binding benzo[a]phenoxazines down-regulate c-KIT expression in human gastric carcinoma cells. *J Am Chem Soc,* 133(8), p. 2658–266.

McNabb, D. & Courtney, R., 1992. Analysis of the UL36 open reading frame encoding the large tegument protein (ICP1/2) of herpes simplex virus type 1. *Journal of Virology,* Volume 66, pp. 7581-4.

Mettenleiter, T., 2002. Herpesvirus Assembly and Egress. *Journal of Virology,* 76(4), p. 1537–1547.

Mettenleiter, T., 2004. Budding events in herpesvirus morphogenesis. *Virus Research,* Volume 106, pp. 167-180.

Mirkin, S., 2013. DNA replication: driving past four-stranded snags. *Nature,* Volume 497, pp. 449-450.

Morissette, G. & Flamand, L., 2010. Herpesviruses and chromosomal integration. *Journal of Virology,* 84(23), pp. 12100-12109.

Mukundan, V. & Phan, A., 2013. Bulges in G-Quadruplexes: Broadening the Definition of G-Quadruplex-Forming Sequences. *J Am Chem Soc,* 135(13), p. 5017–5028.

Nicholas, J., 1994. Nucleotide sequence analysis of a 21-kbp region of the genome of human herpesvirus-6 containing homologues of human cytomegalovirus major immediate-early and replication genes. *Virology,* 204(2), pp. 738-750.

Norseen, J., Johnson, F. & Lieberman, P., 2009. Role for G-quadruplex RNA binding by Epstein-Barr virus nuclear antigen 1 in DNA replication and metaphase chromosome attachment. *Journal of Virology,* Volume 83, pp. 10336-10346.

O'Connor, C., 2008. Telomeres of human chromosomes. *Nature Education,* 1(166).

Orvedahl, A. et al., 2007. HSV-1 ICP34.5 confers neurovirulence by targeting the beclin 1 autophagy protein. *Cell Host & Microbe,* 1(1), pp. 23-35.

O'Sullivan, R. & Karlseder, J., 2010. Telomeres: protecting chromosomes against genome instability. *Nat Rev Mol Cell Biol.,* 11(3), p. 171–181..

Ou, T.-M.et al., 2008. G-quadruplexes: targets in anticancer drug design. *ChemMedChem,* Volume 3, pp. 690 - 713.

Ouyang, Q. et al., 2012. High GC content of simple sequence repeats in Herpes simplex virus type 1 genome. *Gene,* 499(1), pp. 37-40.

Palumbo, S., Ebbinghaus, S. & Hurley, L., 2009. Formation of a unique end-to-end stacked pair of G-quadruplexes in the hTERT core promoter with implications for inhibition of

telomerase by G-quadruplex-interactive ligands. *Journal of the American Chemical Society*, Volume 131, pp. 10878-10897.

Paramasivam, M. et al., 2009. Protein hnRNP A1 and its derivative Up1 unfold quadruplex DNA in the human KRAS promoter: implications for transcription. *Nucleic Acids Research*, Volume 37, pp. 2841-2853.

Parkinson, G., Lee, M. & Neidle, S., 2002. Crystal structure of parallel quadruplexes from human telomeric DNA. *Nature*, Volume 417, pp. 876-880.

Pattingre, S. et al., 2005. Bcl-2 antiapoptotic proteins inhibit Beclin 1-dependent autophagy. *Cell*, Volume 122, pp. 927-939.

Perrone, R. et al., 2014. Anti-HIV-1 activity of the G-quadruplex ligand BRACO-19. *J Antimicrob Chemother*, 69(12), pp. 3248-3258.

Perrone, R. et al., 2013a. A dynamic G-quadruplex region regulates the HIV-1 long terminal repeat promoter. *J. Med. Chem.*, 56(16), pp. 6521-6530.

Perrone, R. et al., 2013b. Formation of a unique cluster of G-quadruplex structures in the HIV-1 Nef coding region: implications for antiviral activity. *PLOS One*, 8(8), p. e73121.

Perry, L. & McGeoch, D., 1988. The DNA sequences of the long repeat region and adjoining parts of the long unique region in the genome of herpes simplex virus type 1. *The Journal of General Virology*, Volume 66, pp. 2831-2846.

Phan, A., Kuryavyi, V., Luu, N. & Patel, D., 2007. Structure of two intramolecular G-quadruplexes formed by natural human telomere sequences. *Nucleic Acids Research*, 35(19), pp. 6517-6525.

Phatak, P. & Burger, A., 2007. Telomerase and its potential for therapeutic intervention. *British Journal of Pharmacology*, 152(7), pp. 1003-1011.

Piekna-Przybylska, D., Sharma, G. & Bambara, R., 2013. Mechanism of HIV-1 RNA dimerization in the central region of the genome and significance for viral evolution. *J Biol Chem*, 288(33), pp. 24140-24150.

Poffenberger, K. & Roizman, B., 1995. A noninverting genome of a viable herpes simplex virus 1: presence of head-to-tail linkages in packaged genomes and requirements for circularization after infection. *Journal of Virology*, 53(2), pp. 587-595.

Post, L., Mackem, S. & Roizman, B., 1981. Regulation of α genes of herpes simplex virus: expression of chimeric genes produced by fusion of thymidine kinase with α gene promoters. *Cell*, Volume 24, pp. 555-565.

Pyles, R., 2001. The association of herpes simplex virus and Alzheimer's disease: a potential synthesis of genetic and environmental factors. *Herpes*, 8(3), pp. 64-68.

Qin, Y. et al., 2010. Molecular cloning of the human platelet-derived growth factor receptor beta (PDGFR-beta) promoter and drug targeting of the G-quadruplex-forming region to repress PDGFR-beta expression. *Biochemistry,* Volume 49, pp. 4208-4219.

Qin, Y. & Hurley, L., 2008. Structures, folding patterns, and functions of intramolecular DNA G-quadruplexes found in eukaryotic promoter regions. *Biochimie,* Volume 90, pp. 1149-1171.

Radtke, K. et al., 2013. Inhibition of the host translation shutoff response by Herpes Simplex virus 1 triggers nuclear envelope-derived autophagy. *Journal of Virology,* 87(7), pp. 3990-3997.

Rankin, S. et al., 2005. Putative DNA quadruplex formation within the human c-kit oncogene. *Journal of th American Chemical Society,* Volume 127, pp. 10584-10589.

Read, M. et al., 2001. Structure-based design of selective and potent G quadruplex-mediated telomerase inhibitors. *Proc Natl Acad Sci USA,* 98(9), pp. 4844-4849.

Reske, A. et al., 2007. Understanding HSV-1 entry glycoproteins. *Review in Medical Virology,* Volume 17, pp. 205-215.

Ribeyre, C. et al., 2009. The yeast Pif1 helicase prevents genomic instability caused by G-quadruplex-forming CEB1 sequences in vivo. *PLoS Genetics,* 5(5), p. e1000475.

Samaniego, L., Neiderhiser, L. & NA, D., 1998. Persistence and expression of the herpes simplex virus genome in the absence of immediate-early proteins. *Journal of Virology,* 72(4), p. 3307–3320.

Sampath, P. & DeLuca, N., 2008. Binding of ICP4, TATA-binding protein, and RNA polymerase II to herpes simplex virus type 1 immediate-early, early, and late promoters in virus-infected cells. *Journal of Virology,* 82(5), pp. 2339-2349.

Sanders, C., 2010. Human Pif1 helicase is a G-quadruplex DNA-binding protein with G-quadruplex DNA-unwinding activity. *Biochem J.,* 430(1), pp. 119-128.

Sarisky, R. & Weber, P., 1994. Role of anisomorphic DNA conformations in the negative regulation of a herpes simplex virus type 1 promoter. *Virology,* 204(2), pp. 569-579.

Shi, D., Wheelhouse, R., Sun, D. & Hurley, L., 2001. Quadruplex-interactive agents as telomerase inhibitors: synthesis of porphyrins and structure-activity relationship for the inhibition of telomerase. *J Med Chem.,* 44(26), pp. 4509-4523.

Siddiqui-Jain, A., Grand, C., Bearss, D. & Hurley, L., 2002. Direct evidence for a G-quadruplex in a promoter region and its targeting with a small molecule to repress c-MYC transcription. *Proceedings of the National Academy of Sciences of the United States of America,* Volume 99, pp. 11593-11598.

Sinha, S. et al., 2008. Molecular basis of the regulation of Beclin 1-dependent autophagy by the gamma-herpesvirus 68 Bcl-2 homolog M11. *Autophagy,* 4(8), pp. 989-997.

Smiley, J., 2004. Herpes simplex virus virion host shutoff protein: immune evasion mediated by a viral RNase?. *Journal of virology,* 70(3), p. 1063–1068.

Smiley, J., Duncan, J. & Howes, M., 1990. Sequence requirements for DNA rearrangements induced by the terminal repeat of herpes simplex virus type 1 KOS DNA. *Journal of Virology,* 64(10), pp. 5036-5050.

Smiley, J., Lavery, C. & Howes, M., 1992. The herpes simplex virus type 1 (HSV-1) a sequence serves as a cleavage/packaging signal but does not drive recombinational genome isomerization when it is inserted into the HSV-2 genome. *Journal of Virology,* 66(12), pp. 7505-7510.

Snoeck, R., 2000. Antiviral therapy of herpes simplex. *International Journal of Antimicrobial Agents,* Volume 16, pp. 157-159.

Sodeik, B., Ebersold, M. & Helenius, A., 1997. Microtubule-mediated transport of incoming herpes simplex virus 1 capsids to the nucleus. *The Journal of Cell Biology,* Volume 136, pp. 1007-1021.

Spear, P., 1993. *Membrane fusion induced by HSV. In Viral Fusion Mecha-*. Boca Raton/Ann Arbor/London/Tokyo: J. Bentz, editor.

Stengel, G. & Kuchta, R., 2011. Coordinated leading and lagging strand DNA synthesis by using the herpes simplex virus 1 replication complex and minicircle DNA templates. *Journal of Virology,* Volume 85, p. 957–967.

Stewart, J. et al., 1995. Herpesvirus Infections in Persons Infected with Human Immunodeficiency Virus. *Clinical Infectious Diseases,* Volume 21, pp. S114-S120.

Stow, N., 1982. Localization of an origin of DNA replication within the TRS/IRS repeated region of the herpes simplex virus type 1 genome. *The EMBO Journal,* 1(7), pp. 863-867.

Sun, D., Guo, K., Rusche, J. & Hurley, L., 2002. Facilitation of a structural transition in the polypurine/polypyrimidine tract within the proximal promoter region of the human VEGF gene by the presence of potassium and G-quadruplex-interactive agents. *Nucleic Acids Research,* Volume 33, pp. 6070-6080.

Sundquist, W. & Heaphy, S., 1993. Evidence for interstrand quadruplex formation in the dimerization of human immunodeficiency virus 1 genomic RNA. *Proceedings of the National Academy of Sciences of the United States of America,* Volume 90, pp. 3393-3397 .

Sun, H., Karow, J., Hickson, I. & Maizels, N., 1998. The Bloom's syndrome helicase unwinds G4 DNA. *J. Biol. Chem.,* Volume 273, p. 27587–27592.

Takahashi, M. et al., 2009. Varicella-zoster virus infection induces autophagy in both cultured cells and human skin vesicles. *Journal of Virology,* Volume 85, pp. 5466-5476.

Thomson, B., Dewhurst, S. & Gray, D., 1994. Structure and heterogeneity of the a sequences of human herpesvirus 6 strain variants U1102 and Z29 and identification of human telomeric repeat sequences at the genomic termini.. *Journal of Virology,* 68(5), pp. 3007-3014.

Tluckova, K. et al., 2013. Human papillomavirus g-quadruplexes. *Biochemistry,* Volume 52, pp. 7207-7216.

Todd, A. & Neidle, S., 2008. The relationship of potential G-quadruplex sequences in cis-upstream regions of the human genome to SP1-binding elements. *Nucleic Acids Research,* 36(8), pp. 2700-2704.

Tong, L. & Stow, N., 2010. Analysis of herpes simplex virus type 1 DNA packaging signal mutations in the context of the viral genome. *Journal of Virology,* 84(1), pp. 321-329.

Vandevenne, P., Sadzot-Delvaux, C. & Piette, J., 2010. Innate immune response and viral interference strategies developed by human herpesviruses. *Biochem. Pharmacol.,* Volume 80, pp. 1955-1972.

Vere Hodge, R. & Field, H., 2013. Antiviral agents for herpes simplex virus. *Advances in Pharmacology,* Volume 6, pp. 1-38.

Verma, A. et al., 2008. Genome-wide computational and expression analyses reveal G-quadruplex DNA motifs as conserved cis-regulatory elements in human and related species. *Journal of Medicinal Chemistry,* Volume 51, pp. 5641-5649.

Wang, Y. & Patel, D., 1993. Solution structure of the human telomeric repeat d[AG3(T2AG3)3] G-tetraplex. *Current Biology,* 1(4), pp. 263-282.

Watt, T. et al., 2012. Response to valganciclovir in chronic fatigue syndrome patients with human herpesvirus 6 and Epstein-Barr virus IgG antibody titers. *J. Med. Virol.*, 84(12), pp. 1967-1974.

Weller, S. & Coen, D., 2012. Herpes Simplex Viruses: Mechanisms of DNA Replication. *Cold Spring Harb Perspect Biol. 4(9),* 4(9), pp. 1-12.

Werstuck, G., Bilan, P. & Capone, J., 1990. Enhanced infectivity of herpes simplex virus type-1 viral DNA in a cell line expressing the trans-inducing factor Vmw65. *Journal of Virology,* Volume 64, pp. 984-991.

Whitley, R., Kimberlin, D. & Roizman, B., 1998. Herpes Simplex Viruses. *Clinical Infectious Diseases,* Volume 26, pp. 541-555.

Whitley, R. & Roizman, B., 2001. Herpes simplex virus infections. *The Lancet,* Volume 357, pp. 1513-1518.

Wu, Y. & Brosh, J. R., 2010. G-quadruplex nucleic acids and human disease. *FEBS J.*, 277(17), pp. 3470-3488.

Wu, Y., Shin-ya, K. & Brosh, R. J., 2008. FANCJ helicase defective in Fanconia anemia and breast cancer unwinds G-quadruplex DNA to defend genomic stability. *Mol. Cell Biol.*, Volume 28, p. 4116–4128.

Xu, F. et al., 2002. Seroprevalence and coinfection with herpes simplex virus type 1 and type 2 in the United States. *Journal of Infectiuos Disease*, 185(8), pp. 1019-1024.

Yamashita, T., Uno, T. & Ishikawa, Y., 2005. Stabilization of guanine quadruplex DNA by the binding of porphyrins with cationic side arms. *Bioorganic & Medicinal Chemistry,* 13(7), p. 2423–2430.

Yang, D. & Okamoto, K., 2010. Structural insights into G-quadruplexes: towards new anticancer drugs. *Future Med Chem.,* 2(4), pp. 619-646.

Zhang, S., Wu, Y. & Zhang, W., 2014. G-quadruplex structures and their interaction diversity with ligands. *ChemMedChem,* Volume 9, pp. 899-911.

Zhou, C. & Knipe, D., 2002. Association of herpes simplex virus type 1 ICP8 and ICP27 proteins with cellular RNA polymerase II holoenzyme. *Journal of Virology,* 76(12), p. 5893–5904.

CONFERENCES

- Artusi S, Nadai M, Perrone R, Biasolo MA, Palù G, Flamand L, Calistri A, Richter SN (2014). *Formation on multiple clusters of repeated G-quadruplex in the HSV-1 genome: implications for antiviral activity*. 2nd Italian Experience in Biomedical Research: young minds at work, Desenzano del Garda (Italy), 24th October 2014. **Oral presentation**.

- Artusi S, Nadai M, Biasolo MA, Palù G, Flamand L, Calistri A, Richter SN (2014). *The Herpes Simplex Virus-1 genome contains multiple clusters of repeated G-quadruplex: implications for the antiviral activity of a G-quadruplex ligand*. 3rd Antivirals Congress, Amsterdam (Netherlands), 12th October 2014.

- Perrone R, Artusi S, Butovskaya E, Nadai M, Richter SN (2014). *G-quadruplexes in the Human Immunodeficiency virus-1 and Herpes Simplex virus-1: new targets for antiviral activity by small molecules*. 5th International Conference on Biomedical Engineering in Vietnam, Ho Chi Minh City (Vietnam), 16th June 2014.

- Artusi S, Nadai M, Biasolo MA, Palù G, Flamand L, Calistri A, Richter SN (2014). *Formation of multiple clusters of repeated G-quadruplex in the HSV-1 genome: implications for antiviral activity*. XII National Congress of the Italian Society of Virology, Orvieto (Italy), 22th September 2014. **Poster presentation**.

- Artusi S, Biasolo MA, Palù G, Calistri A, Richter SN (2013). *Biophysical characterization and antiviral effects of non-canonical DNA structures in the Herpes simplex virus type 1 genome*. 5th European Congress of Virology, Lyon (France), 11th September 2013. **Oral presentation**.

- Artusi S, Nadai M, Doria F, Freccero M, Richter SN (2013). *Synthesis and G-quadruplex binding and selectivity of novel tri- and tetra-substituted ethynyl naphthalene diimides*. IV International Meeting on G-quadruplex Nucleic Acids, Singapore, 1st July 2013. **Poster presentation**.

- Artusi S, Piccoli E, Calistri A, Palù G, Richter SN (2014). *Biophysical characterization and antiviral effects of non-canonical DNA structures in the Herpes simplex virus-1 genome*. XI National Congress of the Italian Society of Virology, Orvieto (Italy), 17th September 2014. **Poster presentation**.